

Universiteit
Leiden
The Netherlands

Unraveling mechanisms of vascular remodeling in arteriovenous fistulas for hemodialysis

Wong, C.Y.

Citation
Wong, C. Y. (2017, March 8). *Unraveling mechanisms of vascular remodeling in arteriovenous fistulas for hemodialysis*. Retrieved from https://hdl.handle.net/1887/46406

Version:	Not Applicable (or Unknown)
License:	Licence agreement concerning inclusion of doctoral thesis in the Institutional Repository of the University of Leiden
Downloaded from:	https://hdl.handle.net/1887/46406

Note: To cite this publication please use the final published version (if applicable).

Cover Page



Universiteit Leiden



The handle http://hdl.handle.net/1887/46406 holds various files of this Leiden University dissertation.

Author: Wong, C.Y.
Title: Unraveling mechanisms of vascular remodeling in arteriovenous fistulas for hemodialysis
Issue Date: 2017-03-08

C.Y. Wong

Unraveling mechanisms of vascular remodeling in arteriovenous fistulas for hemodialysis



Unraveling Mechanisms of Vascular Remodeling in Arteriovenous Fistulas for Hemodialysis

C.Y. Wong

Cover design	Esther Scheide | Proefschriftomslag.nl
Layout	Esther Scheide | Proefschriftomslag.nl
Printed by	Gildeprint BV
ISBN	978-94-92332-18-9

Copyright C.Y. Wong, 2017, Leiden, The Netherlands.
All rights reserved. No parts of this thesis may be reproduced, distributed, stored in a retrieval system or transmitted in any form or by any means, without permission of the author.

Unraveling Mechanisms of Vascular Remodeling in Arteriovenous Fistulas for Hemodialysis

Proefschrift

ter verkrijging van
de graad van doctor aan de Universiteit Leiden,
op gezag van de Rector Magnificus prof. mr. C.J.J.M. Stolker,
volgens besluit van het College voor Promoties
ter verdedigen op woensdag 8 maart 2017
klokke 16:15 uur

door

ChunYu Wong
Geboren te Leidschendam
in 1982

Promotores	Prof. dr. A.J. Rabelink	
	Prof. dr. P.H.A. Quax	
Co-Promotores	dr. J.I. Rotmans	
Promotiecommissie	dr. K.E.A. van der Bogt	
	Prof. dr. H.J.M. Verhagen	Heelkunde, ErasmusMC
	Prof. dr. C.J.M. de Vries	Medische Biochemie, AMC
	Prof. dr. J.F. Hamming	

The research described in this thesis was supported by a grant by the Dutch Kidney Foundation.

Financial support by the Dutch Heart Foundation for the publication of this thesis are gratefully acknowledged.

Financial support by the Alrijne zorggroep is gratefully acknowledged. Publication of the thesis was further supported by Krijnen Medical, Fresenius Medical Care BV, Enceladus Pharmaceuticals BV, Astellas Pharma BV and Chipsoft.

Table of Contents

Chapter 1	General Introduction	7
Chapter 2	Arteriovenous access failure: More than just intimal hyperplasia? *Nephrol Dial Transplant. 2013 May;28(5):1085-92*	17
Chapter 3	Vascular remodeling and intimal hyperplasia in a novel murine model of arteriovenous fistula failure *J Vasc Surg. 2014 Jan;59(1):192-201*	35
Chapter 4	A Novel Murine Model of Arteriovenous Fistula Failure: The Surgical Procedure in Detail *J Vis Exp. 2016 Feb 3;(108)*	59
Chapter 5	Elastin is a key regulator of outward remodeling in arteriovenous fistulas *Eur J Vasc Endovasc Surg. 2015 Apr;49(4):480-6*	77
Chapter 6	Liposomal prednisolone inhibits vascular inflammation and enhances venous outward remodeling in a murine arteriovenous fistula model *Sci Rep. 2016 Jul 27;6:30439*	93
Chapter 7	Deficiency of TLR4 homologue Radio(R) Protective(P)-105 impairs outward remodeling in a murine model of arteriovenous fistula failure *-Submitted-*	117
Chapter 8	Summary and Discussion	139
Chapter 9	Nederlandse Samenvatting	155
	Curriculum Vitae	161
	List of Publications	163
	Dankwoord	165

Chapter 1

General Introduction



End stage renal disease

The kidney is an intricate organ that has many life-sustaining functions, such as removing waste products and excess fluid from the body through secretion of urine, maintaining the balance/homeostasis of electrolytes, acidity and blood pressure. Kidney disease can ultimately lead to permanent failure of the kidney function. The most frequent causes for kidney failure are diabetes mellitus and hypertension. When the kidney function worsens to the stage that the patient is life dependant on renal replacement therapy, the patient then suffers from end-stage renal disease (ESRD). The number of ESRD patients in the Netherlands on January 2015 was 16.316 and every year there are about 2000 new ESRD patients[1].

The treatment for ESRD consists of kidney replacement therapy, which can be divided in two modalities: Kidney transplantation and dialysis. The transplantation of a donor kidney is the preferred type, and although the number of patients with functioning donor kidneys is growing in the Netherlands, there is still a large group of patients who do not have a donor kidney mainly due to the unavailability of donor organs. This group of patients is dependent on dialysis treatment.

Dialysis treatment

There are two dialysis treatment modalities: Haemodialysis (HD) and peritoneal dialysis (PD). In haemodialysis treatment, the exchange of substances and extraction of fluids are carried out directly via the blood, whereas peritoneal dialysis is carried out via the peritoneal cavity. Haemodialysis treatment generally requires patients to travel to the hospital for about 3 times a week. Despite the latter, HD treatment (86%) is favoured greatly over PD (14%) in the Netherlands. On a world-wide scale, the number of haemodialysis patients adds up to approximately 2 million.

Vascular access

One of the prerequisite of HD treatment is gaining access to a blood vessel with a high blood flow. The most simple and quickest option is to gain access to the central venous system using a catheter. However, this direct form of vascular access is not preferred for chronic dialysis due to the high risk of catheter related infections and central vein stenosis. A better and a more practical location for the vascular access point would be in the upper extremity. The veins in the lower arm are located superficially and are therefore suited for easy percutaneous cannulation. However, these veins lack the required high blood flow capacity that is needed for HD. Fortunately, a high blood flow can be acquired surgically by connecting the high pressure arterial system with the low pressure venous system. A direct connection between the artery and vein is called an arteriovenous fistula (AVF) and when a prosthetic graft is used it is called

an arteriovenous graft (AVG). The National Kidney Foundation Dialysis Outcomes Quality Initiative (NKF KDOQI) advocates the use of AVFs whenever possible. This is due to a lower rate of mortality, infection and a higher patency of the AVF when compared to the AVG[2;3]. However, a disadvantage of the AVF is that it needs to "mature" before it can be used. This is a complex process in which the diameters and the blood flow of the involved vessels increase in order to facilitate HD. According to the KDOQI an AVF is matured when the fistula has a flow of at least 600 ml/min, a venous diameter of at least 6 mm and is located no deeper than 6 mm under the skin. The focus of this thesis will be primarily on the AVF.

Pathophysiology of vascular access failure (chapter 1)

Although the AVF is the preferred form of vascular access for chronic haemodialysis, it has significant problems with vascular access dysfunction responsible for a high morbidity rate[4-6]. Moreover, vascular access-related problems account for more than 25% of all hospitalizations in ESRD patients[4] surmounting to more than 1 billion dollars per year being spent on access-related care in the US alone.

From a time point field of view, AVF failure can be categorized in early- and late failure, in which early failure has been defined as an AVF that has never developed adequately for dialysis (maturation failure), or which fails within 3 months of starting dialysis treatment. All other failures are categorized as late failures.

One of the key parameter that determines the success of an AVF is the amount of blood flow that the fistula can facilitate, which is mainly dependant on the available luminal area. How the luminal area develops after AVF creation is mainly determined by two morphological processes that can balance each other out: [1] Intimal hyperplasia (IH) and [2] Outward remodeling (OR). Intimal hyperplasia is the classical histological lesion that appears to be associated with AVF failure, and is mainly composed of vascular smooth muscle cells (VSMCs)[7]. Importantly, IH is considered to be an unwanted process that needs to be reduced as much as possible. On the other hand, outward remodeling is defined by the increase in the vascular diameter and is considered to be a favourable process that can potentially increase the luminal area. The end result that determines the luminal area, and ultimately blood flow, is dependent on the two processes. Which factors determine the favourable or unfavourable outcome remains unclear. In the current literature, therapeutic interventions are predominantly aimed at the reduction of intimal hyperplasia, thereby potentially neglecting the beneficial effects of stimulating outward remodeling.

It is clear that AVF failure remains a significant clinical problem that needs to be improved. In order to develop new therapeutic strategies, it is of utmost importance to first unravel the pathophysiology that is responsible for AVF failure.

Animal models

Although it is still unclear what mechanisms exactly drive maturation failure, the pathogenesis of IH has been well described in the literature and seems to be multifactorial. Factors that are believed to contribute to IH are: (1) Surgical trauma, (2) unfavourable hemodynamic shear stress[8;9], (3) vessel injury due to dialysis needle, (5) uraemia resulting in endothelial dysfunction10 and (6) chronic inflammatory state associated with ESRD[11;12].

Due to the complex nature of the multiple processes involved in AVF failure from which the hemodynamical aspects seems to be of great influence, we believe that basic research is best to be performed in an in-vivo animal model. In the literature, numerous animal models in various animal species have been described that are used to study AVF failure, ranging from a baboon to the mouse[13]. In this great arsenal of animal models, we would prefer the murine variant, due to the widespread availability of genetically altered animals. This allows us to study gene specific factors that might contribute to AVF failure. There are multiple murine models available that all utilize the vasculature in the neck (common carotid artery and jugular vein), however both the models of Kwei et al.[14] and Yang et al.[15] describe a functional end-to-end AVF configuration using a synthetic cuff to complete the anastomosis. Castier et al.[16] introduced an improved murine AVF model in which the end of the common carotid artery was connected to the side of the ipsilateral jugular vein using micro sutures ,thereby taking out the potentially pro-thrombotic and pro-inflammatory effect of the synthetic cuff of the equation. Although this new model is considered to be an important improvement, we believe that the AVF configuration can further be optimized. Unlike in the model described by Castier et al.16, AVFs in the clinical setting most frequently are constructed in a venous end to arterial side manner. This different configuration is very important, as this directly leads to a different hemodynamic profile in the AVF, which is an important factor in AVF biology. We therefore set out to develop a new murine AVF model that incorporates the same vascular configuration as is utilized in humans.

Aims of thesis and thesis outline

The main aim of this thesis was to develop a novel murine model of AVF failure that can be used to further unravel the pathological factors that are involved in AVF maturation failure, in order to develop a basis for the development of novel therapies. Although the exact mechanisms underlying AVF failure remains unclear, both IH and inadequate outward remodelling seem to contribute.

In **chapter 2** the possible factors that might contribute to AVF failure are discussed.

In **chapter 3** and **4** we describe our newly developed murine model of AVF failure, which incorporates a similar vascular configuration as is utilized in humans. We also used an unconventional technique (near infrared fluoroscopy) to visually assess the patency of the AVF in our murine model.

In **chapter 5** we assessed the role of the extracellular matrix protein elastin in vascular remodelling using a mouse that was haplodeficient for the tropoelastin gene. Elastin is the principle extracellular matrix (ECM) protein in the arterial wall constituting about 30-50% of the dry weight of arteries[17]. It provides the blood vessel its unique mechanical property that is needed for proper function. Previous studies have shown that elastin is the major inhibitor of VSMC migration and proliferation[18]. Interestingly, the basal elastin content in veins is relatively low compared to arteries. The latter suggest that the enhanced proliferative response in vein grafts (when compared to arterial grafts) may relate to the less pronounced protective function of elastin in veins. Surprisingly, the role of elastin in AVF failure has not received much attention thus far.

Previous studies have shown that the inflammatory response is involved in the development of IH in vascular injury[19-21]. However, the role of inflammation in AVF biology has not yet been elucidated. Nonetheless, there are clues that AVF failure is linked to inflammation. In a study by Liu et al. , higher levels of inflammatory blood markers such as high-sensitivity C-reactive protein (hs-CRP), interleukin-6 (IL-6) and tumor necrosis factor-alpha (TNF-α) was associated with AVF dysfunction in haemodialysis patients. In **chapter 6**, we investigate the role of inflammation in AVF failure by using prednisolone in our murine model. Too improve local biological activity, we encapsulated prednisolone in liposomes acting as a local target delivery vehicle.

In **chapter 7** we study the effects of the TLR4 inhibitor RP105 on AVF remodeling. RP105 is a structural homologue of TLR4 that lacks the internal signaling domain and can act as an inhibitor of the TLR4 mediated signaling. Based on the hypothesis that TLR4 mediated inflammatory responses contribute to vascular remodeling in several pathophysiological processes, we anticipate an increased AVF maturation in mice that are deficient of the TLR4 inhibitor RP105. Therefore we performed AVF surgery in RP105 deficient mice and studied the effects on the AVF maturation in vivo. In addition we studied in a series of in vitro experiments the effects of RP105 deficiency on smooth muscle cells and inflammatory cells in more detail.

Chapter 8 summarizes the findings in this thesis and reviews future perspectives in the field of AVF research.

Reference List

1. Renine.nl. 2015.
Ref Type: Online Source

2. Dhingra RK, Young EW, Hulbert-Shearon TE, Leavey SF, Port FK. Type of vascular access and mortality in U.S. hemodialysis patients. *Kidney Int* 2001;60:1443-1451.

3. Huber TS, Carter JW, Carter RL, Seeger JM. Patency of autogenous and polytetrafluoroethylene upper extremity arteriovenous hemodialysis accesses: a systematic review. *J Vasc Surg* 2003;38:1005-1011.

4. Feldman HI, Kobrin S, Wasserstein A. Hemodialysis vascular access morbidity. *J Am Soc Nephrol* 1996;7:523-535.

5. McCarley P, Wingard RL, Shyr Y, Pettus W, Hakim RM, Ikizler TA. Vascular access blood flow monitoring reduces access morbidity and costs. *Kidney Int* 2001;60:1164-1172.

6. Roy-Chaudhury P, Kelly BS, Zhang J et al. Hemodialysis vascular access dysfunction: from pathophysiology to novel therapies. *Blood Purif* 2003;21:99-110.

7. Roy-Chaudhury P, Wang Y, Krishnamoorthy M et al. Cellular phenotypes in human stenotic lesions from haemodialysis vascular access. *Nephrol Dial Transplant* 2009;24:2786-2791.

8. Paszkowiak JJ, Dardik A. Arterial wall shear stress: observations from the bench to the bedside. *Vasc Endovascular Surg* 2003;37:47-57.

9. Remuzzi A, Ene-Iordache B, Mosconi L et al. Radial artery wall shear stress evaluation in patients with arteriovenous fistula for hemodialysis access. *Biorheology* 2003;40:423-430.

10. Mezzano D, Pais EO, Aranda E et al. Inflammation, not hyperhomocysteinemia, is related to oxidative stress and hemostatic and endothelial dysfunction in uremia. *Kidney Int* 2001;60:1844-1850.

11. Kokubo T, Ishikawa N, Uchida H et al. CKD accelerates development of neointimal hyperplasia in arteriovenous fistulas. *J Am Soc Nephrol* 2009;20:1236-1245.

12. Liu BC, Li L, Gao M, Wang YL, Yu JR. Microinflammation is involved in the dysfunction of arteriovenous fistula in patients with maintenance hemodialysis. *Chin Med J (Engl)* 2008;121:2157-2161.

13. Rotmans J.I. Animal models for studying pathophysiology of hemodialysis access. The open urology & nephrology journal 7, 14-21. 1-4-2014. Ref Type: Journal (Full)

14. Kwei S, Stavrakis G, Takahas M et al. Early adaptive responses of the vascular wall during venous arterialization in mice. *Am J Pathol* 2004;164:81-89.

15. Yang B, Shergill U, Fu AA, Knudsen B, Misra S. The mouse arteriovenous fistula model. *J Vasc Interv Radiol* 2009;20:946-950.

16. Castier Y, Lehoux S, Hu Y, Foteinos G, Tedgui A, Xu Q. Characterization of neointima lesions associated with arteriovenous fistulas in a mouse model. *Kidney Int* 2006;70:315-320.

17. Brooke BS, Bayes-Genis A, Li DY. New insights into elastin and vascular disease. *Trends Cardiovasc Med* 2003;13:176-181.

18. Ito S, Ishimaru S, Wilson SE. Inhibitory effect of type 1 collagen gel containing alpha-elastin on proliferation and migration of vascular smooth muscle and endothelial cells. *Cardiovasc Surg* 1997;5:176-183.

19. Patel SD, Waltham M, Wadoodi A, Burnand KG, Smith A. The role of endothelial cells and their progenitors in intimal hyperplasia. *Ther Adv Cardiovasc Dis* 2010;4:129-141.

20. Welt FG, Rogers C. Inflammation and restenosis in the stent era. *Arterioscler Thromb Vasc Biol* 2002;22:1769-1776.

21. Welt FG, Tso C, Edelman ER et al. Leukocyte recruitment and expression of chemokines following different forms of vascular injury. *Vasc Med* 2003;8:1-7.

Chapter 2

Arteriovenous access failure: More than just intimal hyperplasia?

Tonia C. Rothuizen, ChunYu Wong, Paul H.A. Quax, Anton Jan van Zonneveld, Ton J. Rabelink and Joris I. Rotmans

Nephrol Dial Transplant. 2013 May;28(5):1085-92



Abstract

Hemodialysis vascular access patency is severely compromised by fistula non-maturation and access stenosis. Intimal hyperplasia (IH) is considered the culprit lesion in failed fistulas, resulting in luminal narrowing and stenosis. This review focuses on the biology and pathophysiology of fistula failure and highlights not only the classically associated intimal hyperplasia but also some relatively neglected but potentially important contributors such as inadequate outward remodeling. In addition, the complex process and fragile balance of successful fistula maturation might be partially hindered by pre-existent chronic kidney disease-mediated vasculopathy. Further unravelling the (patho)physiology of outward remodeling and intimal hyperplasia could contribute to novel therapies and enhance fistula patency.

Introduction

Patients with end-stage renal disease are largely dependent on dialysis as renal replacement therapy. For chronic hemodialysis, an adequately functioning high-flow vascular access is required. Arteriovenous fistulas (AVFs) are the preferred modality in view of the superior patency rates and fewer complications as compared to arteriovenous synthetic grafts[1-3]. Nonetheless, the durability of AVFs is far from optimal with one year primary patency rates ranging from 60-65%[4;5]. In fact, these numbers are too optimistic, as they frequently do not account for fistulas that failed to mature. Maturation failure contributes significantly to the dismal patency rates of AVFs as illustrated by a recent multi-center study which revealed that 60% of the AVFs were not suitable for dialysis between 4-5 months post surgery[6], although, these numbers do vary between different types of AVFs[7]. According to the KDOQI guidelines, an AVF maturation is clinically considered successful if 6 weeks after surgery the fistula supports a flow of 600 mL/min, is located at a maximum of 6 mm from the surface and has a diameter greater than 6 mm[2]. The exact underlying mechanisms responsible for maturation failure are however unknown, but impaired outward remodeling as well as intimal hyperplasia (IH) are both considered to contribute.

Thus far, most research on the pathophysiology of AVF failure focuses on IH. In contrast, the role of vascular outward remodeling in the setting of AVFs is often neglected. However, adequate outward remodeling could preserve luminal caliber and may therefore be valuable for successful fistula maturation. We postulate that the balance between outward expansion and potential luminal narrowing due to IH may ultimately determine fistula flow and patency (Fig.1). This review focuses on the pathophysiology of both AVF maturation failure and failure of already matured AVFs, and highlights some potential contributors thus far gaining relatively little attention, such as outward remodeling and the implications of chronic kidney disease (CKD) mediated vascular pathology.

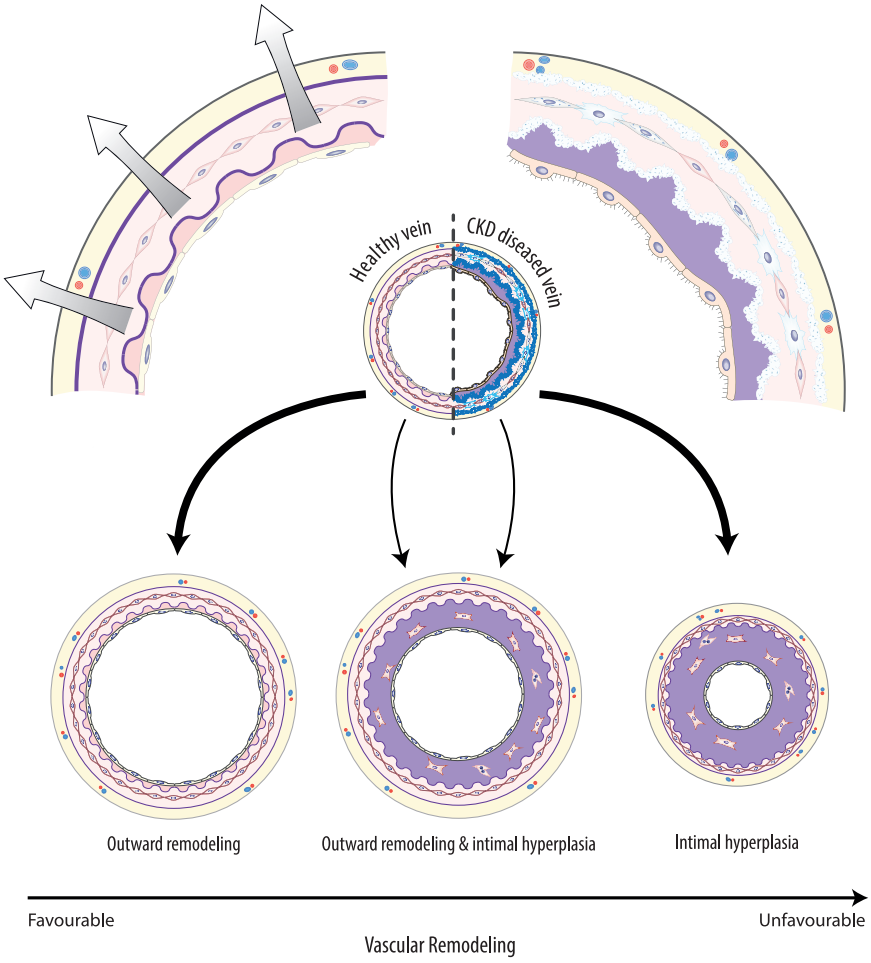


Figure 1. Different modalities of the vascular remodeling response after fistula creation. Whereas a healthy vein has the potential for successful outward remodeling (top left), adequate maturation may be partially hindered by CKD-induced pre-existing vasculopathy such as IH (top right). As shown below, we postulate that the net resultant of IH and outward remodeling may determine ultimate luminal calibre. In case of IH formation, adequate outward remodeling could to a certain extent remain lumen calibre intact, thus providing a patent fistula. However, if IH outbalances outward remodeling this could result in stenosis and fistula failure.

Outward remodeling: an emerging concept in arteriovenous fistulas?

The connection of a low-pressure vein to the high-pressure arterial system results in a chain of vascular events that starts with an immediate increase of blood flow through the both the feeding artery and the draining vein[4;8]. Directly after construction of the AVF, this rapid

increase in flow results in both passive vascular distension and in nitric oxide (NO) synthesis by endothelial cells with subsequent vascular smooth muscle cell (VSMC) relaxatio[n9-11] resulting in acute vasodilation. Concomitantly, the hemodynamic changes following AVF creation initiate a more structural vascular remodeling response leading not only to a further increase in arterial and venous calibre[12-14] but also to thickening of especially the venous wall[15;16]. Increased wall shear stress (WSS) and wall tension are the driving forces. WSS is the frictional force exerted by blood on the vessel wall and is mathematically defined by Poiseuille's formula: $4\eta Q/\pi r^3$ where η = blood viscosity, Q = flow and r = vessel radius. An increase in blood flow will provoke an adaptive response of the vessel in which the luminal diameter increases in attempt to reduce WSS to pre-AVF levels (5-10 dyn/cm^2). Furthermore, due to the pressure increase in the venous outflow tract after fistula creation, the wall tension rises leading to another adaptive response culminating in medial thickening (i.e. venous arterialization). These phenomena are elegantly illustrated in a study of Corpataux et al[12], where hemodynamic changes in the venous part of AVFs in six patients were investigated using echo-tracking and Doppler-ultrasonography. Within the first week after fistula formation the flow increased to 539 mL/min accompanied by an almost threefold increase in WSS to 24.5 dyn/cm^2. The continuous increase in flow resulted in a progressive increment in venous luminal calibre from 2.4 mm preoperative to 6.6 mm after 12 weeks. Since WSS is inversely related to lumen size, the WSS gradually returned to a physiological range (10.4 dyn/cm^2 at 12 weeks). In addition, the venous wall thickness increased, demonstrated by an augmentation of cross sectional wall area. This adaptive response is also applicable for the arterial side of the AVF, where the increment of arterial flow results in an increase of arterial luminal diameter[14], although to a lesser extent than the venous side[12]. This change in diameter does not result in wall thickening but likely rather results in arterial wall remodeling (i.e. an increase in both internal and external diameter without an increase in wall cross sectional area)[14].

On a biological level, these changes in WSS and wall tension are sensed by the endothelial cells, that function as mechanosensors and convert these hemodynamic stimuli to biochemical signals such as vasodilating agents (e.g. NO), growth factors that can control VSMC proliferation and migration and cellular adhesion molecules[10;17-19]. Upregulation of proteases such as matrix metalloproteinases (MMPs) and cathepsins results in matrix degradation and restructuring of the vascular scaffold leading to luminal expansion[15;20-22]. In addition, with an increased circumference of the vessel wall, it seems logical that some VSMC reorganization should occur as well to keep in pace with the expansion, as is also described in arterial setting[23]. However, to date little is known about the role of VSMCs in outward remodeling in AVFs.

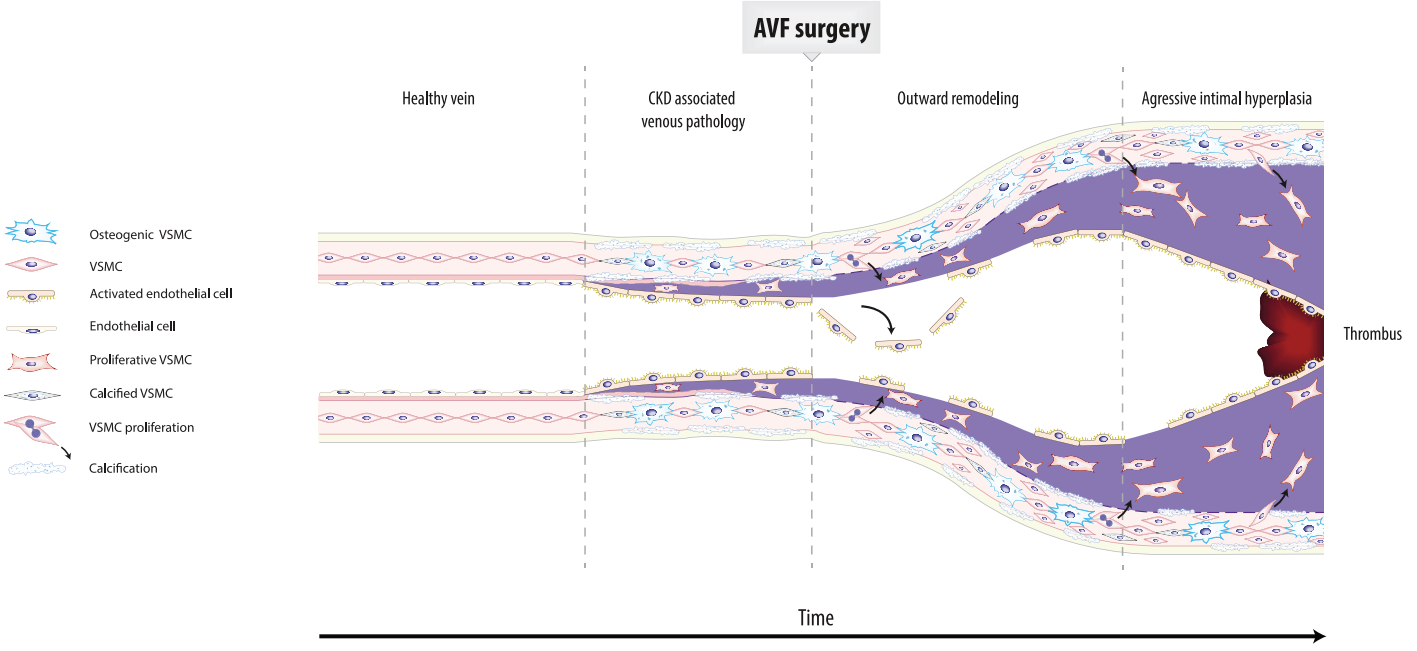


Figure 2. Potential mechanisms of the remodeling response upon fistula creation. Upon fistula creation, in response to the altered hemodynamic environment a plethora of structural changes may occur in the vessel wall; amongst others surgery induced endothelial denudation, matrix reorganization to accommodate outward expansion but possibly also VSMC proliferation and migration contributing to intimal hyperplasia formation. Physiological outward remodeling may to a certain extent compensate for detrimental intimal lesions.

As explained before, the adaptive outward remodeling response occurs both in the feeding artery and in the draining vein of the fistula[12;14]. Nonetheless, the majority of the stenotic lesions in fistulas failing to mature are localized in the venous part, mostly in the juxta-anastomotic region[24;25]. The latter observation could suggest that not only IH but also venous luminal expansion may be important for the preservation of the luminal calibre, thereby allowing the fistula to mature. We postulate that the net resultant of adaptive outward expansion and potential luminal narrowing by IH and thrombosis may ultimately determine luminal calibre, flow and long term AVF patency.

Intimal hyperplasia: adverse vascular response that hampers AVF function

Intimal hyperplasia is the pathologic lesion in AVFs that may result in stenosis and ultimately thrombosis. It is characterized primarily by α-smooth muscle actin (α-SMA) positive cells, extracellular matrix proteins and cytokines such as platelet-derived growth factor, transforming growth factor-β and endothelin within the intima and media of the vein[26-28]. The vast majority of the α-SMA positive cells in the intimal lesions exhibit a myofibroblasts or synthetic VSMC phenotype[29]. These cells could either be differentiated fibroblasts that migrated from the adventitia and acquired α-SMA expression[30], or dedifferentiated medial VSMCs[5]. Furthermore, recent studies of non-AVF models suggest that a proportion of the α-SMA positive cells in IH lesions might originate from multipotent vascular stem cells from the bone marrow[31;3233].

In most physiological conditions, high laminar shear stress triggers endothelial quiescence, endothelial alignment in parallel with the flow and secretion of anti-inflammatory and anti-coagulant substances[17;18;34], thus preventing IH. In contrast, low flow and WSS levels as well as oscillating flow patterns are involved in endothelial cell activation with increased expression of pro-coagulant and pro-inflammatory mediators that predispose for IH[34;35]. Although AVFs merely express high flow profiles, recent studies revealed the coexistence of spot regions with low and oscillating flow and WSS levels in the venous part of the AVF, using a pulsatile computational fluid dynamics simulation[36]. These spot regions corresponded with in previous studies documented IH prone regions in the juxta-anastomotic area of the AVF. Alterations in anastomosis angle could impact the flow rates and patterns, potentially influencing IH formation, with sharper angles (30°) generating favourable outcomes[37]. This was further illustrated by Krishnamoorthy et al[38], demonstrating a correlation between AVF configuration, WSS pattern and the development of IH in a porcine AVF model. Thus, IH in an AVF setting is likely to be associated with an abnormal WSS profile. Nevertheless, IH has also been observed in veins prior to vascular access placement[39] and in saphenous veins[40], suggesting that an abnormal WSS profile is not the sole cause for development of IH. Epidemiological studies have identified diabetes mellitus, race, older age, peripheral vascular disease, female sex and in

some studies also cardiovascular disease as risk factors for maturation failure[41-43]. Furthermore, individual variation in patency outcomes may also in part be explained by genetic susceptibility. Indeed, several single nucleotide polymorphisms are associated with poor functional outcome of vascular access conduits for hemodialysis[44;45].

Most studies on fistula failure focussed on the effect of several parameters on IH, as IH is considered to be the pathognomonical lesion in fistula failure. However, as mentioned above, luminal calibre can be preserved by adequate outward remodeling. Consequently, in addition to IH, impaired outward remodeling may be another important but relatively overlooked contributor to fistula failure. Despite its potential impact on fistula patency, relatively little is known about outward remodeling in AVFs. Future research aiming to gain more insight in the (patho)physiology of outward remodeling in fistulas might therefore contribute to new therapeutic strategies that could improve fistula patency.

Interestingly, some of the elementary factors in outward remodeling are also involved in the process of IH. Whereas outward remodeling in AVFs is related to matrix protease activity such as MMPs and cathepsins[20-22], it is shown that MMPs are also involved in IH formation in AVFs[46;47] and cathepsins in IH formation in balloon-injured artery[48]. The relative contribution of these proteases to expansive remodeling versus IH is not yet established, though the crucial role in outward remodeling suggests a more beneficial than detrimental effect, especially in the initial phase of AVF maturation. The latter suggestion is underscored by a recent report showing increased serum MMP-2 levels in patients with matured fistulas as compared to those with maturation failure[20]. However, as a consequence of elastolytic protease activity the internal elastic lamina is fragmented[21;49]. This disruption of the elastic lamina and loss of integrity of this structural barrier may allow migration of adventitial fibroblasts or medial VSMCs to the intima. Moreover, the elastin degradation products can act as chemo-attractants for VSMCs and fibroblasts and might direct them to the intimal region and support their proliferation[50-52]. Thus, potentially the balance of this partially overlapping beneficial outward remodeling and detrimental IH may affect fistula patency outcomes.

Vascular pathology in chronic kidney disease

Noteworthy, this complex process and fragile balance of successful fistula maturation might be partially hindered by pre-existent vascular abnormalities often present in patients with CKD. Especially in these patients with elevated comorbidity burden, a tailored surgical technique[53;54] and surgical expertise[54] are important in determining fistula patency outcomes. Furthermore, CKD itself is a well-known risk factor for cardiovascular morbidity[55]. The increased prevalence of cardiovascular disease in CKD-patients is only partly explained by traditional risk factors such as hypertension, diabetes, dyslipidemia and increased age. Epidemiological studies revealed

that CKD is an independent risk factor for cardiovascular morbidity[56]. The latter observations implicate a role for additional inimical stimuli in CKD-patients such as chronic inflammation, increased oxidative stress, uremic toxins and endothelial dysfunction, as is reviewed in more detail elsewhere[57-59]. Most studies on CKD mediated vasculopathy concentrate on the arterial system. A functional AVF requires both adequate venous and arterial maturation. Pre-existent arterial vasculopathy may therefore reduce patency. In addition, although not extensively studied, the detrimental effects of CKD on the arterial system may influence veins in a similar manner[60]. Indeed, recent studies elegantly showed marked pre-existing IH in venous segments of patients with end-stage renal disease prior to vascular access surgery[39;61;62]. Another potential contributor to vascular pathology in CKD is vascular calcification. Whereas calcification in the tunica intima is classically associated with atherosclerosis, calcification in the tunica media can occur independently of atherosclerotic plaques and is frequently observed in arteries of any size in CKD-patients[63], resulting in vascular stiffness[64;65]. In arterial setting this is known to impair the vessel's ability to expand upon high flow stimulation[66]. Interestingly, Lee et al[67] recently also demonstrated extensive calcification in the intima and media of venous segments that were harvested at the time of vascular access surgery. This might result, similar to the arterial setting, in reduced venous compliance, thus potentially limiting the utility of AVFs by inhibiting outward remodeling and AVF maturation. Clinical studies already showed that forearm venous distensibility (i.e. increase in luminal diameter upon inflation of an upper arm cuff) rather than baseline venous diameter predicts successful AVF maturation[68]. Although a recent study revealed that medial calcification in the supplying artery of AVFs was not associated with maturation failure[69], future studies should explore the impact of venous calcification prior to access surgery on maturation failure. Indeed, the outward remodeling response is much more pronounced in the venous part of AVFs compared to the feeding artery[12].

Therapeutic strategies to improve vascular access patency

In order to create a proper basis for a successful AVF, pre-operative vein preservation and careful selection of suitable vessels for AVF creation should be performed routinely[2;70]. In case of fistula non-maturation or stenosis a percutaneous transluminal angioplasty (PTA) and/or surgical revision is required[2;70]. To date, there are no adequate therapies improving the remodeling process of the AVF in the intermediary period. Moreover, despite the good results of PTA on the short term, it often induces restenosis on the longer term[71-73]. Therefore there is a strong clinical need for new therapeutic strategies to improve fistula patency.

Possibilities to encourage outward remodeling include the use of elastase, thereby reorganizing the extracellular matrix scaffold of the vessel and promoting rapid dilation. After successful results in an AVF rabbit model[35], the use of recombinant-elastase PRT-201 was recently

clinically evaluated in a randomized controlled trial in human AVFs[74]. Perivascular delivery of PRT-201 appeared to be safe but no effect on primary patency was observed. A larger clinical trial is underway since this first study was not powered to assess efficacy. Given the potential detrimental effects of elastin degradation products on both vascular calcification[75] and VSMC proliferation[51;52], the overall effectiveness of this agent remains to be elucidated.

Potential candidates for targeting IH are agents that inhibit VSMC proliferation, such as paclitaxel and sirolimus, although with data obtained only in AVG setting[76;77] their effect in AVFs remains to be established.

As mentioned above, outward remodeling and IH are two processes that are in part intertwined. Some factors that are involved in outward remodeling such as MMPs may in a later stage also facilitate IH formation. Therefore, the potential of a therapy directed to a factor contributing in both types of remodeling could be influenced by the time of application. Limiting IH in an early stage might also decelerate the outward remodeling response and vice versa. Enhancement of maturation might require a different intervention than prevention of AVF failure once the AVF is successfully used for hemodialysis. Therefore, time dependent delivery might be a suitable approach to tackle fistula failure. Fistulas are ideal targets for such therapy, due to their easy accessibility and the potential to use perivascular delivery methods. However, to create a successful intervention strategy, more insight in the course and (patho)physiology of vascular remodeling is warranted.

Incorporation of other disciplines in the field of vascular access might offer new perspectives. IH is studied extensively in the field of cardiology and vascular surgery and the process of outward remodeling in physiological situations such as pregnancy. Furthermore the technology in slow-release drug delivery systems is rapidly expanding. Another relatively new field with exciting developments is vascular tissue engineering. With vascular tissue engineering it is possible to create a diameter- and length-matched blood vessel free from valves and accessory vessels and has the unique potential to adjust a vessel to patient specific requirements. Importantly, tissue engineered blood vessels are free from pre-existing vascular disease. The potential of a tissue engineered blood vessel (TEBV) as arteriovenous graft was illustrated by the group of l'Heureux and McAllister. Using a so-called sheet-based method, a completely biological TEBV was developed without the use of synthetic material, thereby creating a TEBV that resembles a native vessel in both composition and structure. The TEBV was evaluated as AVG in ten patients resulting in a primary patency rate of 78% and 60% after 1 and 6 months respectively[78]. With spectacular progresses in the field of vascular tissue engineering[79-81], the use of a TEBV might become a realistic alternative in the nearby future.

Conclusion

Upon AVF creation a complex cascade of remodeling events should occur. The net resultant of beneficial outward expansion, potential luminal narrowing by intimal hyperplasia and the possible interference of CKD induced vascular pathology may ultimately determine luminal calibre, flow and long term AVF patency. Due to the potential positive contribution to fistula maturation and its assumed role in luminal calibre preservation, we pledge for more research emphasis on the role of outward remodeling. Further unravelling the complex pathways that mediate both IH and outward remodeling processes after AVF creation could provide new targets and therapies to improve fistula patency.

Acknowledgements

Tonia Rothuizen and Joris Rotmans are supported by the research program of the BioMedical Materials institute, co-funded by the Dutch Ministry of Economic Affairs, Agriculture and Innovation. ChunYu Wong is sponsored by a grant from the Dutch Kidney Foundation (KJPB 08.0003).

Reference List

1. Allon M, Robbin ML. Increasing arteriovenous fistulas in hemodialysis patients: problems and solutions. *Kidney Int* 2002; 62: 1109-1124

2. Clinical practice guidelines for vascular access. *Am J Kidney Dis* 2006; 48 Suppl 1: S248-S273

3. Gibson KD, Gillen DL, Caps MT, Kohler TR, Sherrard DJ, Stehman-Breen CO. Vascular access survival and incidence of revisions: a comparison of prosthetic grafts, simple autogenous fistulas, and venous transposition fistulas from the United States Renal Data System Dialysis Morbidity and Mortality Study. *J Vasc Surg* 2001; 34: 694-700

4. Tordoir JH, Rooyens P, Dammers R, van der Sande FM, de HM, Yo TI. Prospective evaluation of failure modes in autogenous radiocephalic wrist access for haemodialysis. *Nephrol Dial Transplant* 2003; 18: 378-383

5. Roy-Chaudhury P, Spergel LM, Besarab A, Asif A, Ravani P. Biology of arteriovenous fistula failure. *J Nephrol* 2007; 20: 150-163

6. Dember LM, Beck GJ, Allon M *et al*. Effect of clopidogrel on early failure of arteriovenous fistulas for hemodialysis: a randomized controlled trial. *JAMA* 2008; 299: 2164-2171

7. Lazarides MK, Georgiadis GS, Antoniou GA, Staramos DN. A meta-analysis of dialysis access outcome in elderly patients. *J Vasc Surg* 2007; 45: 420-426

8. Saucy F, Haesler E, Haller C, Deglise S, Teta D, Corpataux JM. Is intra-operative blood flow predictive for early failure of radiocephalic arteriovenous fistula? *Nephrol Dial Transplant* 2010; 25: 862-867

9. Cooke JP, Rossitch E Jr, Andon NA, Loscalzo J, Dzau VJ. Flow activates an endothelial potassium channel to release an endogenous nitrovasodilator. *J Clin Invest* 1991; 88: 1663-1671

10. Tronc F, Wassef M, Esposito B, Henrion D, Glagov S, Tedgui A. Role of NO in flow-induced remodeling of the rabbit common carotid artery. *Arterioscler Thromb Vasc Biol* 1996; 16: 1256-1262

11. Moncada S, Higgs A. The L-arginine-nitric oxide pathway. *N Engl J Med* 1993; 329: 2002-2012

12. Corpataux JM, Haesler E, Silacci P, Ris HB, Hayoz D. Low-pressure environment and remodelling of the forearm vein in Brescia-Cimino haemodialysis access. *Nephrol Dial Transplant* 2002; 17: 1057-1062

13. Ene-Iordache B, Mosconi L, Antiga L *et al*. Radial artery remodeling in response to shear stress increase within arteriovenous fistula for hemodialysis access. *Endothelium* 2003; 10: 95-102

14. Girerd X, London G, Boutouyrie P, Mourad JJ, Safar M, Laurent S. Remodeling of the radial artery in response to a chronic increase in shear stress. *Hypertension* 1996; 27: 799-803

15. Chan CY, Chen YS, Ma MC, Chen CF. Remodeling of experimental arteriovenous fistula with increased matrix metalloproteinase expression in rats. *J Vasc Surg* 2007; 45: 804-811

16. Langer S, Heiss C, Paulus N *et al*. Functional and structural response of arterialized femoral veins in a rodent AV fistula model. *Nephrol Dial Transplant* 2009; 24: 2201-2206

17. Garanich JS, Pahakis M, Tarbell JM. Shear stress inhibits smooth muscle cell migration via nitric oxide-mediated downregulation of matrix metalloproteinase-2 activity. *Am J Physiol Heart Circ Physiol* 2005; 288: H2244-H2252

18. Frangos JA, Eskin SG, McIntire LV, Ives CL. Flow effects on prostacyclin production by cultured human endothelial cells. *Science* 1985; 227: 1477-1479

19. Gibbons GH, Dzau VJ. The emerging concept of vascular remodeling. *N Engl J Med* 1994; 330: 1431-1438

20. Lee ES, Shen Q, Pitts RL *et al*. Serum metalloproteinases MMP-2, MMP-9, and metalloproteinase tissue inhibitors in patients are associated with arteriovenous fistula maturation. *J Vasc Surg* 2011; 54: 454-459

21. Tronc F, Mallat Z, Lehoux S, Wassef M, Esposito B, Tedgui A. Role of matrix metalloproteinases in blood flow-induced arterial enlargement: interaction with NO. *Arterioscler Thromb Vasc Biol* 2000; 20: E120-E126

22. Chang CJ, Chen CC, Hsu LA *et al*. Degradation of the internal elastic laminae in vein grafts of rats with aortocaval fistulae: potential impact on graft vasculopathy. *Am J Pathol* 2009; 174: 1837-1846

23. De Mey JG, Schiffers PM, Hilgers RH, Sanders MM. Toward functional genomics of flow-induced outward remodeling of resistance arteries. *Am J Physiol Heart Circ Physiol* 2005; 288: H1022-H1027

24. Nassar GM, Nguyen B, Rhee E, Achkar K. Endovascular treatment of the "failing to mature" arteriovenous fistula. *Clin J Am Soc Nephrol* 2006; 1: 275-280

25. Sivanesan S, How TV, Bakran A. Sites of stenosis in AV fistulae for haemodialysis access. *Nephrol Dial Transplant* 1999; 14: 118-120

26. Rotmans JI, Pasterkamp G, Verhagen HJ, Pattynama PM, Blankestijn PJ, Stroes ES. Hemodialysis access graft failure: time to revisit an unmet clinical need? *J Nephrol* 2005; 18: 9-20

27. Weiss MF, Scivittaro V, Anderson JM. Oxidative stress and increased expression of growth factors in lesions of failed hemodialysis access. *Am J Kidney Dis* 2001; 37: 970-980

28. Lee T, Roy-Chaudhury P. Advances and new frontiers in the pathophysiology of venous neointimal hyperplasia and dialysis access stenosis. *Adv Chronic Kidney Dis* 2009; 16: 329-338

29. Roy-Chaudhury P, Wang Y, Krishnamoorthy M *et al*. Cellular phenotypes in human stenotic lesions from haemodialysis vascular access. *Nephrol Dial Transplant* 2009; 24: 2786-2791

30. Li L, Terry CM, Blumenthal DK *et al*. Cellular and morphological changes during neointimal hyperplasia development in a porcine arteriovenous graft model. *Nephrol Dial Transplant* 2007; 22: 3139-3146

31. Tang Z, Wang A, Yuan F *et al*. Differentiation of multipotent vascular stem cells contributes to vascular diseases. *Nat Commun* 2012; 3: 875

32. Diao Y, Guthrie S, Xia SL *et al*. Long-term engraftment of bone marrow-derived cells in the intimal hyperplasia lesion of autologous vein grafts. *Am J Pathol* 2008; 172: 839-848

33. Caplice NM, Wang S, Tracz M *et al*. Neoangiogenesis and the presence of progenitor cells in the venous limb of an arteriovenous fistula in the rat. *Am J Physiol Renal Physiol* 2007; 293: F470-F475

34. Owens CD. Adaptive changes in autogenous vein grafts for arterial reconstruction: clinical implications. *J Vasc Surg* 2010; 51: 736-746

35. Lee T, Roy-Chaudhury P. Advances and new frontiers in the pathophysiology of venous neointimal hyperplasia and dialysis access stenosis. *Adv Chronic Kidney Dis* 2009; 16: 329-338

36. Ene-Iordache B, Remuzzi A. Disturbed flow in radial-cephalic arteriovenous fistulae for haemodialysis: low and oscillating shear stress locates the sites of stenosis. *Nephrol Dial Transplant* 2012; 27: 358-368

37. Ene-Iordache B, Cattaneo L, Dubini G, Remuzzi A. Effect of anastomosis angle on the localization of disturbed flow in 'side-to-end' fistulae for haemodialysis access. *Nephrol Dial Transplant* 2012;

38. Krishnamoorthy MK, Banerjee RK, Wang Y *et al*. Hemodynamic wall shear stress profiles influence the magnitude and pattern of stenosis in a pig AV fistula. *Kidney Int* 2008; 74: 1410-1419

39. Lee T, Chauhan V, Krishnamoorthy M *et al*. Severe venous neointimal hyperplasia prior to dialysis access surgery. *Nephrol Dial Transplant* 2011; 26: 2264-2270

40. Friedl R, Li J, Schumacher B *et al*. Intimal hyperplasia and expression of transforming growth factor-beta1 in saphenous veins and internal mammary arteries before coronary artery surgery. *Ann Thorac Surg* 2004; 78: 1312-1318

41. Ernandez T, Saudan P, Berney T, Merminod T, Bednarkiewicz M, Martin PY. Risk factors for early failure of native arteriovenous fistulas. *Nephron Clin Pract* 2005; 101: c39-c44

42. Lok CE, Allon M, Moist L, Oliver MJ, Shah H, Zimmerman D. Risk equation determining unsuccessful cannulation events and failure to maturation in arteriovenous fistulas (REDUCE FTM I). *J Am Soc Nephrol* 2006; 17: 3204-3212

43. Monroy-Cuadros M, Yilmaz S, Salazar-Banuelos A, Doig C. Risk factors associated with patency loss of hemodialysis vascular access within 6 months. *Clin J Am Soc Nephrol* 2010; 5: 1787-1792

44. Heine GH, Ulrich C, Sester U, Sester M, Kohler H, Girndt M. Transforming growth factor beta1 genotype polymorphisms determine AV fistula patency in hemodialysis patients. *Kidney Int* 2003; 64: 1101-1107

45. Lin CC, Yang WC, Lin SJ *et al*. Length polymorphism in heme oxygenase-1 is associated with arteriovenous fistula patency in hemodialysis patients. *Kidney Int* 2006; 69: 165-172

46. Tummers AM, Mountain DJ, Mix JW *et al*. Serum levels of matrix metalloproteinase-2 as a marker of intimal hyperplasia. *J Surg Res* 2010; 160: 9-13

47. Misra S, Fu AA, Anderson JL *et al*. The rat femoral arteriovenous fistula model: increased expression of matrix metalloproteinase-2 and -9 at the venous stenosis. *J Vasc Interv Radiol* 2008; 19: 587-594

48. Cheng XW, Kuzuya M, Sasaki T *et al*. Increased expression of elastolytic cysteine proteases, cathepsins S and K, in the neointima of balloon-injured rat carotid arteries. *Am J Pathol* 2004; 164: 243-251

49. Abeles D, Kwei S, Stavrakis G, Zhang Y, Wang ET, Garcia-Cardena G. Gene expression changes evoked in a venous segment exposed to arterial flow. *J Vasc Surg* 2006; 44: 863-870

50. Amabile PG, Wong H, Uy M *et al*. In vivo vascular engineering of vein grafts: directed migration of smooth muscle cells by perivascular release of elastase limits neointimal proliferation. *J Vasc Interv Radiol* 2002; 13: 709-715

51. Mochizuki S, Brassart B, Hinek A. Signaling pathways transduced through the elastin receptor facilitate proliferation of arterial smooth muscle cells. *J Biol Chem* 2002; 277: 44854-44863

52. Reddel CJ, Weiss AS, Burgess JK. Elastin in asthma. *Pulm Pharmacol Ther* 2012; 25: 144-153

53. Palmes D, Kebschull L, Schaefer RM, Pelster F, Konner K. Perforating vein fistula is superior to forearm fistula in elderly haemodialysis patients with diabetes and arterial hypertension. *Nephrol Dial Transplant* 2011; 26: 3309-3314

54. Konner K, Hulbert-Shearon TE, Roys EC, Port FK. Tailoring the initial vascular access for dialysis patients. *Kidney Int* 2002; 62: 329-338

55. Vanholder R, Massy Z, Argiles A, Spasovski G, Verbeke F, Lameire N. Chronic kidney disease as cause of cardiovascular morbidity and mortality. *Nephrol Dial Transplant* 2005; 20: 1048-1056

56. Go AS, Chertow GM, Fan D, McCulloch CE, Hsu CY. Chronic kidney disease and the risks of death, cardiovascular events, and hospitalization. *N Engl J Med* 2004; 351: 1296-1305

57. Brunet P, Gondouin B, Duval-Sabatier A *et al*. Does uremia cause vascular dysfunction? *Kidney Blood Press Res* 2011; 34: 284-290

58. Gunthner T, Jankowski V, Kretschmer A *et al*. Endothelium and vascular smooth muscle cells in the context of uremia. *Semin Dial* 2009; 22: 428-432

59. Moody WE, Edwards NC, Madhani M *et al*. Endothelial dysfunction and cardiovascular disease in early-stage chronic kidney disease: cause or association? *Atherosclerosis* 2012; 223: 86-94

60. Kokubo T, Ishikawa N, Uchida H *et al*. CKD accelerates development of neointimal hyperplasia in arteriovenous fistulas. *J Am Soc Nephrol* 2009; 20: 1236-1245

61. Wali MA, Eid RA, Dewan M, Al-Homrany MA. Pre-existing histopathological changes in the cephalic vein of renal failure patients before arterio-venous fistula (AVF) construction. *Ann Thorac Cardiovasc Surg* 2006; 12: 341-348

62. Wasse H, Huang R, Naqvi N, Smith E, Wang D, Husain A. Inflammation, oxidation and venous neointimal hyperplasia precede vascular injury from AVF creation in CKD patients. *J Vasc Access* 2012; 13: 168-174

63. O'Neill WC, Lomashvili KA. Recent progress in the treatment of vascular calcification. *Kidney Int* 2010; 78: 1232-1239

64. Blacher J, Guerin AP, Pannier B, Marchais SJ, London GM. Arterial calcifications, arterial stiffness, and cardiovascular risk in end-stage renal disease. *Hypertension* 2001; 38: 938-942

65. Guerin AP, London GM, Marchais SJ, Metivier F. Arterial stiffening and vascular calcifications in end-stage renal disease. *Nephrol Dial Transplant* 2000; 15: 1014-1021

66. Huang PH, Chen LC, Leu HB *et al*. Enhanced coronary calcification determined by electron beam CT is strongly related to endothelial dysfunction in patients with suspected coronary artery disease. *Chest* 2005; 128: 810-815

67. Lee T, Safdar N, Mistry MJ *et al*. Preexisting Venous Calcification Prior to Dialysis Vascular Access Surgery. *Semin Dial* 2012;

68. van der Linden J, Lameris TW, van den Meiracker AH, de Smet AA, Blankestijn PJ, van den Dorpel MA. Forearm venous distensibility predicts successful arteriovenous fistula. *Am J Kidney Dis* 2006; 47: 1013-1019

69. Allon M, Litovsky S, Young CJ *et al*. Medial fibrosis, vascular calcification, intimal hyperplasia, and arteriovenous fistula maturation. *Am J Kidney Dis* 2011; 58: 437-443

70. Tordoir J, Canaud B, Haage P *et al*. EBPG on Vascular Access. *Nephrol Dial Transplant* 2007; 22 Suppl 2: ii88-117

71. Chang CJ, Ko PJ, Hsu LA *et al*. Highly increased cell proliferation activity in the restenotic hemodialysis vascular access after percutaneous transluminal angioplasty: implication in prevention of restenosis. *Am J Kidney Dis* 2004; 43: 74-84

72. Beathard GA. Percutaneous transvenous angioplasty in the treatment of vascular access stenosis. *Kidney Int* 1992; 42: 1390-1397

73. Lee T, Ullah A, Allon M *et al*. Decreased cumulative access survival in arteriovenous fistulas requiring interventions to promote maturation. *Clin J Am Soc Nephrol* 2011; 6: 575-581

74. Peden EK, Leeser DB, Dixon BS *et al*. A multi-center, dose-escalation study of human type I pancreatic elastase (PRT-201) administered after arteriovenous fistula creation. *J Vasc Access* 2012; 0: 0

75. Pai AS, Giachelli CM. Matrix remodeling in vascular calcification associated with chronic kidney disease. *J Am Soc Nephrol* 2010; 21: 1637-1640

76. Paulson WD, Kipshidze N, Kipiani K *et al*. Safety and efficacy of local periadventitial delivery of sirolimus for improving hemodialysis graft patency: first human experience with a sirolimus-eluting collagen membrane (Coll-R). *Nephrol Dial Transplant* 2012; 27: 1219-1224

77. Kelly B, Melhem M, Zhang J *et al*. Perivascular paclitaxel wraps block arteriovenous graft stenosis in a pig model. *Nephrol Dial Transplant* 2006; 21: 2425-2431

78. McAllister TN, Maruszewski M, Garrido SA *et al*. Effectiveness of haemodialysis access with an autologous tissue-engineered vascular graft: a multicentre cohort study. *Lancet* 2009; 373: 1440-1446

79. Dahl SL, Kypson AP, Lawson JH *et al*. Readily available tissue-engineered vascular grafts. *Sci Transl Med* 2011; 3: 68ra9

80. Peck MK, Dusserre N, Zagalski K *et al*. New biological solutions for hemodialysis access. *J Vasc Access* 2011; 12: 185-192

81. Wu W, Allen RA, Wang Y. Fast-degrading elastomer enables rapid remodeling of a cell-free synthetic graft into a neoartery. *Nat Med* 2012; 18: 1148-1153

Chapter 3

Vascular remodeling and intimal hyperplasia in a novel murine model of arteriovenous fistula failure

C.Y. Wong, M.R. de Vries, Y. Wang, J.R. van der Vorst, A.L. Vahrmeijer , A.J. van Zonneveld, P. Roy-Chaudhury, T.J. Rabelink, P.H.A Quax and J.I. Rotmans

J Vasc Surg. 2014 Jan;59(1):192-201



Abstract

Objective

The arteriovenous fistula (AVF) still suffers from a high number of failures caused by insufficient outward remodeling and intimal hyperplasia (IH) formation from which the exact mechanism is largely unknown. A suitable animal model is of vital importance in the unraveling of the underlying pathophysiology. However, current murine models of AVF failure do not incorporate the surgical configuration that is commonly used in humans. Since the hemodynamic profile is one of the key determinants that play a role in vascular remodeling in the AVF, it is preferable to use this same configuration in an animal model. Here we describe a novel murine model of arteriovenous fistula failure, in which the configuration (end-to-side) is similar to what is most frequently performed in humans.

Methods

An AVF was created in 45 C57BL/6 mice by anastomosing the end of a branch of the external jugular vein to the side of the common carotid artery with interrupted sutures. The fistulas were harvested and analyzed histologically at days 7, 14 and 28. Identical veins of unoperated mice served as controls. Intravenous near-infrared fluorescencent fluorophores were used to assess the patency of the fistula.

Results

The patency rates at days 7, 14 and 28 days were 88%, 90% and 50%, respectively. The mean circumference increased up to day 14 with a maximum 1.4-fold increase at day 7 as compared to the control group (1.82±0.7mm vs 1.33±0.3mm;P= .443). Between days 14 and 28, the circumference remained constant (2.36±0.2mm vs 2.45±0.2mm;P= .996). At 7 days after surgery, the intimal area consisted mainly of an acellular layer that was structurally analogous to a focal adherent thrombus Starting at 14 days after surgery, venous IH increased significantly as compared to the unoperated group (14 days:115090±22594μm^2, 28 days:234619±47828μm^2, unoperated group:2368±1056μm^2;P= .001 and P< .001, respectively) and was mainly composed of α-smooth muscle actin-positive cells. We observed leukocytes in the adventitial side of the vein at all time points.

Conclusion

Our novel murine arteriovenous fistula model, which incorporates a clinically relevant configuration of the anastomosis, displays similar features that are characteristic of failing human fistulas. Moreover, our findings suggest that both coagulation and inflammation could potentially play an important role in the formation of intimal hyperplasia and subsequent arteriovenous fistula failure. Near infrared fluoroscopy proved to be a suitable alternative for conventional imaging techniques. We conclude that this murine AVF-model is a valuable addition to the AVF animal model arsenal.

Clinical relevance

The autologous arteriovenous fistula is considered to be the preferred choice of vascular access in hemodialysis. However, this type of vascular access suffers from a high failure rate of which the exact pathophysiology is poorly understood. The use of a clinically relevant murine model provides us with a tool to unravel the pathophysiology and also to develop new therapeutic strategies that can improve the patency of the arteriovenous fistula in hemodialysis patients.

Introduction

A durable vascular access is of vital importance for patients on chronic hemodialysis. In view of their superior patency rates, the construction of native arteriovenous fistulas (AVF) is currently the preferred choice for vascular access. However, the utility of AVFs is hampered by two distinct causes of failure: (1) an initial failure to mature; and (2) the later development of stenotic lesions in the venous outflow tract. The exact pathophysiology that results in maturation failure is unclear although both intimal hyperplasia (IH) and impaired outward remodelling (OR) seem to contribute [1]. Various studies report poor one-year primary patency rates of AVFs not exceeding 60-65% [2-4].

To date, numerous animal models [5-17] have been designed to study AVF failure. While large animals such as pigs are more suitable for intervention studies, murine models have the greatest potential to gain more insight in the molecular mechanisms underlying this pathologic process due to the availability of transgenic mice.

In previous studies, two groups have described a murine AVF model in which the fistula was constructed in an end-to-end manner [7, 17]. In 2006, an improved model was introduced by Castier et al. [5, 18] where the end of the common carotid artery is connected to the side of the external jugular vein. However, in hemodialysis patients, AVFs are usually constructed by anastomosing the end of a vein to the side of an artery. The exact configuration of the AVF is crucial since it determines the hemodynamic profile [19], an important contributor to endothelial dysfunction and subsequent development of IH [20-22]. Therefore, incorporating an AVF configuration resembling the human situation is preferable. In the present study, we developed a novel murine model with an identical anatomical configuration as utilized in humans. In our analysis, we focused on outward remodeling as well as the formation of IH in the venous outflow tract.

Material and Methods

Animals and study design

The Institutional Committee for Animal Welfare at the LUMC approved all experiments. Forty-five male C57bl6 mice (Charles River) aged 8-13 weeks were used. Unilateral AVFs were created in an end-to-side manner between the dorsomedial branch of the external jugular vein and the common carotid artery. The animals were sacrificed at days 7, 14 and 28 after the surgical procedure. Identical veins of unoperated mice served as controls.

Anesthesia, analgesia and anticoagulant therapy

At the start of the procedure, animals were injected subcutaneously with buprenorphin (0.1 mg/kg) (MSD, Whitehouse Station, NJ, USA) and 0.5 mL saline. Isoflurane inhalation anesthesia with oxygen (40%) enriched air was used, with isoflurane concentrations of 4% for induction and 1.5% for maintenance. To prevent acute AVF thrombosis, acetylsalicylic acid (Sigma, St Louis, MO, USA) dosed at 30 mg/kg was dissolved in drinking water. However, this approach was not successful as it caused severe hemorrhage at the anastomosis. As an alternative, heparin was administered intravenously at a dose of 0.2 IU/gram bodyweight (LEO Pharma, Ballerup, Denmark).

Surgical procedure

After anesthetizing the animal, eyes were covered with an ointment (Oculentum simplex, Pharmachemie BV, Haarlem, The Netherlands) and the surgical area was shaved. Next, the animal was fixed in a supine position on a heating blanket. The skin was disinfected and a ventral midline incision was made in the neck under a dissecting microscope (M80, Leica, Wetzlar, Germany). After dissecting the dorsomedial distal branch of the right external jugular vein, a vascular clamp (S&T, Neuhausen, Switzerland) was placed proximally and a 10.0 ligature (BBraun, Melsungen, Germany) was placed distally followed by transection of the vein just proximal from the ligature. (Fig 1, A-E) The vein was then rinsed with saline containing 100 IU/mL heparin. The right sternocleidomastoid muscle was then dissected and ligated proximally and distally with a 6.0 suture thread (BBraun, Melsungen, Germany). The muscle was then transsected between the two ligations with a heat cauterizer (Fine Science Tools, Heidelberg, Germany). Next, the right common carotid artery was dissected and clamped, followed by an incision of approximately 1.0 mm longitudinally with micro-scissors (Fine Science Tools, Heidelberg, Germany). Subsequently, the carotid artery was rinsed with heparin (100 IU/mL), whereupon the end of the vein was anastomized to the side of the artery using 10.0 interrupted sutures (BBraun, Melsungen, Germany). Heparin (0.2 IU/gram bodyweight) was injected intravenously halfway during suturing. After completion of the anastomosis, the remaining clamps were removed and patency was assessed. The skin was closed with a 6.0 running suture suture (BBraun, Melsungen, Germany). A more detailed description is available in the online supplement.

Following completion of the surgery 0.5 mL of saline was injected subcutaneously and the animals were kept warm until full recovery. A peroperative patent AVF, followed by a complete recovery from the anesthesia, was considered a surgical success.

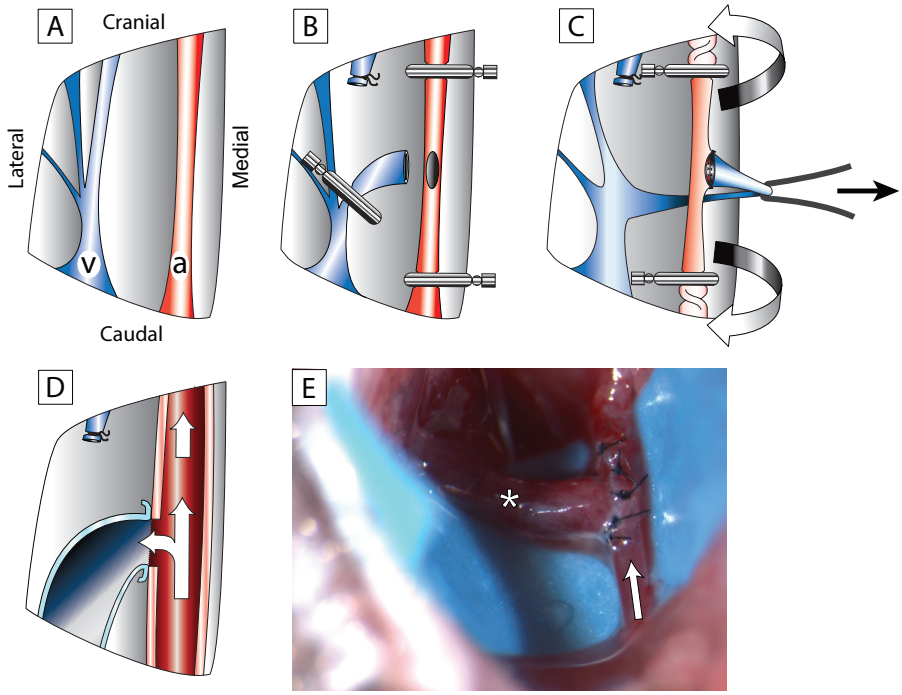


Figure 1. Surgical procedure. A, Dissection of the carotid artery (*a*) and external jugular vein (*v*). B, After placement of vascular clamps and ligation of the vein, an incision was made in the artery, followed by the transection of the vein. C, After the front side of the anastomosis is completed with interrupted sutures, the backside is exposed using a suture wire and by simultaneously twisting the vascular clamps 180°. D, Blood flow direction (*arrows*) in the arteriovenous fistula (AVF). E, Photograph of completed AVF. The *white arrow* depicts blood flow in the artery, and the *asterisk* (*) designates the venous outflow tract.

Near-infrared fluorescence imaging

To assess direct postoperative AVF patency and at the time of sacrifice (day 14 or day 28), near infrared fluorescence (NIRF) imaging was used as previously described [23 24]. Each animal received 200 µL via the femoral vein of a 500 µM indocyanine green solution (ICG) (Pulsion Medical Systems, Munich, Germany) that was dissolved in a 20% human serum albumin (HSA) (Sanquin, Amsterdam,The Netherlands).

Directly after the injection, the Fluorescence Assisted Resection and Exploration (FLARE) imaging system (Center for Molecular Imaging, Boston, MA, USA) was positioned approximately 46 cm above the AVF and video images were captured with 30 frames-per-second. Multiple video channels (color video, 700 nm and 800 nm) were obtained simultaneously with

60 milliseconds (16.7 Hz) exposure times. After computer-controlled image acquisition, color video and NIRF images were displayed individually and/or merged in real-time. The 800 nm channel was used for imaging ICG.

Tissue harvesting and processing

Upon sacrifice, animals received an intraperitoneal injection with an anesthetic-mixture containing midazolam (5 mg/kg) (Roche, Basel, Switzerland), medetomidine (0.5 mg/kg) (Orion, Espoo, Finland) and fentanyl (0.05 mg/kg) (Janssen, High Wycombe, UK) whereupon a reincision was made over the scar. The AVF was dissected and patency was assessed. After a thoracotomy, the inferior vena cava was transected followed by an intracardiac perfusion with subsequently 4% formalin. The tissue was processed to paraffin and sections of 5 μm were made perpendicular to the vein at 12 locations with an interval of 150 μm. The small size of the murine vasculature and the configuration of the AVF preclude simultaneous perpendicular analysis of the carotid artery and the jugular vein. Since most of the stenotic lesions in human AVFs occur in the venous outflow tract, we focused our analysis on the vein.

Morphometric analysis

A histochemical staining with hematoxylin, phloxin and saffron (HPS) was used for a morphological overview. Fibrin deposition was assessed by using a Movat pentachrome staining. Morphometric analysis was performed on Weigert's elastin stained sections. All venous sections were analyzed using quantitative imaging software (Qwin, Leica, Wetzlar, Germany). The intimal area was calculated by subtracting the luminal area from the area within the internal elastic lamina (IEL). The circumference of the vessel was determined by the length of the IEL (Fig 2, *A*). The percentage stenosis was defined as the intimal area divided by the intimal area plus the lumen area (intima/(intima+lumen) X 100). AVFs were defined patent histologically, when the maximum stenosis percentage in all included venous sections was ≤ 95%. Additionally, the venous sections were divided in 4 equal segments of 300 μm (A-D) by grouping 2 consecutive slides starting from the area closest to the anastomosis (Fig 3, *C*). Results are expressed as mean ± standard error of the mean.

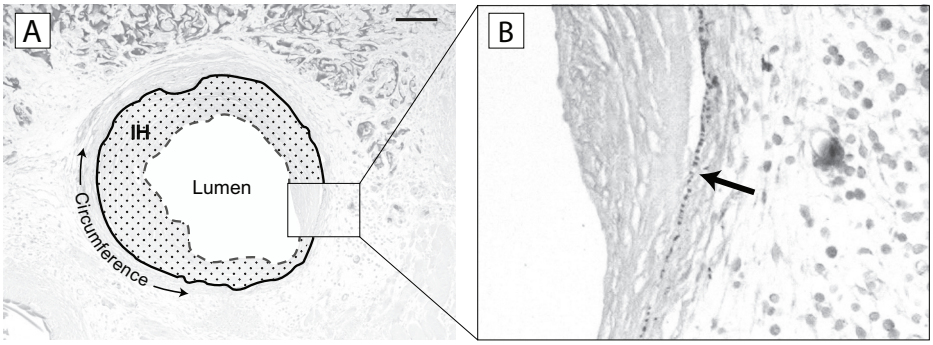


Figure 2. Morphometric parameters and fragmentation of internal elastic lamina (IEL). Venous section in the arteriovenous fistula (AVF) stained with Weigert elastin. (A), The IEL, traced in *black*, is used to quantify the circumference. Intimal hyperplasia (*IH*) and luminal (*lumen*) area are shown. (B), High magnification photomicrograph shows fragmentation of the IEL, which is indicated by the *black arrow* (original magnification, ×100; *scale bar*: 100 μm).

Collagen quantification

Collagen content was determined in sirius red stained sections using quantitative imaging software (Qwin, Leica, Wetzlar, Germany). This was measured in the whole vessel and was expressed as total positive surface area (μm2) and as positive area divided by the total vessel area (%).

Immunohistochemical analysis

Serial sections from each AVF were stained with the following antibodies: anti- α-smooth muscle actin (α-sma) for vascular smooth muscle cells (VSMC) and myofibroblasts, at 1:1000 dilution; (Dako, Glostrup, Denmark); anti-CD31 for endothelial cells, at 1:200 dilution (Abcam, Cambridge, UK); anti-CD45 for leukocytes, at 1:200 dilution (BD Pharmingen, San Diego, California, USA). Slides were digitized at a resolution of 2080 x 1542 by a camera connected to a microscope (Carl Zeiss, Oberkochen, Germany). Detailed protocols of the stainings are listed in the supplement.

Statistical analysis

Results are expressed as mean ± standard error of the mean. Comparison between the time points was performed by one-way ANOVA followed by a Tukey HSD test. Differences were considered statistically significant at a value of $P < .05$.

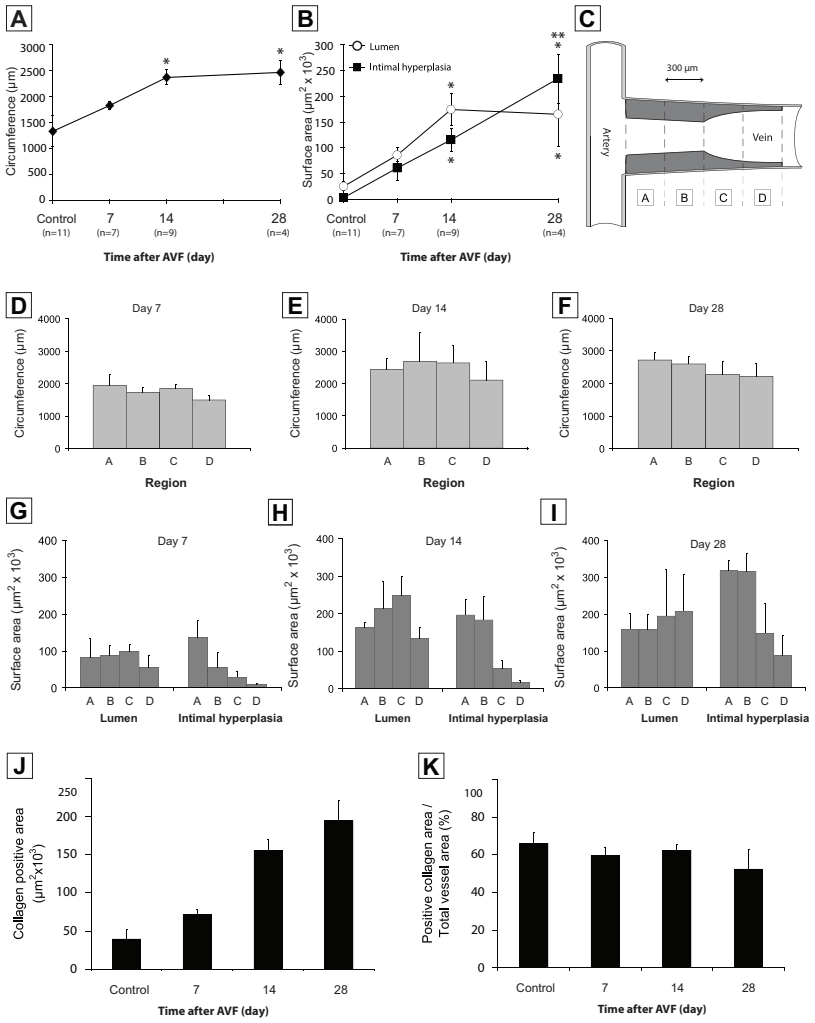


Figure 3. Quantification of outward remodeling (OR) and intimal hyperplasia (IH). (A), OR was present in the first 14 days after arteriovenous fistula (*AVF*) creation. (B), IH increased progressively in time, whereas the luminal area only increased in the first 14 days after AVF placement due to a reduction in OR after this time point. Furthermore, the increase in IH between consecutive time points was significant between days 14 and 28. (C), The venous outflow tract was divided in four equal segments of 300 µm (*A-D*) and shows that the maximum IH (*shaded area*) was located at the site closest to the anastomosis. OR at days (D) 7, (E) 14, and (F) 28 and luminal area at days (G) 7, (H) 14, and (I) 28 were not differently distributed in the vein. At days 14 and 28, IH was the highest in the first 600 µm. (J), The total amount of collagen increased in time. (K), However, the amount of collagen divided by the total vessel area remained the same between the control and arterialized vein. $^{*}P < .05$ compared with control. $^{**}P < .05$ compared with the previous time point. Mean data are presented with the standard error of the mean (*error bars*).

Results

Surgical outcome

In total, 45 mice were operated and in 30 mice the surgical procedure was successful (67%). The main cause of failure was hemorrhage (60%), followed by acute thrombosis (27%) and anesthesia related death (13%). In the group where the surgical intervention was successful, 3 mice died post-operatively of unknown causes and 1 mouse developed a wound abscess. These 4 mice were excluded from the study. The remaining 26 mice were sacrificed at days 7 (8 mice), 14 (10 mice) and 28 (8 mice) after surgery. Eleven animals without AVF surgery served as control. The average time of the surgical procedure was 60 minutes.

Patency

Patency of the AVF was assessed visually using the dissecting microscope at time of sacrifice and was confirmed histologically. This resulted in patency rates of 88%, 90% and 50% at days 7, 14 and 28, respectively. In addition, the patency was assessed in 10 mice by NIRF. As shown in Fig 4, *A-C*, representative NIRF images are depicted of a patent AVF directly after creation and at 28 days.

The patency assessed by NIRF matched the visual assessment in 10 out of 11 cases (91%). In the remaining mouse, the AVF appeared patent by NIRF while no perfusion could be observed macroscopically. A representative movie of the patency assessment using NIRF is available as online supplement.

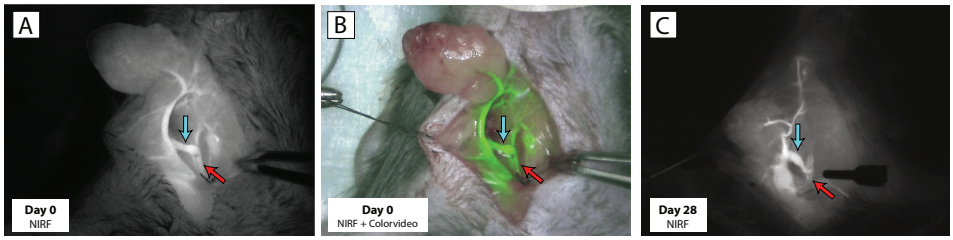


Figure 4. Visualization of the arteriovenous fistula (AVF) with near-infrared fluorescence imaging. The proximal carotid artery and venous outflow tract are depicted by a *red* and *blue arrow*, respectively. (A), Intravenous administration of indocyanine green (*white*) that is detected at 800 nm using a fluorescence-assisted resection and exploration (FLARE) imaging system indicates AVF patency directly after completion of the surgical intervention. (B), Merged image of color video and 800-nm near-infrared fluorescence channel. (C), At 28 days after surgery, the luminal area is reduced in the perianastomotic area due to intimal hyperplasia (IH).

Morphometric analysis

For the quantification of OR and IH, only patent AVFs were included in the analysis (7, 8 and 4 mice for 7, 14 and 28 days of follow-up, respectively).

Outward remodeling

The venous circumference at days 14 (2.36 ± 0.15 mm) and 28 (2.45 ± 0.24 mm) was higher compared to that of the unoperated control mice (1.33 ± 0.30 mm; P = .01 and P= .037, respectively). The highest increase in mean venous circumference (1.4-fold) was observed within 7 days after surgery (1.33 ± 0.30 mm vs 1.82 ± 0.07 mm; P = .443). Between days 7 and 14, a 1.3-fold increase was observed (P = .397), whereas no increase in venous circumference was observed from days 14 to 28 (P = .996). (Fig 3, *A*).

No difference in OR was observed between various sections of the AVF (Fig 3, *D-F*). Of note, the venous circumference of the occluded AVFs (1.69 ± 0.2 mm) at day 28 was smaller when compared to patent AVF (2.45 ± 0.2 mm) at the same time point. In all AVFs, we observed fragmentation of the IEL in the venous outflow tract (Fig 2, *B*).

Intimal hyperplasia and luminal area

Already 7 days after surgery, we observed intimal hyperplasia (60138 ± 23626 μm^2) in the venous outflow tract (Fig 5, *B-D*). This area further increased at days 14 and 28 (115090 ± 22594 μm^2 and 234619 ± 47828 μm^2, respectively) and was significantly higher as compared to control mice (2368 ± 1056 μm^2 ; P = .001 and P <.001). (Fig 3, *B*). Detailed analysis of the various sections within the venous outflow tract revealed that IH was most prominent in the first 600 μm from the anastomosis (Fig 3, *G-I*). The combined effect of the OR process and IH resulted in a markedly higher luminal area both at day 14 and 28 (173965 ± 30829 μm^2 and 164842 ± 63411 μm^2) when compared to the control (24679 ± 8462 μm^2 ; P< .001 and P= .010, respectively). Between the consecutive time points, we observed a 3.5-fold increase in the luminal area at day 7 (85693 ± 13541 μm^2) as compared to the control veins (P= .294). Between days 7 and 14, a 2-fold increase in lumen area was observed (P= .082). At day 28 the luminal area of the patent AVFs decreased with 5% compared to day 14 (P= .996) (Fig 3, *B*).

The mean stenosis at days 7, 14 and 28 were 30%, 38% and 59%, respectively. Seven days after surgery, the highest percentage of stenosis was observed in the first 300 μm from the anastomosis (segment A). At days 14 and 28 after surgery, the percentage stenosis was the highest in segment A and B (data not shown). In the occluded AVFs at day 28, IH was 23% lower compared to patent vessels at the same time point (180866 ± 49332 μm2 vs 234619 ± 47828 μm^2).

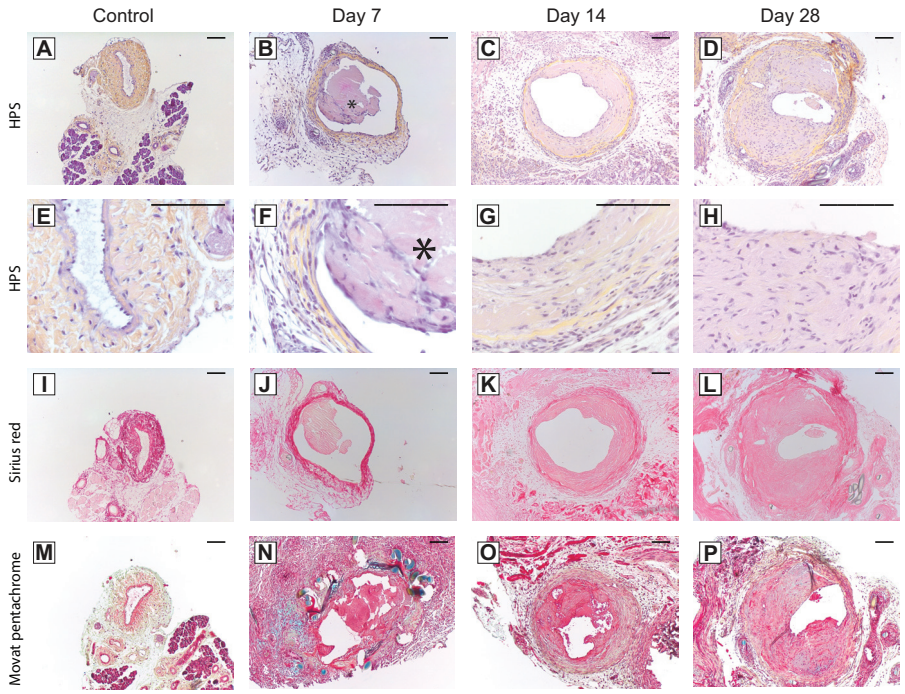


Figure 5. Outward remodeling (OR), intimal hyperplasia (IH), and collagen distribution are shown in time. Venous sections stained with hematoxylin, phloxine, and saffron (HPS) at days 7, 14 and 28 after creation of arteriovenous fistula (AVF). A control vein (A) before arterialization shows no IH and has a modest circumference compared with the veins (B-D) after AVF placement. OR was primarily observed at (B) day 7 and (C) day 14 and was less evident at (D) day 28. E-H, Higher magnification photomicrographs of panels (A-D) shows the development of neo-IH, which starts with a (F) thrombus that has been repopularized with cells as time progresses. I-L, Sirius red staining shows the collagen content in time. M-P, Movat pentachrome staining shows fibrin-rich areas (*bright red*) in the intimal lesion at the different time points. (A-D, I-P: original magnification, ×100; E-H: original magnification, ×400). Partially repopularized thrombus indicated by *asterisk* (*), and *black arrow* indicates fibrin-rich area. *Scale bar*: 100 μm.

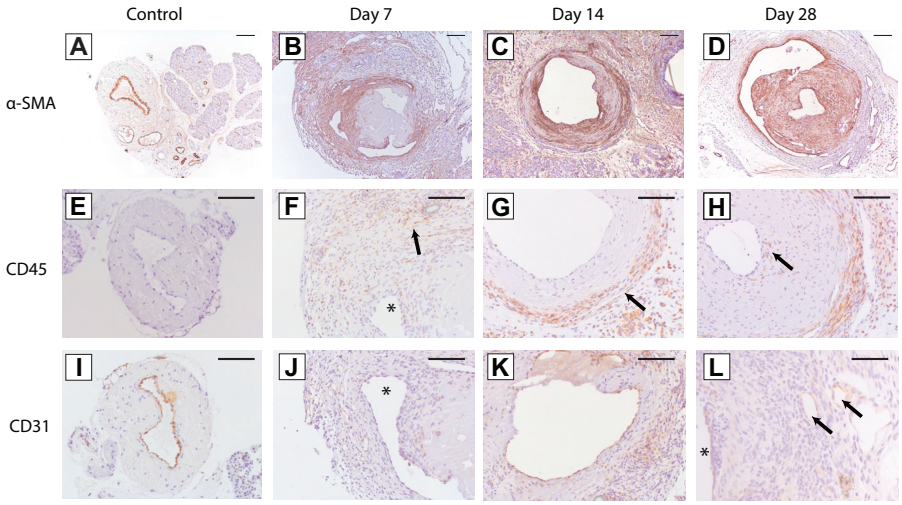


Figure 6. Immunohistochemical stainings. (A), Immunohistochemical assessment of cells positive for α-smooth muscle actin (*SMA*) revealed a small band in the control vein, compared with a (B-D) time-dependant increase of α-SMA-positive cells in the intimal hyperplasia (IH) after arteriovenous fistula (AVF) surgery. (E), The presence of leukocytes, which was absent in the control vein, was located in the (F-H) media and adventitia of the AVF vein at all time points. (H), However, leukocytes were also found in the intima at day 14 and 28 as depicted by the *black arrow*. (J) and (K), The luminal lining with cluster of differentiation (*CD*)31-positive endothelial cells, was disrupted at all time points but showed re-endothelialization in a time dependant manner. (L), Adventitial capillaries were present at all time points (*black arrow*). (I), The control vein showed an intact lining of endothelial cells. (A-D: original magnification, ×100; E-L: original magnification, ×200). The *asterisk* (*) indicates the lumen. *Scale bar*: 100 μm.

Composition of intimal hyperplasia

Histological analysis revealed a dynamic composition of the intimal lesions. Starting from day 7 the intimal lesion consisted mainly of an acellular fibrin-rich layer, consistent with a focal adherent thrombus (Fig 5, *B,F,N-P*). Concomitant with increased lesion size at later time points (day 14 and 28), progressive cellular density was observed (Fig 5, *F-H*). The majority of cells within the intima were α-sma-positive (Fig 6, *B-D*). Analysis of CD45-stained sections demonstrated the presence of leukocytes, mainly in the adventitia and outer circumference of the vessel wall at all time points and in the intima starting at day 14 (Fig 6, *F-H*). The endothelial layer was disrupted at all time points, although CD31(+) cells did increase in time. Furthermore, starting from day 7, an increased density of adventitial capillaries was observed (Fig 6, *J-L*).

Quantification of collagen content in the venous outflow tract revealed a time-dependent increase in absolute collagen content (Fig 3, *J-K* and Fig 5, *J-L*). However, no differences in collagen-positive area were observed between the control group and all time points were expressed as a percentage of the total vessel area. Thus, the relative contribution of collagen in the total vessel composition remained stable.

Discussion

In the present study, we describe a novel murine model of AVF failure in which the AVF configuration resembles the human situation (venous end to arterial side). We observed that the venous outflow tract of AVFs is characterized by OR in the first 14 days. Furthermore, we hypothesize that focal adherent thrombi appear to serve as fertile soil for the formation of progressive α-sma positive intimal lesions ultimately leading to a 50% loss of patency at 28 days after surgery.

Anticoagulant therapy was necessary for creating a patent AVF and finding the correct balance between acute thrombosis and hemorrhage proved to be of crucial importance. Importantly, we observed a very high incidence 69% of bleeding complications when using acetylsalicylic acid. Therefore, as an alternative, we administered a single dose of heparin which was effective in preventing acute thrombosis. Using our protocol with heparin, we observed early thrombosis and bleeding complications in 3% and 7% of the mice, respectively.

Outward remodeling

Although IH is widely considered to be the most important determinant of AVF failure, the functionality of the AVF is generally determined by the luminal area, which is defined by the net result of OR and IH formation. To the best of our knowledge, we are the first to quantify OR by measuring the circumference of the venous outflow tract in murine AVF. Studies in rats and mice have revealed that OR is induced by the increase in flow that evokes an adaptive response of the vessel in which the luminal diameter increases in attempt to reduce wall shear stress to pre-AVF levels [8, 25, 26]. In our study, we observed a 1.4-fold increase in venous circumference within 7 days after AVF placement. Unfortunately, data on wall shear stress could not be collected in this study. The decrease in OR at later time points could be the result of the partial normalization of shear stress levels as previously observed in murine [26] and human [27] AVF studies. Furthermore, we observed fragmentation of the IEL of the venous outflow tract, a phenomenon that has been described in previous studies [28-30]. This effect is likely driven by flow-induced matrix metalloproteinase (MMP)-2 and MMP-9 activation, a process that is

essential in facilitating outward remodeling [28, 29]. In keeping with this notion, serum levels of MMP-2 have been shown to be significantly higher in patients with matured AVFs as compared to non-matured AVFs [31].

We observed a smaller venous circumference in the occluded AVFs at 4 weeks after surgery. The latter might suggests that the cause of AVF failure in these cases could potentially be the result of impaired OR. However, these data should be interpreted with caution since we cannot exclude the possibility that the circumference decreased upon occlusion of the vessel.

Intimal hyperplasia formation

In failing human AVFs, IH is designated as one of the main contributors in the pathophysiology and is typically located in the juxta-anastomotic area of the venous outflow tract [32, 33]. In our study, progressive IH developed in this same region of the AVF, illustrating the resemblance to failing human fistulas.

Interestingly, we observed a remarkable pattern in the development of IH not previously described in AVF studies. In our murine AVFs, IH appears to commence with the focal adherence of thrombi. In the following weeks, these lesions showed progressive cellularity, culminating in a high cellular density at 28 days after surgery. At this time, intimal lesions possessed the hallmarks of classic IH of failed human AVFs, as evidenced by the presence of high numbers of α-sma(+) cells [32, 34].

Thus far, IH is considered primarily to be the direct result of migrating and proliferating VSMCs, and that thrombus formation in the early phase after surgery would be considered a separate entity [5, 11, 13, 35]. Although the venous morphology in the early phase after AVF surgery has not been described in great detail in humans, the sequence of events in the development of IH in our study does resemble the pathophysiology of intimal lesions after (arterial) angioplasty and in vein grafts [36, 37]. Furthermore, Castier et al. also showed partly acellular lesions in the venous outflow tract of murine AVF [5]. The adherence of small (platelet and fibrin-rich) thrombi to the vessel wall most likely results from endothelial denudation and the subsequent exposure of the subendothelial matrix leading to platelet adhesion and activation [36, 38, 39]. Indeed, we observed marked endothelial denudation in the venous outflow tract in the first 7 days after surgery, a phenomenon that also was observed in previous animal studies of AVF failure [8, 11].

This observation might suggests that anticoagulatory interventions could be an eligible strategy to inhibit intimal hyperplasia. Previous studies in a murine vascular endothelial injury model indeed revealed reduced IH upon treatment with human soluble CD39, an inhibitor of ADP-mediated platelet activation [40]. In contrast, a randomized clinical controlled trial by Dember et al. showed no significant effect on AVF maturation, despite a reduction in incidence of early thrombosis in patients treated with clopidogrel [41]. In our opinion, the limited effect of

systemic antiplatelet therapy on AVF maturation in humans does not necessarily preclude a contributing role of platelets in local development of IH in AVF.

Role of inflammation in vascular adaptation in arteriovenous fistulas

The inflammatory response is a crucial process involved in vascular injury and is linked to development of IH [37, 39, 42]. Upon injury, leukocytes are recruited via activated platelets lining the denudated endothelium and release chemokines such as MCP-1 [43], IL-6 and IL-8, which further stimulates leukocyte recruitment [42]. Similar to the pathophysiology in occlusive vein graft disease and arterial restenosis, we observed a marked influx of leukocytes at the adventitial side of the vein throughout all time points. In contrast, hardly any CD45(+) cells were present in the intima in the first 14 days. This might suggests that leukocyte infiltration in the early phase predominantly occurs via adventitial capillaries rather than the lumen [44, 45] such as demonstrated by Gotoh et al. [45]. However, the role of inflammation in outward remodeling in the AVF has gained little attention. Future experiments using anti-inflammatory therapeutic agents could aid in the elucidation of the contribution of inflammation in AVF remodeling.

Animal models

In concordance with other rodent AVF models [5, 7, 8, 11-13], we observed rapid development of IH. Furthermore, as previously described in AVF studies in rats 8, marked venous OR was observed in the first 14 days following surgery. As a result of this venous OR, we observed an increase in luminal area in the first 14 days, whereas Castier et al. described a decrease in luminal area from the first week after AVF creation[5]. In Castier's study however, the arterial rather than the venous segment of the AVF was analyzed. Together with the difference in AVF configuration, this might explain the observed difference in luminal area since previous studies in rats have revealed that arterial OR is less prominent than venous OR. [8] However, this explanation remains speculative since no data on OR were reported by Castier et al.

Near infrared fluorescence imaging

We were unable to visualize the AVF with conventional techniques such as ultrasonography (US) and magnetic resonance imaging (MRI). Therefore, we utilized NIRF technology, which proved to be a quick and accurate method to assess the patency of murine AVFs.

Study limitation

Although animal models are useful in gaining insight into the pathophysiology of various human diseases, we should remain cautious in the interpretation and extrapolation, as the pathology in animals does not necessarily mimic to that of humans.

A multitude of risk factors, including the uremic milieu and the hemodialysis procedure itself are likely to contribute to premature vascular diseases [46, 47]. Uremia can play a major role in this regard, and more specifically can directly lead to venous IH in end stage renal disease patients prior to hemodialysis access surgery [48]. For future studies, incorporation of chronic renal failure in mice as described by Kokubo et al. [35] will be considered.

The complex microsurgical procedure remains a challengeable one that requires a skilled surgeon. However, the surgical difficulty is comparable to the existing murine AVF model as described by Castier [5]. Importantly, sufficient training has led to a surgical success rate during ongoing experimental studies of 97%.

In conclusion, we describe a novel murine AVF model with a similar configuration as is used most frequently in humans. This end-to-side configuration, while providing a more accurate reflection of human AVF pathophysiology, can also yield novel insight into this process by being effectively applied in a myriad of transgenic animals. In view of the different proposed mechanisms that are involved in venous remodeling in the AVF, disabling genes that play an important role in coagulation, inflammation and VSMC biology can help us to elucidate the complex pathophysiology of AVF failure. The obtained knowledge from these studies will hopefully result in the development of new therapeutic strategies that improve the patency of AVFs in patients that require hemodialysis.

Acknowledgments

This study was supported by a grant from the Dutch Kidney Foundation (KJPB 08.0003).

We thank Carolien Rothuizen for her contribution to the study; Hoang Pham for his assistance with the pathology work-up; and Eric van der Veer for his valuable review of the manuscript.

Reference List

1. Asif A, Roy-Chaudhury P, Beathard GA. Early arteriovenous fistula failure: a logical proposal for when and how to intervene. *Clin J Am Soc Nephrol* 2006;1:332-9.

2. Falk A. Maintenance and salvage of arteriovenous fistulas. *J Vasc Interv Radiol* 2006;17:807-13.

3. Tordoir JH, Rooyens P, Dammers R, van der Sande FM, de HM, Yo TI. Prospective evaluation of failure modes in autogenous radiocephalic wrist access for haemodialysis. *Nephrol Dial Transplant* 2003;18:378-83.

4. Dixon BS, Novak L, Fangman J. Hemodialysis vascular access survival: upper-arm native arteriovenous fistula. *Am J Kidney Dis* 2002;39:92-101.

5. Castier Y, Lehoux S, Hu Y, Foteinos G, Tedgui A, Xu Q. Characterization of neointima lesions associated with arteriovenous fistulas in a mouse model. *Kidney Int* 2006;70:315-20.

6. Johnson MS, McLennan G, Lalka SG, Whitfield RM, Dreesen RG. The porcine hemodialysis access model. *J Vasc Interv Radiol* 2001;12:969-77.

7. Kwei S, Stavrakis G, Takahas M, Taylor G, Folkman MJ, Gimbrone MA, Jr., et al. Early adaptive responses of the vascular wall during venous arterialization in mice. *Am J Pathol* 2004;164:81-9.

8. Langer S, Heiss C, Paulus N, Bektas N, Mommertz G, Rowinska Z, et al. Functional and structural response of arterialized femoral veins in a rodent AV fistula model. *Nephrol Dial Transplant* 2009;24:2201-6.

9. Lemson MS, Daemen MJ, Kitslaar PJ, Tordoir JH. A new animal model to study intimal hyperplasia in arteriovenous fistulas. *J Surg Res* 1999;85:51-8.

10. Lin T, Horsfield C, Robson MG. Arteriovenous fistula in the rat tail: a new model of hemodialysis access dysfunction. *Kidney Int* 2008;74:528-31.

11. Manning E, Skartsis N, Orta AM, Velazquez OC, Liu ZJ, Asif A, et al. A new arteriovenous fistula model to study the development of neointimal hyperplasia. *J Vasc Res* 2012;49:123-31.

12. Misra S, Fu AA, Anderson JL, Sethi S, Glockner JF, McKusick MA, et al. The rat femoral arteriovenous fistula model: increased expression of matrix metalloproteinase-2 and -9 at the venous stenosis. *J Vasc Interv Radiol* 2008;19:587-94.

13. Nath KA, Kanakiriya SK, Grande JP, Croatt AJ, Katusic ZS. Increased venous proinflammatory gene expression and intimal hyperplasia in an aorto-caval fistula model in the rat. *Am J Pathol* 2003;162:2079-90.

14. Ramacciotti E, Galego SJ, Gomes M, Goldenberg S, De Oliveira GP, Pinto OJ. Fistula size and hemodynamics: an experimental model in canine femoral arteriovenous fistulas. *J Vasc Access* 2007;8:33-43.

15. Tronc F, Wassef M, Esposito B, Henrion D, Glagov S, Tedgui A. Role of NO in flow-induced remodeling of the rabbit common carotid artery. *Arterioscler Thromb Vasc Biol* 1996;16:1256-62.

16. Wang Y, Krishnamoorthy M, Banerjee R, Zhang J, Rudich S, Holland C, et al. Venous stenosis in a pig arteriovenous fistula model--anatomy, mechanisms and cellular phenotypes. *Nephrol Dial Transplant* 2008;23:525-33.

17. Yang B, Shergill U, Fu AA, Knudsen B, Misra S. The mouse arteriovenous fistula model. *J Vasc Interv Radiol* 2009;20:946-50.

18. Kang L, Yamada S, Hernandez MC, Croatt AJ, Grande JP, Juncos JP, et al. Regional and systemic hemodynamic responses following the creation of a murine arteriovenous fistula. *Am J Physiol Renal Physiol* 2011;301:F845-F851.

19. Krishnamoorthy MK, Banerjee RK, Wang Y, Zhang J, Roy AS, Khoury SF, et al. Hemodynamic wall shear stress profiles influence the magnitude and pattern of stenosis in a pig AV fistula. *Kidney Int* 2008;74:1410-9.

20. Sivanesan S, How TV, Bakran A. Sites of stenosis in AV fistulae for haemodialysis access. *Nephrol Dial Transplant* 1999;14:118-20.

21. Ene-Iordache B, Cattaneo L, Dubini G, Remuzzi A. Effect of anastomosis angle on the localization of disturbed flow in 'side-to-end' fistulae for haemodialysis access. *Nephrol Dial Transplant* 2012.

22. Ene-Iordache B, Remuzzi A. Disturbed flow in radial-cephalic arteriovenous fistulae for haemodialysis: low and oscillating shear stress locates the sites of stenosis. *Nephrol Dial Transplant* 2012;27:358-68.

23. Gioux S, Kianzad V, Ciocan R, Gupta S, Oketokoun R, Frangioni JV. High-power, computer-controlled, light-emitting diode-based light sources for fluorescence imaging and image-guided surgery. *Mol Imaging* 2009;8:156-65.

24. Troyan SL, Kianzad V, Gibbs-Strauss SL, Gioux S, Matsui A, Oketokoun R, et al. The FLARE intraoperative near-infrared fluorescence imaging system: a first-in-human clinical trial in breast cancer sentinel lymph node mapping. *Ann Surg Oncol* 2009;16:2943-52.

25. Guzman RJ, Abe K, Zarins CK. Flow-induced arterial enlargement is inhibited by suppression of nitric oxide synthase activity in vivo. *Surgery* 1997;122:273-9.

26. Castier Y, Brandes RP, Leseche G, Tedgui A, Lehoux S. p47phox-dependent NADPH oxidase regulates flow-induced vascular remodeling. *Circ Res* 2005;97:533-40.

27. Corpataux JM, Haesler E, Silacci P, Ris HB, Hayoz D. Low-pressure environment and remodelling of the forearm vein in Brescia-Cimino haemodialysis access. *Nephrol Dial Transplant* 2002;17:1057-62.

28. Tronc F, Mallat Z, Lehoux S, Wassef M, Esposito B, Tedgui A. Role of matrix metalloproteinases in blood flow-induced arterial enlargement: interaction with NO. *Arterioscler Thromb Vasc Biol* 2000;20:E120-E126.

29. Martin BJ, Stehbens WE, Davis PF, Ryan PA. Scanning electron microscopic study of hemodynamically induced tears in the internal elastic lamina of rabbit arteries. *Pathology* 1989;21:207-12.

30. Rotmans JI, Velema E, Verhagen HJ, Blankensteijn JD, de Kleijn DP, Stroes ES, et al. Matrix metalloproteinase inhibition reduces intimal hyperplasia in a porcine arteriovenous-graft model. *J Vasc Surg* 2004;39:432-9.

31. Lee ES, Shen Q, Pitts RL, Guo M, Wu MH, Sun SC, et al. Serum metalloproteinases MMP-2, MMP-9, and metalloproteinase tissue inhibitors in patients are associated with arteriovenous fistula maturation. *J Vasc Surg* 2011;54:454-9.

32. Roy-Chaudhury P, Arend L, Zhang J, Krishnamoorthy M, Wang Y, Banerjee R, et al. Neointimal hyperplasia in early arteriovenous fistula failure. *Am J Kidney Dis* 2007;50:782-90.

33. Beathard GA, Arnold P, Jackson J, Litchfield T. Aggressive treatment of early fistula failure. *Kidney Int* 2003;64:1487-94.

34. Roy-Chaudhury P, Wang Y, Krishnamoorthy M, Zhang J, Banerjee R, Munda R, et al. Cellular phenotypes in human stenotic lesions from haemodialysis vascular access. *Nephrol Dial Transplant* 2009;24:2786-91.

35. Kokubo T, Ishikawa N, Uchida H, Chasnoff SE, Xie X, Mathew S, et al. CKD accelerates development of neointimal hyperplasia in arteriovenous fistulas. *J Am Soc Nephrol* 2009;20:1236-45.

36. Mitra AK, Gangahar DM, Agrawal DK. Cellular, molecular and immunological mechanisms in the pathophysiology of vein graft intimal hyperplasia. *Immunol Cell Biol* 2006;84:115-24.

37. Muto A, Model L, Ziegler K, Eghbalieh SD, Dardik A. Mechanisms of vein graft adaptation to the arterial circulation: insights into the neointimal algorithm and management strategies. *Circ J* 2010;74:1501-12.

38. Wilentz JR, Sanborn TA, Haudenschild CC, Valeri CR, Ryan TJ, Faxon DP. Platelet accumulation in experimental angioplasty: time course and relation to vascular injury. *Circulation* 1987;75:636-42.

39. Patel SD, Waltham M, Wadoodi A, Burnand KG, Smith A. The role of endothelial cells and their progenitors in intimal hyperplasia. *Ther Adv Cardiovasc Dis* 2010;4:129-41.

40. Drosopoulos JH, Kraemer R, Shen H, Upmacis RK, Marcus AJ, Musi E. Human solCD39 inhibits injury-induced development of neointimal hyperplasia. *Thromb Haemost* 2010;103:426-34.

41. Dember LM, Beck GJ, Allon M, Delmez JA, Dixon BS, Greenberg A, et al. Effect of clopidogrel on early failure of arteriovenous fistulas for hemodialysis: a randomized controlled trial. *JAMA* 2008;299:2164-71.

42. Welt FG, Rogers C. Inflammation and restenosis in the stent era. *Arterioscler Thromb Vasc Biol* 2002;22:1769-76.

43. Juncos JP, Grande JP, Kang L, Ackerman AW, Croatt AJ, Katusic ZS, et al. MCP-1 contributes to arteriovenous fistula failure. *J Am Soc Nephrol* 2011;22:43-8.

44. Maiellaro K, Taylor WR. The role of the adventitia in vascular inflammation. *Cardiovasc Res* 2007;75:640-8.

45. Gotoh R, Suzuki J, Kosuge H, Kakuta T, Sakamoto S, Yoshida M, et al. E-selectin blockade decreases adventitial inflammation and attenuates intimal hyperplasia in rat carotid arteries after balloon injury. *Arterioscler Thromb Vasc Biol* 2004;24:2063-8.

46. Kennedy R, Case C, Fathi R, Johnson D, Isbel N, Marwick TH. Does renal failure cause an atherosclerotic milieu in patients with end-stage renal disease? *Am J Med* 2001;110:198-204.

47. Cheung AK, Sarnak MJ, Yan G, Dwyer JT, Heyka RJ, Rocco MV, et al. Atherosclerotic cardiovascular disease risks in chronic hemodialysis patients. *Kidney Int* 2000;58:353-62.

48. Lee T, Chauhan V, Krishnamoorthy M, Wang Y, Arend L, Mistry MJ, et al. Severe venous neointimal hyperplasia prior to dialysis access surgery. *Nephrol Dial Transplant* 2011;26:2264-70.

Supplemental Data

Surgical procedure

After anesthetizing the mice, we covered the eyes with a sterile ointment and shaved the surgical area. Next, the animal was fixed in a supine position on a heating blanket. The skin was then disinfected with ethanol and a ventral midline incision was made in the neck under a dissecting microscope (M80, Leica, Wetzlar, Germany). After dissecting the dorsomedial distal branch of the right external jugular vein, a vascular clamp (B1-V, S&T, Neuhausen, Switzerland) was placed proximally and a 10.0 ligature (BBraun, Melsungen, Germany) was placed distally followed by transection of the vein just proximal from the ligature. (Fig 1, A-E) The vein was then rinsed with saline containing 100 IU/ml heparin.

The right sternocleidomastoid muscle was then resected with a cauterizer (Fine Science Tools, Heidelberg, Germany). Next, the right common carotid artery was dissected and clamped, followed by an incision with a micro-scissor (Fine Science Tools, Heidelberg, Germany) of approximately 1.0 mm longitudinally. Subsequently, the carotid artery was rinsed with saline containing 100 IU/ml heparin, whereupon the end of the vein was anastomized to the side of the artery using 10.0 interrupted sutures. The first two interrupted sutures were inserted at the twelve- and six o'clock position of the vein and at the ends of the incision in the artery, providing mild tissue tension and a good starting position by dividing the suture area of the vein in two even portions. Tension was then also applied longitudinally using a 6.0 suture thread (BBraun, Melsungen, Germany) that was placed below the vein, and was followed by placing interrupted 10.0 sutures at the exposed half of the anastomosis. Next, heparin was injected intravenously in the femoral vein at a dose of 0.2 IU/gram bodyweight. The rear unexposed part of the anastomosis was then exposed by a 180 degrees axial rotation of the arterial clamps and the partly anastomosed vein with the help of a suture thread that now is placed above the vein and below the artery. The venous clamp was removed during the rotational procedure. After completion of the anastomosis, the remaining arterial clamps were removed starting with the distal clamp. After confirming the patency of the AVF, the skin was closed with a 6.0 running suture (BBraun, Melsungen, Germany).

Immunohistochemistry

For immunohistochemical stainings, deparaffinization and hydration was followed by a treatment with 1% hydrogen peroxide and 5% bovine serum albumine in order to block the endogenous peroxidase and aspecific binding sites respectively. Antigen retrieval in the anti-CD31 and CD45 staining consisted of a treatment with 0.1% trypsin (Sigma-Aldrich, St. Louis, MO, USA) for 30 minutes at 37 degrees Celsius.

Incubation of the primary antibodies was performed overnight at room temperature. Subsequently, sections were incubated at room temperature for 1 hour with HRP labeled antibodies against: mouse IgG (Dako, Glostrup, Denmark) in the α-smooth muscle actin staining at 1:1000 dilution and rabbit IgG (Envision, Dako, Glostrup, Denmark) in the staining against CD31 Biotinylated anti rat antibody (Vector laboratories, Burlingame, CA, USA) was used in the stainings against CD45, followed by a treatment with a 0.2 % streptavidin-AB complex (Dako, Glostrup, Denmark) for 30 minutes at room temperature. Immunoreactive tissue was then developed by using a DAB peroxidase substrate kit (Dako, Glostrup, Denmark). Sections were counterstained with hematoxylin.

Near infrared fluoroscopy

Video 1

Visualization of a patent arteriovenous fistula directly after creation using near infrared fluorescence imaging. Two hundred μL of indocyanine green adsorbed to human serum albumin (500μM) was injected intravenously in the femoral vein. The fluorescent signal signal of indocyanine green was pseudo-colored green and merged with the color video.

Video 2

Visualization of a patent arteriovenous fistula 28 days after creation using near infrared fluorescence imaging. Two hundred μL of indocyanine green adsorbed to human serum albumin (500μM) was injected intravenously in the femoral vein seconds after the start of the recording. The fluorescent signal signal of indocyanine green was pseudo-colored green and merged with the color video. The video shows direct antegrade filling of the venous outflow tract demonstrating a patent arteriovenous fistula.

Chapter 4

A novel murine model of arteriovenous fistula failure: The surgical procedure in detail

Wong, C.Y., de Vries, M.R., Wang, Y., van der Vorst, J.R., Vahrmeijer, A.L., van Zonneveld, A.J, Hamming, J.F., Roy-Chaudhury, P., Rabelink, T.J. , Quax, P.H.A. and Rotmans, J.I.

J Vis Exp. 2016 Feb 3;(108)



Abstract

The arteriovenous fistula (AVF) still suffers from a high number of failures caused by insufficient remodeling and intimal hyperplasia from which the exact pathophysiology remains unknown. In order to unravel the pathophysiology a murine model of AVF-failure was developed in which the configuration of the anastomosis resembles the preferred situation in the clinical setting. A model was described in which an AVF is created by connecting the venous end of the branch of the external jugular vein to the side of the common carotid artery using interrupted sutures. At a histological level, we observed progressive stenotic intimal lesions in the venous outflow tract that is also seen in failed human AVFs. Although this procedure can be technically challenging due to the small dimensions of the animal, we were able to achieve a surgical success rate of 97% after sufficient training. The key advantage of a murine model is the availability of transgenic animals. In view of the different proposed mechanisms that are responsible for AVF failure, disabling genes that might play a role in vascular remodeling can help us to unravel the complex pathophysiology of AVF failure.

Introduction

A functional vascular access conduit is of vital importance for patients with renal failure that depend on chronic hemodialysis to stay alive. The construction of an arteriovenous fistula (AVF) is currently the preferred choice for vascular access. However, AVF related complications constitute a major cause of morbidity for patients on chronic hemodialysis. Despite extensive scientific efforts, none of the novel approaches to reduce AVF access-related complications did result in substantial improvement of AVF durability. Part of this disappointing progress relates to incomplete understanding of the underlying pathophysiology of hemodialysis access failure. To unravel the pathophysiology of AV access failure, animal models that closely mimic human pathology are of utmost importance. In this respect, not only the animal species but also the anastomotic site, the required anti-coagulatory therapy and the duration of follow up after surgery should be taken into account[1]. While large animals are the most suitable for intervention studies aimed to develop new therapeutic strategies, murine models have the greatest potential to gain more insight in the molecular mechanisms underlying AV access failure due to the availability of transgenic mice. In addition, a large number of mice can be used for this purpose at lower costs compared to larger animal use.

The first murine model of AVF failure was described in 2004 by Kwei and coworkers[2]. In this model, AVFs were constructed using the carotid artery and the jugular vein in an end-to-end manner using an intravascular catheter. This model could be useful to study early venous adaptation in AVFs although the end-to-end configuration and the presence of an intravascular catheter limit the validity of this model for human AVFs. An improved AVF model was introduced by Castier and coworkers3 in which the end of the carotid artery is connected to the side of the jugular vein. However, AVFs in hemodialysis patients are usually constructed by anatomizing the end of a vein to the side of an artery. The exact configuration of the AVF is a crucial characteristic of an AV access model since it determines the hemodynamic profile within the conduit4. The latter is an important contributor to endothelial dysfunction and subsequent development of intimal hyperplasia (IH) [5].

A novel murine model was recently developed with an identical anatomical configuration as is utilized in humans[6]. In this model, AVF are created in C57BL/6 mice by anastomosing the end of a branch of the external jugular vein to the side of the common carotid artery with interrupted sutures. In the present paper, we focus on the microsurgical procedure of this model in order to facilitate the widespread use of this murine model, aimed to unravel the complex pathophysiology of hemodialysis access failure.

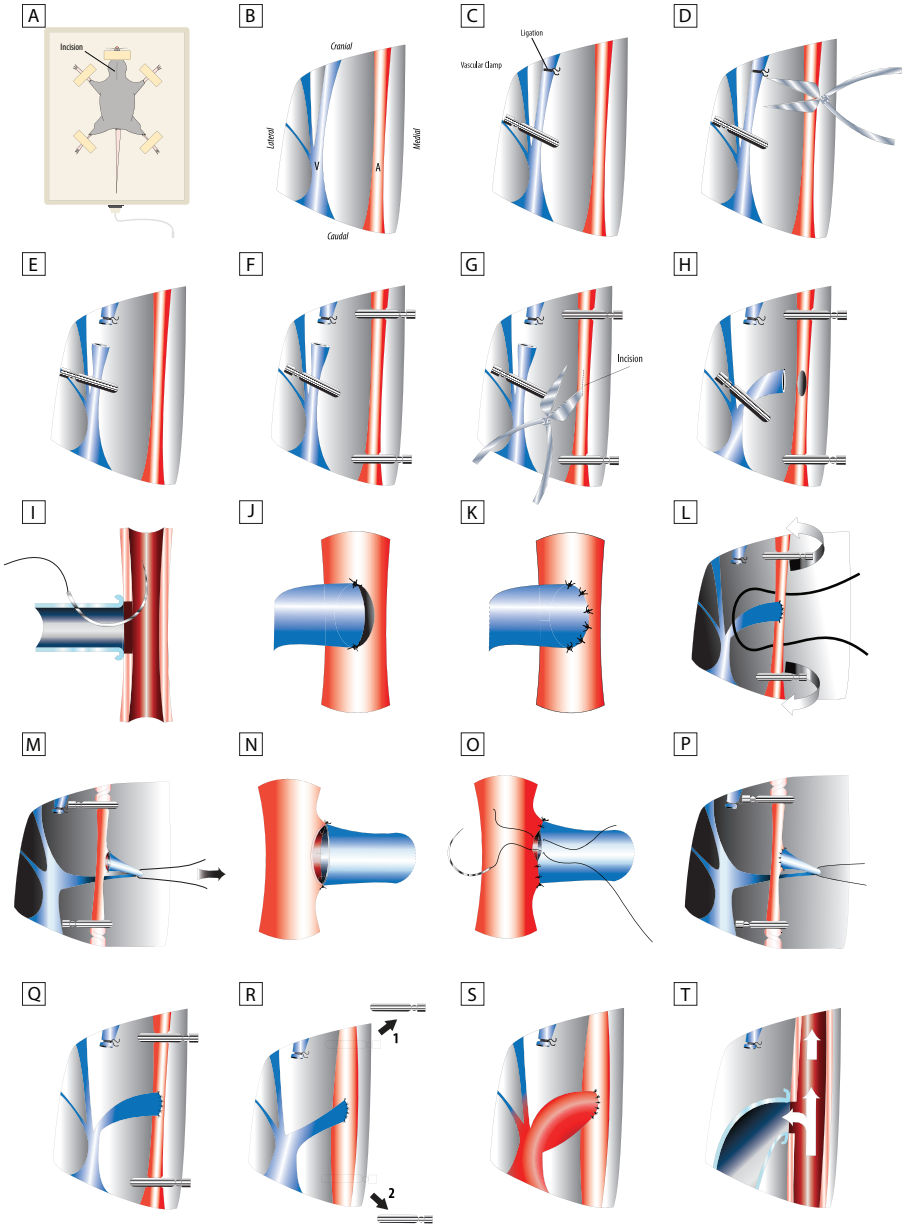


Figure 1. Detailed scheme of surgical procedure. (A-T) Key steps for successful creation of an AVF.

Protocol:

All experiments were approved by the committee on animal welfare of the Leiden University Medical Center.

1. Animal preparation and anesthesia

1.1 Anesthetize the mouse (1-3 months old) in a continuous anaesthetic induction chamber filled with 3-4 % isoflurane.

1.2 Shave the ventral side of the neck and the inside part of the left upper leg using an electrical razor and use a piece of tape to remove the hair.

1.3 Apply ocular ointment on both eyes.

1.4 Position the animal on the heating blanket on which the nose ventilation mask is fixed. Fixate the head to the nose mask using adhesive tape. Deliver isoflurane at a concentration of 1.5-2.0 % using oxygen enriched air set at the following flow: air 0.3 L/min, 100% oxygen 0.2 L/min. Pinch the skin between the toes to assess the depth of anaesthesia and adjust the concentration of isoflurane if needed.

1.5 Fixate the animal to the heating blanket with adhesive tape on all the limbs that is set at approximately 37 °C in a supine position.

1.6 Inject buprenorphine dissolved in sodium chloride (NaCl) 0.9% at a dosage of 0.1 mg/kg together with 0.5 mL of sterile NaCl 0.9% subcutaneously in the flank of the animal.

1.7 Apply chlorhexidine tincture 0.5% to the prepared area.

2. Skin incision

2.1 Position the animal under the microscope with its head towards the surgeon.

2.2 Make a longitudinal incision of approximately 1.5 cm in the midline of the ventral neck using a micro scissor.

2.3 Grab the salivary glands with forceps and displace the right salivary gland cranially until it is partly outside the wound.

3. Dissecting and preparing the vein

3.1 Identify and bluntly dissect the dorsomedial branch of the right external jugular vein completely from its perivascular tissue by spreading just alongside and in the direction of the blood vessel.

3.2 Place a loop (10.0 suture) around the dissected vein and apply one knot without locking it.

4. Removing the sternocleidomastoid muscle

4.1 Using forceps, bluntly dissect the right sternocleidomastoid muscle from its surroundings by spreading along its border. Place a pair of open forceps under the isolated muscle and ligate it proximally and distally with a 6.0 suture. Subsequently, excise the muscle using a cauterizer.

5. Dissecting and preparing the common carotid artery

5.1 Identify and dissect the right common carotid artery using forceps. Place a 6.0 suture thread around the artery to aid in the manipulation of the artery.
5.2 Apply vascular clamps as distally and proximally as possible.
5.3 Make a longitudinal incision in the middle of the artery of approximately 1 mm using the specialised micro scissor.
5.4 Rinse the artery with a heparin solution [100 IU/mL] until the vessel is clear of blood.
5.5 Measure and adjust the length of the incision if necessary to match the width the vascular clamp [1.1 mm].

6. Ligation of the vein

6.1 Apply a vascular clamp proximally of the already prepared vein and place a suture thread around the vein.
6.2 Apply gentle caudal traction to the vein using a haemostat that is placed on the suture thread and ligate the vein as distally as possible using the 10.0 suture that was placed earlier.
6.3 Cut the vein using a scissor just proximally to the ligation.
6.4 Using vascular forceps, gently open the lumen of the vein and rinse it with a heparin solution [100 IU/mL].

7. Creation of anastomosis part 1

7.1 Connect the vein to the artery with an interrupted suture (10.0) using 2 square knots at the twelve o'clock position followed by a suture at the six o'clock position. Make sure to connect the vein to the artery without allowing it to rotate around its own axis. Rotate the animal in order to improve the surgical exposure.
7.2 Position a suture thread around the vein and apply gentle lateral traction using a haemostat.
7.3 Using the same interrupted sutures, complete the anastomosis by placing approximately 3-4 additional sutures at the visible ventral side of the anastomosis.

8. Heparin administration

8.1 Rotate heating blanket 180 degrees and focus the microscope on the left upper leg.

8.2 Identify the femoral vein/artery/nerve bundle by looking for a vascular structure that runs longitudinally in the medial part of the upper leg and can be seen through the skin. Make an incision with the micro scissor of approximately 1 cm directly above the femoral vein in a lengthwise manner.

8.3 Carefully dissect the perivascular tissue of femoral vein and inject heparin at a dose of 0.2 IU/gram bodyweight in the femoral vein.

9. Creation of anastomosis part 2

9.1 Return to the neck area and remove the suture thread that was placed around the vein.

9.2 Place a suture thread (6.0) that subsequently passes below the carotid artery, over the vein and again below the carotid artery. (Figure 1-L)

9.3 Remove the venous vascular clamp.

9.4 Next, twist the half completed arteriovenous fistula 180 degrees along the axis of the carotid artery in a clockwise manner by simultaneously twisting both the vascular clamps and apply medial traction to the ends of the suture thread.

9.5 Complete the anastomosis in the same fashion as is described in step 7.2.

10. Vascular clamp removal

10.1 Remove the suture thread and rotate the vascular clamps 180 degrees counter clockwise.

10.2 Remove the distal vascular clamp followed by the proximal vascular clamp.

10.3 Assess the patency of the anastomosis by gently occluding the venous outflow tract with the vascular forceps. In case of a patent anastomosis, the pre-occluding venous section will expand in a pulsatile fashion. Relocate the right salivary gland to its original anatomical position using forceps.

11. Skin closure and postoperative care

11.1 Close the skin of the upper leg with an uninterrupted suture (6.0).

11.2 Close the skin of the neck with an uninterrupted suture (6.0).

11.3 Remove the animal from the heating blanket and inject 0.5 mL NaCl 0.9% subcutaneously.

11.4 Place the animal in a darkened cage that is heated with a heating lamp and let it recover fully. When an animal does not recover fully, make sure it does not suffer from a hemodynamic shock due to bleeding in the surgical area. Look for signs such as a swollen neck and the leakage of blood.

11.5 After approximately 6 hours after the first injection of buprenorphine, inject a single dose of a sustained-release formulation of buprenorphine subcutaneously in a dose that is recommended by the manufacturer, in order to provide adequate analgesia for an additional 72 hours.

12. Tissue harvesting

12.1 Anesthetize the animal with an anesthetic-mixture containing midazolam (5 mg/kg), medetomidine (0.5 mg/kg) and fentanyl (0.05 mg/kg) administered intraperitoneally.

12.2 Fixate the animal in a supine position by inserting needles through its paws and cheeks into a non-heated silicon mat.

12.3 Make an incision of approximately 1.5-2.0 cm over the scar in the neck with the micro scissor.

12.4 Dissect the AVF, and place suture threads (6.0) around the proximal-, distal artery and venous outflow tract for easy identification.

12.5 Assess the patency of the AVF as is described in section 10.3 of the protocol.

12.6 Open the peritoneal cavity by performing a medial laparotomy using the micro scissor.

12.6.1 Cut through the left and right ventral rib cage using a pair of scissors starting caudally in the midclavicular line. Using a micro scissor, transect the diaphragm that is attached to the middle part of the ventral rib cage and subsequently displace this section cranially using forceps.

12.6.2 Locate the inferior caval vein and transect it with a micro scissor.

12.7 Insert a needle 23 gauge needle in the left ventricle and perfuse with PBS at a pressure of approximately 100 mmHg until the intravasal fluid is nearly clear.

12.8 Without removing the needle, now perfuse with 4% formalin for 10 minutes at a pressure of approximately 100 mmHg.

12.9 Excise the AVF by transecting both the arteries and vein with the micro scissor and submerge it in a 4% formalin solution overnight.

13. Tissue embedding and sectioning

13.1 Process the tissue to paraffin according to the manufacture's protocol. The protocol applied consisted of the following:

13.1.1 Immerse in Ethanol 70% for 1 hour at room temperature. Repeat 2X.

13.1.2 Immerse in Ethanol 96% for 1 hour at room temperature. Repeat 2X.

13.1.3 Immerse in Ethanol 99.5% for 1 hour at room temperature. Repeat once.

13.1.4 Immerse in Ethanol 99.5% for 1.5 hour at room temperature.

13.1.5 Immerse in xylene 100% for 1 hour at room temperature. Repeat once.

13.1.6 Immerse in Paraffin for 1 hour at 62°C. Repeat 2X.

13.2 Embed the AVF in paraffin so that the venous outflow tract is orientated perpendicular to the embedding cassette.

13.3 Using a microtome, create 12 serial sections each consisting of 30 sections with a 5 μm thickness. Then of each serial section, place one section on a single mounting glass starting from position one up to twelve in an orderly fashion starting with the area closest to the anastomosis.

Representative results

After the creation of the anastomosis (Figure 1), the patency should be assessed by shortly occluding the venous outflow tract with a vascular forceps. When the anastomosis is patent, the vascular tract proximal to the occlusion should clearly expand in a pulsatile manner. In addition, the patency is confirmed by using near infrared fluoroscopy (NIRF) that effectively functions as an angiography (Figure 2). A failure in the surgical procedure can lead to an occlusion of the anastomosis as is depicted in (Figure 2). This failure can be caused by a too narrow anastomotic area, torsion of the vessels, inadequate heparin dose or an accidental suture placement that connects the front side of the anastomosis to the back side.

At a histological level, the process of vascular remodeling in AVF can be investigated elegantly using this model. Vascular remodeling in AVF occurs as a result of the increase in blood flow and pressure. In mice, this response is characterized by an increase in circumference (e.g. outward remodeling) leading to an increase in luminal area in the first 2 weeks after surgery. After these 2 weeks, the luminal area progressively decreases due to a stop in the outward remodeling and ongoing thickening of the tunica intima. The formation of these progressive stenotic lesions results in occlusion of 50% of AVF at 4 weeks after surgery. Therefore, the optimal time point to harvest the AVFs would be at 2 weeks after surgery, since in this phase, proper analysis of the vascular response in patent AVF is still feasible. Immunostaining of the venous outflow tract at 2 weeks after surgery shows that the cellular compartment of the intima mainly consists of alpha-smooth muscle actin (α-SMA) positive cells (Figure 3), as observed in failed human AVFs as well[7].

In view of the complexity of the microsurgical procedure, it's realistic to reckon with technical failure of the procedure in a proportion of the mice. In our hands, the success rate of the procedure was 67% in the beginning. However, with further training this rate was increased up to 97%. The main cause of failure was hemorrhage (60%), followed by acute thrombosis (27%) and anesthesia- related death (13%). After sufficient training, the surgical procedure can be performed in approximately 1 hour.

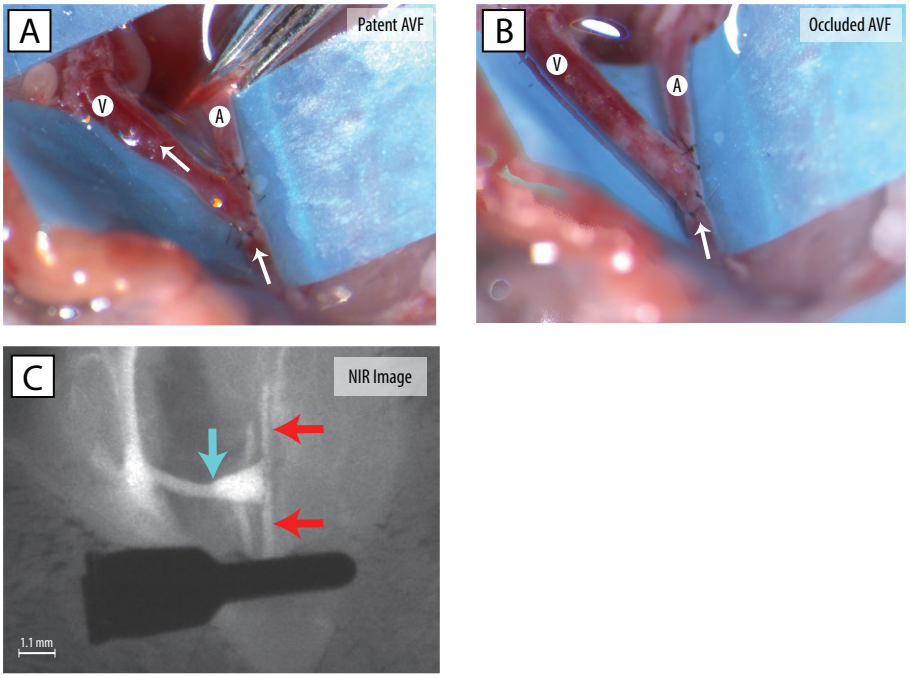


Figure 2. Macroscopic pictures of patent and occluded AVFs. (A) A patent AVF with a vascular clamp on the distal common carotid artery. (B) An occluded AVF. (*White arrow*) indicates the direction of the blood flow. (C) A patent AVF demonstrated using Near Infrared Fluoroscopy. (*red arrow*) indicates artery. (*blue arrow*) indicates venous outflow tract.

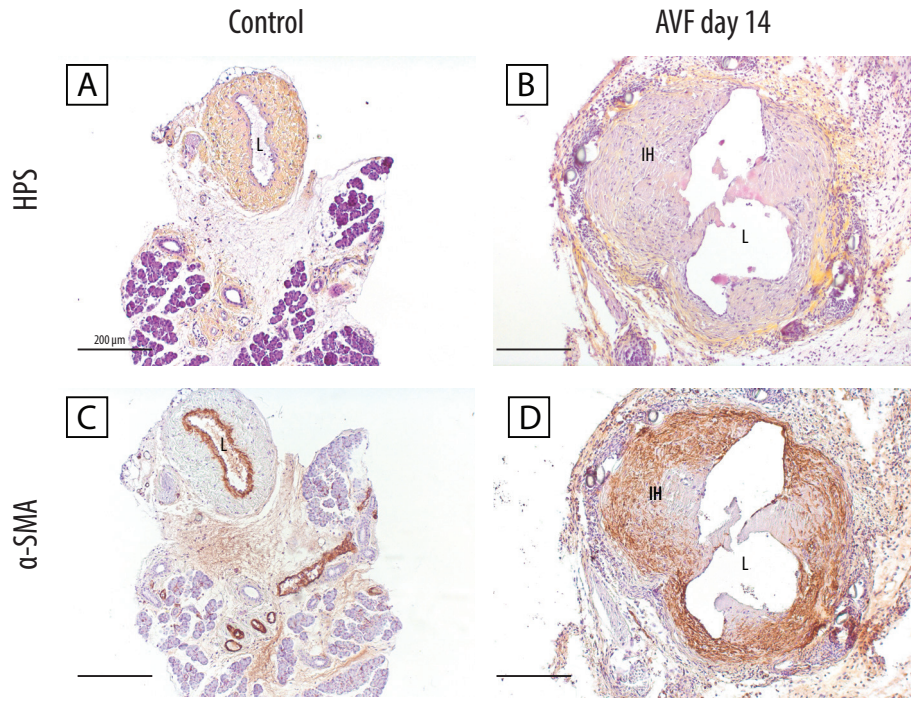


Figure 3. Histological stainings of the venous outflow tract of the AVF at day 14 versus unoperated control vessels. (A-B) Morphologic overview using hematoxylin, phloxin and saffron showing a clear increase in vessel circumference and intimal hyperplasia development 14 days after AVF creation. (C-D) Immunohistochemical staining demonstrating that the majority of the cells present the intimal hyperplasia are alpha smooth muscle actin positive. *(L) Lumen*; *(IH) Intimal hyperplasia; scale bar: 200 µm*

Discussion

The AVF is considered to be the Achilles' heel in hemodialysis treatment. Unfortunately, the AVF still suffers from a high number of failure[8-10]. Despite extensive research on the underlying mechanisms, the exact pathophysiology remains unknown. Numerous murine models for AVF failure have already been described in literature [2,3,11,12]. However, none of these models incorporate a venous end to arterial side anastomosis configuration that is most used in the clinical situation. This is very relevant since the resultant hemodynamic profile plays an important role in vascular remodeling. Moreover, some of the models used a synthetic cuff for the connection between the artery and vein [2,11], which is not used in the clinical setting.

To improve the clinical relevance, we therefore developed a murine model in which a unilateral venous end to arterial side anastomosis was created between a branch of the jugular vein and common carotid artery with interrupted sutures6. In this model crucial histomorphological changes were observed including outward remodeling and progressive intimal hyperplasia, ultimately leading to AVF failure.

A crucial aspect of the surgical procedure is the anaesthesia protocol. It is recommended to use isoflurane inhalation anaesthesia, as this is a safe and easy method for obtaining prolonged periods of anaesthesia. The latter is especially important for the training phase in which the whole procedure can take up to 3 hours.

In order to create the necessary room for the traversing outflow vein of the arteriovenous fistula, the ipsilateral sternocleidomastoid muscle needs to be excised.

With respect to the vessel handling during surgery, dissection of vessels should be performed in a blunt manner using forceps. The use of specialised vascular straight forceps are recommended for direct handling and manipulation of the vessels as they provide more precision and produce less mechanical damage due to the rounded tip. The usage of suture threads as vessel loops combined with a hemostat can aid in safe tissue handling and moreover, in presenting the tissue in an optimal manner when used as a third hand which is crucial so this procedure can be performed without any direct assistance.

Undoubtedly, the most difficult step in the procedure are the suture placements between the artery and vein. Care must be taken not to suture the "back"-side of the anastomosis with the "front"-side, as this will lead to narrowing of the anastomosis that can lead to early failure of the AVF. To prevent this from happening, position the tip of the vascular forceps between the two walls of the vessel in order to separate them. The technical difficulty can be considered to be a limitation of this model. However, we do not think that this procedure is more challenging than the model that is presently most widely used[3,6].

It's difficult to make a general remark on the sample size for future studies, as the calculated sample size does not only depend on the variability between animals but also on the 'strength' of the intervention. We estimate that a group size of approximately 10 mice (excluding mice that drop out of the study because of technical failure of the AVF) should be sufficient for studies that focus on the role of a specific gene in AVF failure. Recently, we were able to obtain significant results with an average group size of 10 animals in a study on the role of elastin in murine AVF remodeling[13].

One aspect of our murine model requires further discussion. It is known that the uremic milieu in patients with end stage renal disease contributes to a multitude of vascular diseases including venous intimal hyperplasia even prior to hemodialysis access surgery[14-16]. This present model does not incorporate the uremic milieu. Therefore, the incorporation of a model of chronic

renal failure [17] would be a valuable additive step to further improve the validity of this murine model.

Acknowledgements

This study was supported by a grant from the Dutch Kidney Foundation (KJPB 08.0003). Carolien Rothuizen is acknowledged for her contribution to the study. Hoang Pham is acknowledged for his assistance with the pathology work-up.

Reference List

1. Rotmans, J.I. Animal Models for Studying Pathophysiology of Hemodialysis Access. *The Open Urology & Nephrology Journal.* **7** 14-21, doi:10.2174/1874303X01407010014 (2014).

2. Kwei, S. *et al.* Early adaptive responses of the vascular wall during venous arterialization in mice. *Am.J.Pathol.* **164** (1), 81-89, doi:S0002-9440(10)63099-4 [pii];10.1016/S0002-9440(10)63099-4 [doi] (2004).

3. Castier, Y. *et al.* Characterization of neointima lesions associated with arteriovenous fistulas in a mouse model. *Kidney Int.* **70** (2), 315-320, doi:5001569 [pii];10.1038/sj.ki.5001569 [doi] (2006).

4. Krishnamoorthy, M.K. *et al.* Hemodynamic wall shear stress profiles influence the magnitude and pattern of stenosis in a pig AV fistula. *Kidney Int.* **74** (11), 1410-1419, doi:ki2008379 [pii];10.1038/ki.2008.379 [doi] (2008).

5. Ene-Iordache, B., Cattaneo, L., Dubini, G., & Remuzzi, A. Effect of anastomosis angle on the localization of disturbed flow in 'side-to-end' fistulae for haemodialysis access. *Nephrol.Dial.Transplant.* **28** (4), 997-1005, doi:gfs298 [pii];10.1093/ndt/gfs298 [doi] (2013).

6. Wong, C.Y. *et al.* Vascular remodeling and intimal hyperplasia in a novel murine model of arteriovenous fistula failure. *J.Vasc.Surg.* **59** (1), 192-201, doi:S0741-5214(13)00553-3 [pii];10.1016/j.jvs.2013.02.242 [doi] (2014).

7. Rekhter, M., Nicholls, S., Ferguson, M., & Gordon, D. Cell proliferation in human arteriovenous fistulas used for hemodialysis. *Arterioscler.Thromb.* **13** (4), 609-617, (1993).

8. Falk, A. Maintenance and salvage of arteriovenous fistulas. *J.Vasc.Interv.Radiol.* **17** (5), 807-813, doi:17/5/807 [pii];10.1097/01.RVI.0000217928.43396.35 [doi] (2006).

9. Tordoir, J.H. *et al.* Prospective evaluation of failure modes in autogenous radiocephalic wrist access for haemodialysis. *Nephrol.Dial.Transplant.* **18** (2), 378-383, (2003).

10. Dixon, B.S., Novak, L., & Fangman, J. Hemodialysis vascular access survival: upper-arm native arteriovenous fistula. *Am.J.Kidney Dis.* **39** (1), 92-101, doi:S0272-6386(02)34055-1 [pii];10.1053/ajkd.2002.29886 [doi] (2002).

11. Yang, B., Shergill, U., Fu, A.A., Knudsen, B., & Misra, S. The mouse arteriovenous fistula model. *J.Vasc.Interv.Radiol.* **20** (7), 946-950, doi:S1051-0443(09)00346-7 [pii];10.1016/j.jvir.2009.03.044 [doi] (2009).

12. Kang, L. *et al.* Regional and systemic hemodynamic responses following the creation of a murine arteriovenous fistula. *Am.J.Physiol Renal Physiol.* **301** (4), F845-F851, doi:ajprenal.00311.2011 [pii];10.1152/ajprenal.00311.2011 [doi] (2011).

13. Wong, C.Y. *et al.* Elastin is a key regulator of outward remodeling in arteriovenous fistulas. *Eur.J.Vasc.Endovasc.Surg.* **49** (4), 480-486, doi:S1078-5884(15)00037-4 [pii];10.1016/j.ejvs.2014.12.035 [doi] (2015).

14. Kennedy, R. *et al.* Does renal failure cause an atherosclerotic milieu in patients with end-stage renal disease? *Am.J.Med.* **110** (3), 198-204, doi:S0002-9343(00)00695-1 [pii] (2001).

15. Cheung, A.K. *et al.* Atherosclerotic cardiovascular disease risks in chronic hemodialysis patients. *Kidney Int.* **58** (1), 353-362, doi:kid173 [pii];10.1046/j.1523-1755.2000.00173.x [doi] (2000).

16. Lee, T. *et al.* Severe venous neointimal hyperplasia prior to dialysis access surgery. *Nephrol.Dial.Transplant.* **26** (7), 2264-2270, doi:gfq733 [pii];10.1093/ndt/gfq733 [doi] (2011).

17. Kokubo, T. *et al.* CKD accelerates development of neointimal hyperplasia in arteriovenous fistulas. *J.Am.Soc.Nephrol.* **20** (6), 1236-1245, doi:ASN.2007121312 [pii];10.1681/ASN.2007121312 [doi] (2009).

Supplemental data

Name	Company	Catalog Number
Dissecting microsocpe	Leica	M80
Forceps	Medicon	07.61.25
Vascular forceps	S&T	JFL-3D.2
Vascular forceps	S&T	D-5a.2
Forceps	Roboz	SS/45
Micro scissor 5 mm blade	Fine science tools	15000-08
Micro scissor 2 mm blade	Fine science tools	15000-03
Scissor	Medicon	05.12.21
Clip applier 1	S&T	CAF-4
Vascular clamp 1	S&T	B-1V
Clip applier 2	BBraun	FE572K
Vascular clamp 2	BBraun	FE740K
Hemostatic forceps	BBraun	BH110
10.0 sutures	BBraun	G1117041
6.0 sutures	BBraun	768464
Cauterizer	Fine science tools	18010-00
Needle holder	Medicon	11.82.18
Ocular ointment	Pharmachemie	41821101
Chlorhexidine tincture 0,5%	Leiden University Medical Center	NA
Heparin	Leo Pharma	012866-08
Buprenorphin	RB Pharmaceuticals	283732
Isoflurane	Pharmachemie	45.112.110
Anesthesia mask	Maastricht university	custom made
Midazolam	Actavis	AAAC6877
Dexmedetomidine	Orion	141-267
Fentanyl	Bipharma	15923002
Continuous anaesthetic induction chamber	Vet-tech solutions	AN010R

Table 1. Materials used for the surgical procedure

Chapter 5

Elastin is a key regulator of outward remodeling in arteriovenous fistulas

C.Y. Wong, T.C. Rothuizen, M.R. de Vries, T.J. Rabelink, J.F. Hamming, A.J. van Zonneveld, P.H.A Quax and J.I. Rotmans

Eur J Vasc Endovasc Surg. 2015 Apr;49(4):480-6



Introduction

An adequate functioning arteriovenous fistula (AVF) is of the preferred type of vascular access for patients requiring chronic hemodialysis. AVF maturation (e.g. increase in flow and venous diameter) is a prerequisite for successful cannulation of the venous outflow tract. Unfortunately, 30-50% of fistulae fail to mature[1] eventually leading to a poor one-year primary patency of 60-65%[2, 3]. The pathophysiology responsible for inadequate maturation is incompletely understood.

AVF maturation results from a cascade of processes after AVF surgery that leads to the reorganization of the extracellular matrix (ECM)[4]. This matrix-metalloproteinase (MMP)-mediated process of vascular remodeling allows the vessels of the fistula to enlarge. The main ECM components that are involved in this outward remodeling (OR) are collagen and elastin. In vascular physiology, elastic fibers provide the vessel its elasticity and resilience, thereby providing the ability to absorb hemodynamic stress[5, 6]. Elastin is a cross-linked, insoluble polymer of the monomeric secreted form of the protein tropoelastin that is secreted primarily by vascular smooth muscle cells (VSMCs) and diverse fibroblasts[6, 7]. Elastin homeostasis has emerged as an important determinant of vascular OR. Indeed, elastic fiber degradation mediates physiological OR as occurs in the uterine artery during pregnancy[8, 9]. Additional support for a role of elastin degradation in OR comes from studies in patients with aortic aneurysms showing that polymorphisms in the elastin gene[10] may contribute to the pathogenesis of this pathological arterial dilation. In the present study, we hypothesized that elastin might be an important regulator in outward remodeling in AVF. For this purpose, end-to-side AVFs were created in haplodeficient tropoelastin KO mice[11].

Material and Methods

Animals and study design

The Institutional Committee for Animal Welfare at the LUMC approved all experiments. Adult male C57BL/6 (WT) (Charles River) and $eln^{+/-}$ mice with a C57BL/6 background aged 10-17 weeks (weighing 23-35 grams) were used for the experiments and received unilateral AVFs. The animals were sacrificed at day 21 after the surgical procedure. Identical veins of unoperated mice were used to assess elastic fiber density before surgery.

Surgical procedure

An unilateral AVF was created as previously described[12] (Fig 1, A). In short, the animal was anesthetized using isoflurane followed by shaving and disinfection of the skin in the ventral neck area and fixed in a supine position on a heating blanket. The mouse was then injected with buprenorphin (0.1 mg/kg) (MSD, Whitehouse Station, NJ, USA) and 0.5 mL saline. Under a dissecting microscope (M80, Leica, Wetzlar, Germany), an incision in the ventral midline of the neck area was made, followed by a dissection of the right dorsomedial branch of the external jugular vein and ipsilateral common carotid artery after the excision of the sternocleidomastoid muscle using a heat cauterizer. Next, after applying a vascular clamp (S&T, Neuhausen, Switzerland) on the proximal and distal artery an approximate 1 mm incision was made using a microscissor (Fine Science Tools, Heidelberg, Germany) and the lumen was rinsed with a heparin solution (100 IU/mL) (LEO Pharma, Ballerup, Denmark). The vein was then clamped proximally and ligated distally, followed by a transsection just proximal to the ligation. After rinsing the vein with a heparin solution, an end-to-side anastomosis was created using 10.0 interrupted sutures (BBraun, Melsungen, Germany). Halfway during the suturing procedure heparin was injected intravenously with a dose of 0.2 IU/gram bodyweight. After completion of the anastomosis, the remaining clamps were removed and patency was assessed. The skin was closed with a 6.0 running suture suture (BBraun, Melsungen, Germany). Following completion of the surgery 0.5 mL of saline was injected subcutaneously and the animals were kept warm until recovery.

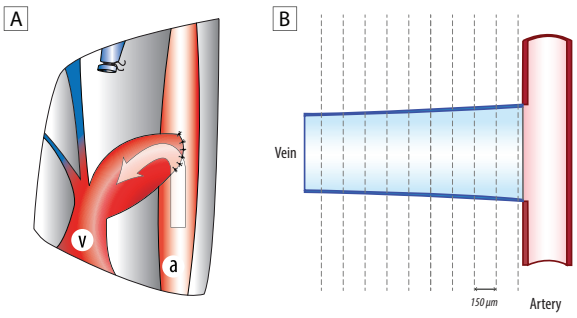


Figure 1. Surgical scheme and orientation of sectioning. (A) Schematic visualization of an arterial side to venous end arteriovenous anastomosis between the common carotid artery (a) and the dorsomedial distal branch of the external jugular vein (v) using 10.0 interrupted sutures. (B) Schematic overview of sectioning locations within the arteriovenous fistula, in which every dashed line represents a sectioning area with a fixed interval of approximately 150 µm.

Tissue harvesting and processing

Upon sacrifice, animals received an intraperitoneal injection with an anesthetic-mixture containing midazolam (5 mg/kg) (Roche, Basel, Switzerland), medetomidine (0.5 mg/kg) (Orion, Espoo, Finland) and fentanyl (0.05 mg/kg) (Janssen, High Wycombe, UK) whereupon a reincision was made over the scar. The AVF, including its venous and arterial limb, was dissected and the patency was assessed clinically. For this purpose, the blood flow was disrupted by compressing the distal arterial as well as the distal venous limb with vascular forceps. The AVF was considered patent when the venous limb proximal to the forceps expands in diameter. In case this phenomenon was not clearly visible, the AVF was considered not patent. Next, a thoracotomy was performed and the inferior vena cava was transected followed by an intracardial perfusion with subsequently phosphate buffered saline and formalin 4% at a pressure of approximately 100 mmHg. The small size of the murine vasculature and the configuration of the AVF preclude simultaneous perpendicular analysis of the artery and the vein. Since most of the stenotic lesions in human AVFs occur in the venous outflow tract, we focused our analysis on the vein. (Fig 1, B) The tissue was processed to paraffin and sections of 5 μm were made perpendicular to the vein at 12 locations with an interval of 150 μm. For the purpose of RNA isolation, 20 μm thick sections were obtained from additional animals.

RNA islolation and real-time quantitative polymerase chain reaction (RT-QPCR)

Twenty paraffin embedded sections section of 20 μm-thick representing the entire AVF were freshly collected and RNA was isolated from the tissue using RNeasy FFPE Kit (Qiagen, Gaitherburg, Maryland, USA). RNA concentration, purity and integrity were examined by nanodrop (Nanodrop® Technologies). Relative quantitative mRNA PCR was performed on reverse transcribed cDNA (High Capacity RNA-to-cDNA kit - Applied Biosystems art.nr. 4387406) using primers against mouse eln (Mm00514670_m1, Life technologies, Grand Island, New York, USA). qPCRs were run on a 7900HT Fast Real-Time PCR System (Applied Biosystems). Normalization of data was performed using stably expressed endogenous controls (HPRT).

Spectral microscopy

To study the dispersion of elastic fibers in more detail, sections stained with Weigert's elastin were analyzed using multispectral imaging system comprised of a fluorescent microscope (DM4000B, Leica, Wetzlar) and a Nuance imaging unit (N-MSI-FX, PerkinElmer, Massachusetts, USA). In short, the specific spectrum of elastin was selected using the elastic lamellae present in the carotid artery. This tissue specific selection was then located in the venous outflow tract of the AVF and assigned the color red. The background was assigned the color green.

Morphometric analysis

A histochemical staining with hematoxylin, phloxin and saffron (HPS) was used for a morphological overview. After digitalization of all the venous sections with a microscope (Carl Zeiss, Oberkochen, Germany), morphometric analysis was performed on Weigert's elastin stained sections using quantitative imaging software (Qwin, Leica, Wetzlar, Germany). The intimal area was calculated by subtracting the luminal area from the area within the internal elastic lamina (IEL). The circumference of the vessel was determined by measuring the length of the IEL. Results are expressed as mean ± standard error of the mean.

Alpha smooth muscle actin staining and quantification

All sections were stained against α-smooth muscle actin (α-sma) to identify vascular smooth muscle cells (VSMC) and myofibroblasts using a dilution of 1:1000 for the primary antibody (Dako, Glostrup, Denmark). Subsequently, the slides were digitized at a resolution of 2080 x 1542 pixels by a camera connected to a microscope (Carl Zeiss, Oberkochen, Germany). A detailed protocol of the staining is listed in the appendix. The α-sma positive area in the total vessel was measured using quantitative imaging software (ImageJ) and was expressed in μm^2.

Collagen quantification

In order to quantify the collagen content in the vessels, the tissue sections were first stained using a picro-sirius red staining and followed by digitalization using the method as described above. Using ImageJ software, collagen content in all the venous sections was determined by selecting the stain specific color for collagen at a fixed average threshold12, and was expressed in μm2. In order to obtain qualitative information about the deposition pattern of collagen additional images were produced using digital image microscopy with circularly polarized light (Olympus, Shinjuku-ku, Tokyo, Japan.).

Statistical analysis

All data except the patency outcome were expressed as mean ± standard error of the mean. A Fisher's exact test was used for the data on AVF patency. For the histomorphometric and RT-QPCR results an unpaired t-test was used. The results from the α-sma quantification were tested using a Mann-Whitney U test. A P-value < 0.05 was considered statistically significant.

Results

Surgical outcome

Twenty animals (11 WT mice and 9 eln$^{+/-}$ mice) successfully received an AVF out of which 2 (18%) from the WT group and 1 (11%) from the eln+/- group were occluded 21 days after surgery (P = 1.0). No difficulties were encountered during the surgical procedure in the eln$^{+/-}$ mice. These occluded AVFs were excluded from morphometric analysis, resulting in an inclusion of 9 WT mice and 8 eln$^{+/-}$ mice.

Elastin expression

At the mRNA level, a relative reduction of 53% in expression of the mELN gene in eln$^{+/-}$ mice was observed as compared to the WT mice (1.0 ± 0.19 vs 0.47 ± 0.07, P < 0.001) (Fig 2, *A*). Using spectral microscopy, we observed a reduction in elastin accumulation in the IEL of eln$^{+/-}$ mice before AVF placement, resulting in a more fragmented IEL structure (Fig 2, B-*E*). After 21 days of venous arterialization, elastin content in the vessel wall is greatly fragmented and diminished in both the WT (n=5) and eln$^{+/-}$ mice (n=6), retaining the pre-existing difference in elastin content favouring the WT group.

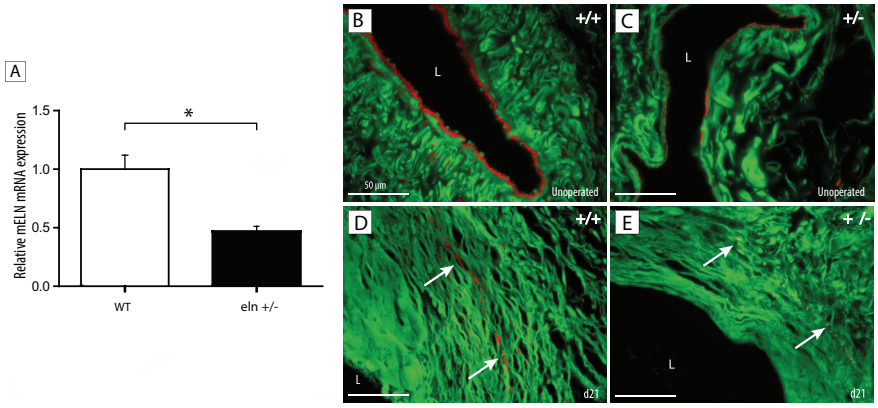


Figure 2. The presence of elastin in the venous outflow tract prior to, and after arteriovenous fistula creation. (A) Relative mRNA expression of murine elastin in the AVF at day 21 after surgery. (B–E) Visualization of elastin (red) (white arrow) in the venous outflow tract before (control) and after surgery (day 21) using spectral microscopy. *Note*. Original magnification 100×. Scale bar, 50 µm; L = Lumen; +/+ = wild type; +/− = haplodeficient. *$p < .05$.

Morphometric analysis

Twenty one days after AVF placement, the circumference in eln$^{+/-}$ mice (2936 ± 191 μm) was 21% larger as compared to the WT mice (2424 ± 126 μm; P = 0.037), whereas the intimal area was comparable between the groups (WT: 112908 ± 16029 μm^2 vs eln$^{+/-}$:134967 ± 24673 μm^2;P = 0.45). The luminal area of the venous outflow tract in the eln$^{+/-}$ mice was 53% larger as compared to the WT mice, although this difference was borderline significant (eln$^{+/-}$: 350116 ± 45073 μm^2, WT: 229405 ± 40453 μm^2; P = 0.064). (Fig 3, *A-F*).

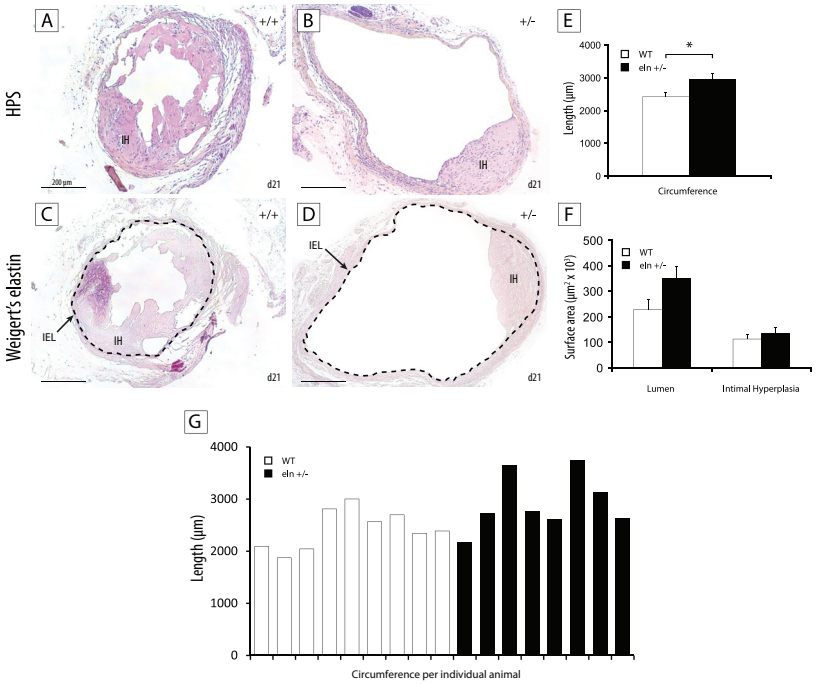


Figure 3. Morphometric parameters 21 days after AVF creation. (A,B) Hematoxylin, phloxin, and saffron staining (HPS). (C,D) Weigert's elastin staining used for the histomorphometric analysis in which the internal elastic lamina (IEL) is highlighted (dashed line). (E,F) Histomorphometric data after AVF creation. (G) Mean circumference displayed per individual animal. Original magnification 100×. Scale bar, 200 μm. IH = intimal hyperplasia. * $p < .05$.

Alpha smooth muscle actin

Although the amount of intimal hyperplasia was equal in both groups after 21 days, we did observe an 2.4 fold larger area of α-sma positive cells in the venous outflow tract of the haplodeficient mice as compared to the WT (132169 ± 30725 μm^2 vs 55331 ± 8053 μm^2; P = 0 .036) (Fig 4, *A-C*).

Collagen

At day 21, the amount of collagen observed in the eln$^{+/-}$ mice (129539 ± 19246 μm^2) was 87 % higher as compared to the WT mice (69180 ± 11574 μm^2, P = 0.015). (Fig 4, *D-F*). The pico-sirius red stained sections, analyzed with circularly polarized light revealed that collagen type I and III was mainly located in the media and adventitia, with limited collagen content in the intima.

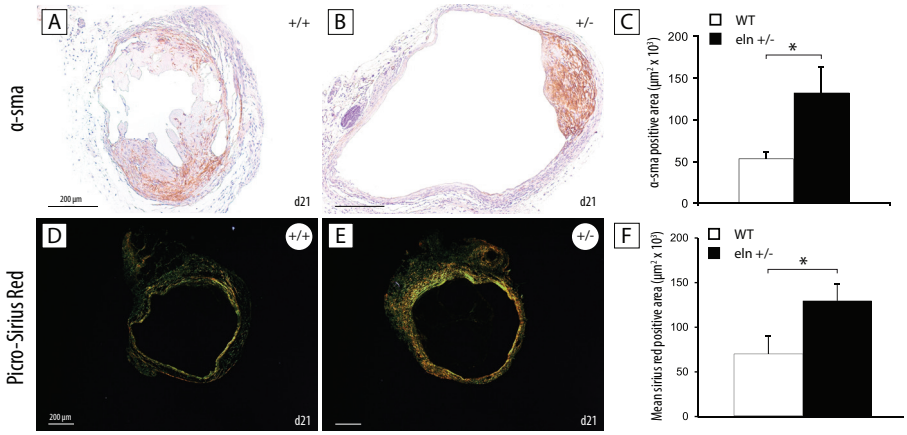


Figure 4. Alpha smooth muscle actin and picro-sirius red staining. (A,B) Immunohistochemical staining using antibodies against α-sma. (C) Quantification of α-sma positive area in the venous outflow tract. (D,E) Picro-sirius red staining visualized using circular polarized light microscopy. (Original magnification 40×). (F) Quantification of collagen positive area using the picro-sirius red staining. Original magnification 100×. Scale bar, 200 μm. * $p < 0.05$.

Discussion

In the present study we investigated the effect of elastin deficiency on venous remodeling in a murine model of AVF failure. We observed that eln+/- mice have a lower density of elastic fibers present in the venous IEL prior to AVF creation when compared to WT mice. Upon AVF creation, $eln^{+/-}$ mice showed an accelerated venous outward remodeling response while no effect was observed on intimal hyperplasia. This adaptive response in the $eln^{+/-}$ mice resulted in a trend towards a larger luminal area of the venous outflow tract when compared to WT mice.

The role of elastin in outward remodeling after arteriovenous fistula creation

The main objective of AVF surgery in hemodialysis patients is to create a high-flow vascular circuit with a sufficient venous intraluminal diameter to allow safe cannulation. According to the KDOQI guidelines, AVF maturation is considered clinically successful if 6 weeks after surgery, the fistula supports a flow of 600 mL/min, is located at a maximum of 6 mm from the surface and has a diameter of > 6 mm[13]. In order to achieve the latter, adequate outward remodeling of the venous outflow tract is required. The data from the present study in which we observed enlarged OR in the elastin haplodeficient mice provides support for the hypothesis that a low elastin content in the venous outflow tract might facilitate AVF maturation. In addition, a reduced elastin expression in the carotid artery might also have contributed to the increase in venous outward remodeling since increased arterial outward remodeling could stimulate flow-induced venous remodeling. Unfortunately, the end-to-side configuration of the AVF precluded morphometric analysis of cross-sections of the arterial segment. Since intimal hyperplastic lesions in AVF mostly occur in the venous outflow tract, we chose to focus on this segment by cross-sectioning the venous part.

Previous clinical studies have also suggested that elastin degradation might be beneficial for AVF maturation by showing that patients with matured AVF have higher circulating levels of MMP 2 (an elastinolytic protease), when compared to those with maturation failure[14]. A similar association has been observed between high MMP-2 expression in venous segments of AVFs and maturation of these fistulas[15]. Conversely, peri-adventitial application of recombinant elastase has been shown to stimulate OR in rabbit AVF[16]. Interestingly, this approach has recently been investigated in a phase II clinical trial that revealed increased maturation of radiocephalic fistulas that were treated with 30 μg elastase[17].

The role of collagen in AVF adaptation is more complex since MMPs are not only involved in collagen degradation, but they also induce collagen synthesis[18]. The higher amount of total collagen observed in the $eln^{+/-}$ mice corresponds with the larger vessel wall area as compared to the WT mice. Indeed, newly synthesized collagen fibers are required in order to keep in

pace with the growing dimensions of the venous vessel wall. Most likely, VSMCs are the major source of collagen since during vascular remodelling, proliferating VSMCs synthesize large amounts of collagen[19].

Intimal hyperplasia in elastin haplodeficient mice

In our study, we did not observe a significant difference in intimal hyperplasia (IH) between the eln $^{+/-}$ and WT mice 21 days after surgery. Obviously, increased IH might be the downside of impaired elastin synthesis since elastin is an important inhibitor of VSMC migration and proliferation[20-22] one of the main mechanisms underlying the development of IH[23]. The importance of elastin in vascular function and integrity becomes clear, as homozygous knock-out mice are not viable due to the formation of occlusive arterial lesions consisting of VSMCs[24]. In line, increased activity of MMP-2 and MMP-9, have also been associated with IH in arteriovenous conduits[25-27]. In the previous studies in the murine AVF model, we observed progressive growth of intimal hyperplastic lesions up to 4 weeks after surgery[12]. In view of the inhibitory effect of elastin on VSMC proliferation, we cannot exclude that elastin deficiency might result in enhanced IH at later time points after surgery.

Interestingly, Franano and coworkers observed an 84% reduction in intimal area in the outflow vein of an rabbit AVF after perivascular application of porcine elastase[28]. This beneficial effect on IH is most likely driven by the perivascular delivery method of elastase resulting in a directional VSMC proliferation and migration to the adventitia rather than the intima[29, 30]. This location specific elastolytic process, however, is absent in our used model as we only study the effect of impaired elastin synthesis that does not specifically target the adventitia.

While the size of the intimal area did not differ between the WT en eln$^{+\backslash -}$ mice, we did observe a larger content of α-sma positive cells in the venous outflow tract of the eln$^{+/-}$ mice. The latter results from a higher density of α-sma positive cells in the intima. In addition, the enhanced OR response in eln$^{+/-}$ mice also resulted in a larger VSMCs content in the adventitia and media. This observation supports the hypothesis that VSMC proliferation in the initial phase after AVF surgery is required in order to keep pace with the expansion of the venous outflow tract, as demonstrated previously in flow induced arterial OR in rats[31].

Study limitations

The uremic milieu has a clear impact on the progression of vascular diseases in end-stage renal disease patients. Recent studies have suggested that uremic conditions also contribute to the formation of IH in veins prior to AVF surgery[32, 33]. In order to further elucidate the mechanisms involved in AVF maturation, the incorporation of chronic renal failure[34] would be of added value.

Another limitation of our experiments is the absence of data on flow measurements since a high blood flow is one of the main characteristics of a functional AVF for hemodialysis access. Due to technical reasons, quantification of blood flow using ultrasonography or MRI was not successful in our hands.

Although murine models are useful to study the pathophysiology of human diseases, we should remain cautious in the extrapolation of these results to the human setting because the pathology in animals does not necessarily mimic the pathology in humans.

Finally, we should take into account that we could not incorporate the homozygous $eln^{-/-}$ mouse into our AVF model, due to its lethal phenotype. Nevertheless, we think the haplodeficient mice still provide a good indication of the vascular remodeling process in elastin deficient blood vessels.

In conclusion, in the present study we showed that elastin is a crucial factor in OR in murine AVF. This study provides further evidence that interventions aimed at the promotion of elastin degradation such as local application of elastase could be a viable option to enhance maturation of AVFs.

Acknowledgements

This study was supported by a grant from the Dutch Kidney Foundation (KJPB 08.0003). We would like to thank Erna Peters and Iris Schmidt for their assistance on the RT-QPCR and pathology work-up. The knockout mice were generated at the University of Utah by Dr. Dean Li and coworkers. We thank him as well as Dr. Hiromi Yanagisawa from Southwestern Medical Center, Dallas, Texas for providing the elastin haplodeficient mice.

Reference List

1. Tordoir JH, Rooyens P, Dammers R, van der Sande FM, de HM, Yo TI. Prospective evaluation of failure modes in autogenous radiocephalic wrist access for haemodialysis. Nephrol Dial Transplant 2003 Feb;18(2):378-83.

2. Falk A. Maintenance and salvage of arteriovenous fistulas. J Vasc Interv Radiol 2006 May;17(5):807-13.

3. Dixon BS, Novak L, Fangman J. Hemodialysis vascular access survival: upper-arm native arteriovenous fistula. Am J Kidney Dis 2002 Jan;39(1):92-101.

4. Rothuizen TC, Wong C, Quax PH, van Zonneveld AJ, Rabelink TJ, Rotmans JI. Arteriovenous access failure: more than just intimal hyperplasia? Nephrol Dial Transplant 2013 May;28(5):1085-92.

5. Li DY, Faury G, Taylor DG, Davis EC, Boyle WA, Mecham RP, et al. Novel arterial pathology in mice and humans hemizygous for elastin. J Clin Invest 1998 Nov 15;102(10):1783-7.

6. Wise SG, Weiss AS. Tropoelastin. Int J Biochem Cell Biol 2009 Mar;41(3):494-7.

7. Wagenseil JE, Mecham RP. New insights into elastic fiber assembly. Birth Defects Res C Embryo Today 2007 Dec;81(4):229-40.

8. Harris LK, Aplin JD. Vascular remodeling and extracellular matrix breakdown in the uterine spiral arteries during pregnancy. Reprod Sci 2007 Dec;14(8 Suppl):28-34.

9. Harris LK, Smith SD, Keogh RJ, Jones RL, Baker PN, Knofler M, et al. Trophoblast- and vascular smooth muscle cell-derived MMP-12 mediates elastolysis during uterine spiral artery remodeling. Am J Pathol 2010 Oct;177(4):2103-15.

10. Saracini C, Bolli P, Sticchi E, Pratesi G, Pulli R, Sofi F, et al. Polymorphisms of genes involved in extracellular matrix remodeling and abdominal aortic aneurysm. J Vasc Surg 2012 Jan;55(1):171-9.

11. Li DY, Faury G, Taylor DG, Davis EC, Boyle WA, Mecham RP, et al. Novel arterial pathology in mice and humans hemizygous for elastin. J Clin Invest 1998 Nov 15;102(10):1783-7.

12. Wong CY, de Vries MR, Wang Y, van der Vorst JR, Vahrmeijer AL, van Zonneveld AJ, et al. Vascular remodeling and intimal hyperplasia in a novel murine model of arteriovenous fistula failure. J Vasc Surg 2013 May 15.

13. Clinical practice guidelines for vascular access. Am J Kidney Dis 2006 Jul;48 Suppl 1:S248-S273.

14. Lee ES, Shen Q, Pitts RL, Guo M, Wu MH, Sun SC, et al. Serum metalloproteinases MMP-2, MMP-9, and metalloproteinase tissue inhibitors in patients are associated with arteriovenous fistula maturation. J Vasc Surg 2011 Aug;54(2):454-9.

15. Lee ES, Shen Q, Pitts RL, Guo M, Wu MH, Yuan SY. Vein tissue expression of matrix metalloproteinase as biomarker for hemodialysis arteriovenous fistula maturation. Vasc Endovascular Surg 2010 Nov;44(8):674-9.

16. Burke SK, Franano FN, Mendenhall V, Howk K, LaRochelle A, Wong M, et al. Recombinant human elastase (PRT-201) dilates outflow veins in a rabbit model of arteriovenous fistula. Abstract at Kidney Week, American Society of Nephrology; 2008. .

17. Hye RJ, Peden EK, O'Connor TP, Browne BJ, Dixon BS, Schanzer AS, et al. Human type I pancreatic elastase treatment of arteriovenous fistulas in patients with chronic kidney disease. J Vasc Surg 2014 Aug;60(2):454-61.

18. Strauss BH, Robinson R, Batchelor WB, Chisholm RJ, Ravi G, Natarajan MK, et al. In vivo collagen turnover following experimental balloon angioplasty injury and the role of matrix metalloproteinases. Circ Res 1996 Sep;79(3):541-50.

19. Owens GK, Kumar MS, Wamhoff BR. Molecular regulation of vascular smooth muscle cell differentiation in development and disease. Physiol Rev 2004 Jul;84(3):767-801.

20. Brooke BS, Bayes-Genis A, Li DY. New insights into elastin and vascular disease. Trends Cardiovasc Med 2003 Jul;13(5):176-81.

21. Ito S, Ishimaru S, Wilson SE. Inhibitory effect of type 1 collagen gel containing alpha-elastin on proliferation and migration of vascular smooth muscle and endothelial cells. Cardiovasc Surg 1997 Apr;5(2):176-83.

22. Ooyama T, Fukuda K, Oda H, Nakamura H, Hikita Y. Substratum-bound elastin peptide inhibits aortic smooth muscle cell migration in vitro. Arteriosclerosis 1987 Nov;7(6):593-8.

23. Roy-Chaudhury P, Arend L, Zhang J, Krishnamoorthy M, Wang Y, Banerjee R, et al. Neointimal hyperplasia in early arteriovenous fistula failure. Am J Kidney Dis 2007 Nov;50(5):782-90.

24. Li DY, Brooke B, Davis EC, Mecham RP, Sorensen LK, Boak BB, et al. Elastin is an essential determinant of arterial morphogenesis. Nature 1998 May 21;393(6682):276-80.

25. Misra S, Doherty MG, Woodrum D, Homburger J, Mandrekar JN, Elkouri S, et al. Adventitial remodeling with increased matrix metalloproteinase-2 activity in a porcine arteriovenous polytetrafluoroethylene grafts. Kidney Int 2005 Dec;68(6):2890-900.

26. Misra S, Shergill U, Yang B, Janardhanan R, Misra KD. Increased expression of HIF-1alpha, VEGF-A and its receptors, MMP-2, TIMP-1, and ADAMTS-1 at the venous stenosis of arteriovenous fistula in a mouse model with renal insufficiency. J Vasc Interv Radiol 2010 Aug;21(8):1255-61.

27. Rotmans JI, Velema E, Verhagen HJ, Blankensteijn JD, de Kleijn DP, Stroes ES, et al. Matrix metalloproteinase inhibition reduces intimal hyperplasia in a porcine arteriovenous-graft model. J Vasc Surg 2004 Feb;39(2):432-9.

28. Franano FN, Hance K, Bland KS, Burke SK. PRT-201 dilates outflow veins and improves maturation rates in a rabbit model of AVF. 22 ed. 2007.

29. Amabile PG, Wong H, Uy M, Boroumand S, Elkins CJ, Yuksel E, et al. In vivo vascular engineering of vein grafts: directed migration of smooth muscle cells by perivascular release of elastase limits neointimal proliferation. J Vasc Interv Radiol 2002 Jul;13(7):709-15.

30. Wong AH, Waugh JM, Amabile PG, Yuksel E, Dake MD. In vivo vascular engineering: directed migration of smooth muscle cells to limit neointima. Tissue Eng 2002 Apr;8(2):189-99.

31. Buus CL, Pourageaud F, Fazzi GE, Janssen G, Mulvany MJ, De Mey JG. Smooth muscle cell changes during flow-related remodeling of rat mesenteric resistance arteries. Circ Res 2001 Jul 20;89(2):180-6.

32. Cheung AK, Sarnak MJ, Yan G, Dwyer JT, Heyka RJ, Rocco MV, et al. Atherosclerotic cardiovascular disease risks in chronic hemodialysis patients. Kidney Int 2000 Jul;58(1):353-62.

33. Kennedy R, Case C, Fathi R, Johnson D, Isbel N, Marwick TH. Does renal failure cause an atherosclerotic milieu in patients with end-stage renal disease? Am J Med 2001 Feb 15;110(3):198-204.

34. Kokubo T, Ishikawa N, Uchida H, Chasnoff SE, Xie X, Mathew S, et al. CKD accelerates development of neointimal hyperplasia in arteriovenous fistulas. J Am Soc Nephrol 2009 Jun;20(6):1236-45.

Supplemental Data

Alpha smooth muscle actin staining

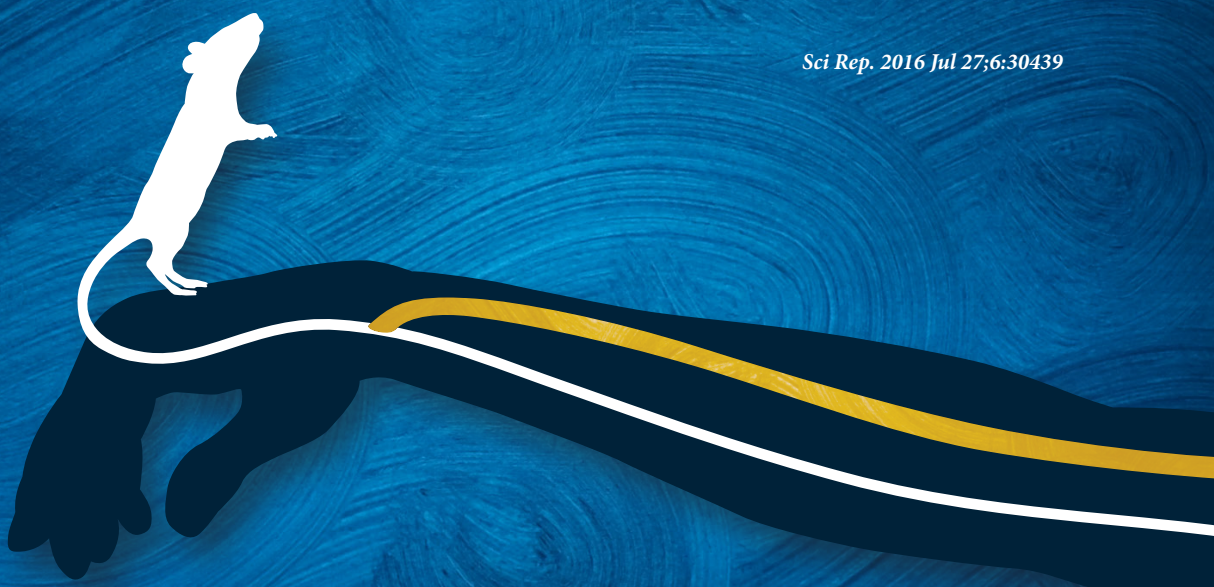
For the α-sma staining, deparaffinization and hydration of the 5 μm sections was followed by a treatment with 1% hydrogen peroxide and 5% bovine serum albumine in order to block the endogenous peroxidase and aspecific binding sites respectively. Incubation of the primary antibody was performed overnight at room temperature. Subsequently, sections were incubated at room temperature for 1 hour with HRP labelled antibodies against mouse IgG (Dako, Glostrup, Denmark) at 1:1000 dilution. Immunoreactive tissue was then developed by using a DAB peroxidase substrate kit (Dako, Glostrup, Denmark). Sections were counterstained with hematoxylin.

Chapter 6

Liposomal prednisolone inhibits vascular inflammation and enhances venous outward remodeling in a murine arteriovenous fistula model

ChunYu Wong, Taisiya Bezhaeva, Tonia C. Rothuizen, Josbert M. Metselaar, Margreet R. de Vries, Floris P.R. Verbeek, Alexander L. Vahrmeijer, Anouk Wezel, Anton-Jan van Zonneveld, Ton. J. Rabelink, Paul H.A. Quax and Joris I. Rotmans

Sci Rep. 2016 Jul 27;6:30439



Abstract

Arteriovenous fistulas (AVF) for hemodialysis access have a 1-year primary patency rate of only 60%, mainly as a result of maturation failure that is caused by insufficient outward remodeling and intimal hyperplasia. The exact pathophysiology remains unknown, but the inflammatory vascular response is thought to play an important role. In the present study we demonstrate that targeted liposomal delivery of prednisolone increases outward remodeling of the AVF in a murine model. Liposomes accumulate in the post-anastomotic area of the venous outflow tract in which the vascular pathology is most prominent in failed AVFs. On a histological level, we observed a reduction of lymphocytes and granulocytes in the vascular wall. In addition, a strong anti-inflammatory effect of liposomal prednisolone on macrophages was demonstrated *in vitro*. Therefore, treatment with liposomal prednisolone might be a valuable strategy to improve AVF maturation.

Introduction

Arteriovenous fistulas (AVFs) are the preferred type of permanent vascular access for hemodialysis in view of their superior patency and lower rate of infectious complications, when compared to prosthetic arteriovenous grafts. However, the durability of AVFs is far from optimal with a 1-year primary patency of only 60%[1]. AVF maturation refers to the process of enlargement of the lumen of the access conduit and the concomitant increase in blood flow, both needed to allow safe cannulation and adequate hemodialysis treatment. The exact mechanisms underlying maturation failure are unknown, but impaired outward remodeling as well as intimal hyperplasia (IH) are both considered to contribute[2]. Animal studies have shown that the adaptive response that occurs upon AVF creation, is characterized by marked vascular inflammation as illustrated by the infiltration of macrophages and lymphocytes[3, 4] as well as the up regulation of pro-inflammatory cytokines[5]. In addition, recent clinical studies suggest that this inflammatory response is harmful for AVF maturation, by showing that plasma levels of C-reactive protein are inversely correlated with successful AVF maturation[6].

Glucocorticoids (GCs) are well-known anti-inflammatory drugs that are widely used for the treatment of numerous inflammatory diseases[7]. Despite their excellent anti-inflammatory efficacy, the therapeutic use of systemic GCs is hampered by the high risk of occurrence of adverse side effects. Nanoparticle therapeutics such as liposomes have shown to facilitate selective delivery of drugs to inflamed tissues with a highly permeable microvasculature[8], where liposomes are being phagocytized by macrophages[9].

In the present study, we evaluated the feasibility and efficacy of liposomal prednisolone (L-Pred) to target the inflamed peri-anastomotic region of murine AVFs and assessed its effect on the morphometry and composition of the venous outflow tract. Subsequently, we assessed the efficacy of L-Pred to reduce the inflammatory profile of cultured macrophages and evaluated its effect on vascular smooth muscle cell (VSMC) proliferation *in vitro*.

Results

Surgical outcome

In total, 54 mice received an AVF (PBS; n=10, L-PBS; n=8 Pred; n=9, L-Pred; n=10, gold-containing PEG-liposomes; n=3), of which 14 mice (26%) did not survive the surgical procedure. The number of deaths did not differ significantly between the different intervention groups when compared to the PBS treated group. In 6 of the 14 mice (43%), the cause of death was clearly due to postoperative bleeding in the surgical area. In the rest of the cases, the cause

of death was unclear. The surviving mice showed normal behavior after recovering from the surgery until time to sacrifice. Figure 1, A-B and video 1-2 illustrate the AVF directly after surgery as well as circulating liposomes shortly after intravenous administration.

With regard to adverse effects of systemic prednisolone phosphate therapy, animals that received either liposomal prednisolone phosphate or free prednisolone phosphate both showed disturbed wound healing in the ears that was caused by the placement of earmarks at the start of the surgical procedure. However, we did not observe any disturbance in the wound healing of the skin incisions located in the neck and upper leg. Apart from this adverse effect, the general condition of all the animals remained normal during the study.

Patency

Using near infrared fluorescence (NIRF) (Figure 1, C-D and video 3-4), we observed a 100% patency in all the groups except for the mice treated with prednisolone in which 2 out of the 9 (22%) AVFs were occluded at time of sacrifice. This difference in patency was not significant when compared to PBS (P=0.15). These two occluded AVFs were excluded from further analysis.

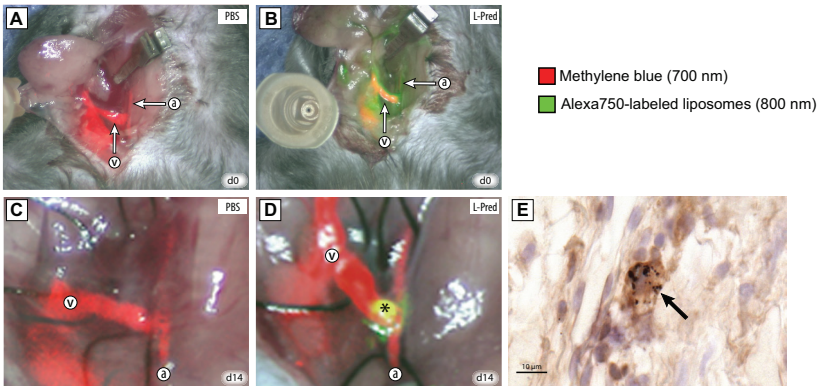


Figure 1. Localization of liposomes using near infrared fluoroscopy and immunohistochemistry. (A-B) In vivo imaging using NIRF of the AVF directly after creation (day 0) in mice that were injected with PBS (A) or L-Pred (B). Red color overlay corresponds to the intravenously administered methylene blue visualized on the 700 nm channel. Green color overlay corresponds to the intravenously administered liposomes that are labeled with the Alexa-750 fluorochrome visualized on the 800 nm channel. (C-D) In vivo imaging using NIRF of the AVF at time of sacrifice (day 14) in mice that were injected with either PBS (C) or L-Pred (D) at day 0, 2, 5 and 10. (*) Extravasation of liposomes in the anastomotic area of the AVF. (E) Double staining against F4/80 and gold particles showing accumulation of gold-labeled liposomes in macrophages in the venous outflow tract (black arrows). (a) Artery, (v) Vein. Bar = 10 µm

Distribution of liposomes in murine AVF

At 14 days after surgery, liposomes accumulated in the peri-anastomotic area of the AVF as assessed, by NIRF imaging (Figure 1D and video 4). At this time, 4 days after the last injection, no circulating liposomes were detected. Histological analysis of the venous outflow tract in mice that were injected with the gold-labeled liposomes, showed marked accumulation of gold in F4/80(+) macrophages (Figure 1E).

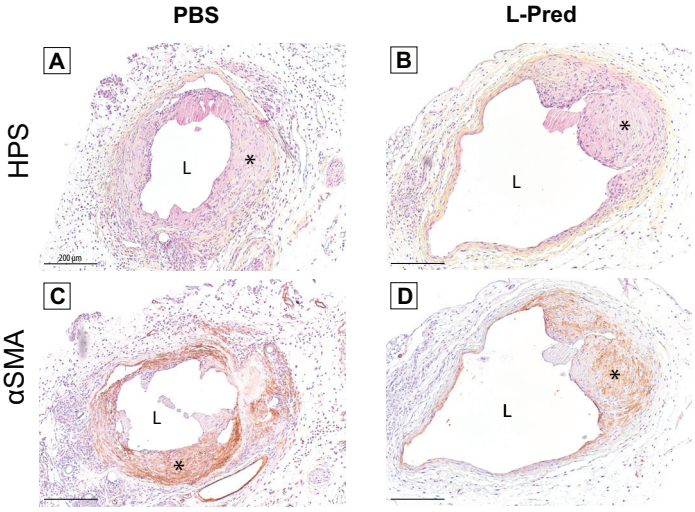


Figure 2. Histological stainings of the venous outflow tract of the AVF at day 14 after surgery. (A-B) Hematoxylin, phloxin and saffron staining (HPS). (C-D) Immunohistological staining against α-smooth muscle actin. (*) Intimal hyperplasia, (L) Lumen, Original magnification 100x. Bar = 200 µm

Morphometric analysis

Representative sections from the venous outflow tract of the AVF are shown in figure 2A-B. At day 14 after surgery, the mice that were treated with L-Pred showed a 27 % larger circumference of the external jugular vein when compared to the PBS-treated group (P=0.004), whereas no significant differences were observed in the Pred-treated mice (P= 0.195) or L-PBS treated mice (P=0.396) (Figure 3A).

No significant differences were observed in intimal area in the experimental groups (L-Pred: P=0.052, Pred: P=0.350, L-PBS: P=0.494) when compared to PBS-treated mice (Figure 3B). Immunohistochemical staining revealed that the vast majority of the cells in the intima stained positive for α-SMA in all the groups (Figure 2, C-D).

The luminal area in the L-pred treated mice showed a 47% increase compared to the PBS treated mice (P=0.042), whereas the mice treated with Pred (P=0.766) or L-PBS (P=0.861) did not show a significant difference when compared to the PBS-treated mice (Figure 3C).

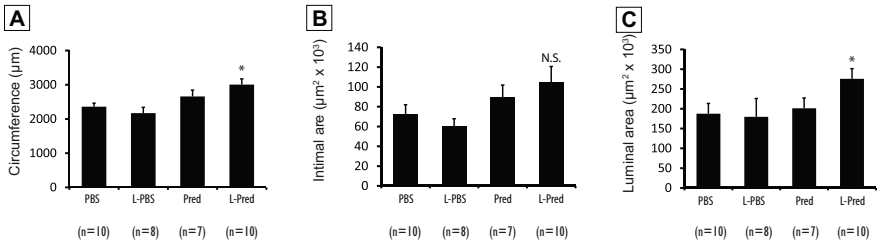


Figure 3. Histomorphometric parameters 14 days after AVF surgery. (A) Venous circumference. (B) Intimal area at the venous outflow tract. (C) Luminal area at the venous outflow tract. (*) $P < 0.05$ compared to PBS, (N.S) not significant compared to PBS.

Inflammatory response in the AVF

Representative sections of the immunohistochemical staining against CD45 and CD3 are shown in figure 4, A-F. Immunohistochemical analysis of sections obtained from the venous outflow tract revealed that the mean number of CD45(+) cells present in the venous outflow tract of the L-Pred treated mice was reduced by 83%, when compared to the mice treated with PBS (P<0.001). A trend towards reduction of CD45-positive cells in the venous vascular wall was observed in the Pred-treated mice, when compared to PBS (P=0.069) (Figure 5A). Additional immunohistochemical stainings for subsets of inflammatory cells revealed a 86% decrease in CD3(+) T-cells (p<0.001) and a 51% decrease in GR1(+) granulocytes (P=0.008) in the L-Pred treated group when compared to the PBS treated group (Figure 5, B-D).

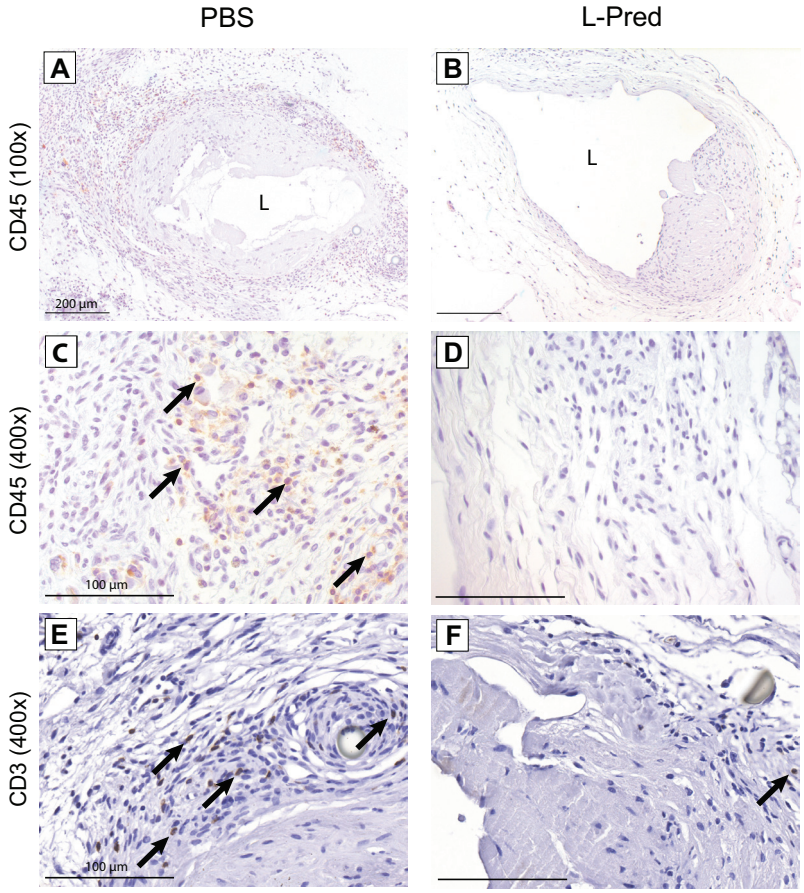


Figure 4. Representative sections of immunohistochemical stainings against CD45 and CD3 at 14 days after AVF surgery. (A-D) CD45(+) cells (black arrow) in the venous outflow tract of the AVF. (E-F) CD3(+) cells (black arrow) in the venous outflow tract of AVF. Original magnification (A-B): 100x. Bar = 200 µm, (C-F): 400x, Bar = 100 µm (L) Lumen.

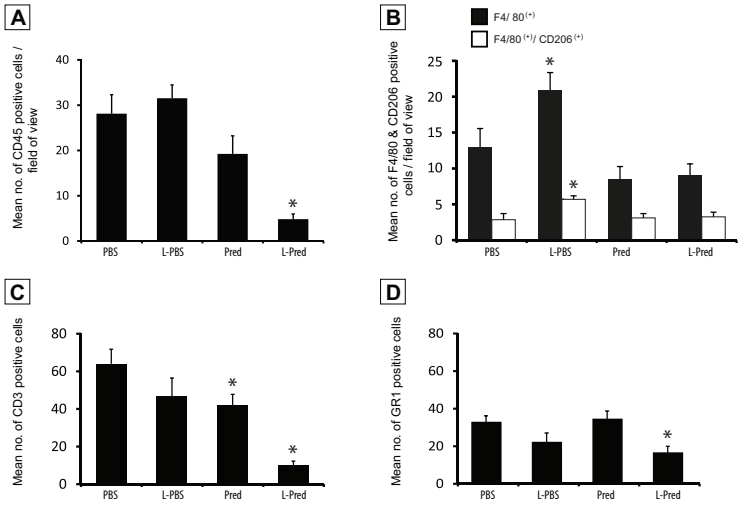


Figure 5. Quantification of immunohistological staining against different inflammatory cells at day 14. (A): CD45(+) leucocytes. (B) F4/80(+) macrophages and F4/80(+)CD206(+) M2 macrophages. (C) CD3(+) granulocytes. (D) GR1(+) granulocytes in the venous outflow tract of AVF at day 14. (*) $P < 0.05$ compared to PBS.

Inflammatory effect of L-Pred in cultured macrophages

To study the inflammatory effects on a mRNA level, we exposed murine M1 and M2 macrophages to L-Pred, L-PBS, Pred and PBS. Upon incubation with L-Pred and Pred, a strong reduction was observed in the expression of pro-inflammatory genes including TNF-α, MCP-1 and IL-6 (all P<0.01) by M1 polarized macrophages, whereas M2 macrophages showed a significant increase in the expression of the anti-inflammatory cytokine IL-10 after addition of L-Pred and L-PBS (both P<0.01) when compared to the incubation with PBS (Figure. 6, A-D).

Effect of liposomal prednisolone on the expression of MMPs and TIMP.

We measured the expression of matrix metalloproteinases (MMP-2 and MMP-9) and their endogenous inhibitors (TIMP-2 and TIMP-1, respectively) on RNA level in M1 macrophages. Upon incubation with L-Pred, both MMP-2 and MMP-9 expression decreased when compared to PBS incubation. In addition, both the TIMP1/MMP-9 and the TIMP2/ MMP-2 ratio increased upon incubation with L-Pred when compared to PBS incubation (Figure 7, A-D).

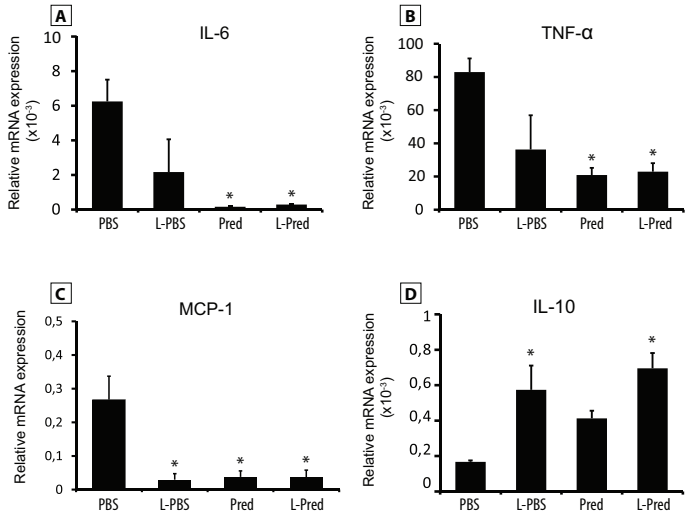


Figure 6. mRNA expression levels of pro- and anti-inflammatory cytokines in macrophages in vitro after incubation with PBS (control medium), L-PBS, Pred and L-Pred. (A-C) Relative mRNA expression of pro-inflammatory cytokines (IL-6, TNF-α and MCP-1) in M1 macrophages and (D) the anti-inflammatory cytokine IL-10 in M2 macrophages. The relative expression is normalized against GAPDH. (*) $P < 0.05$ compared to PBS.

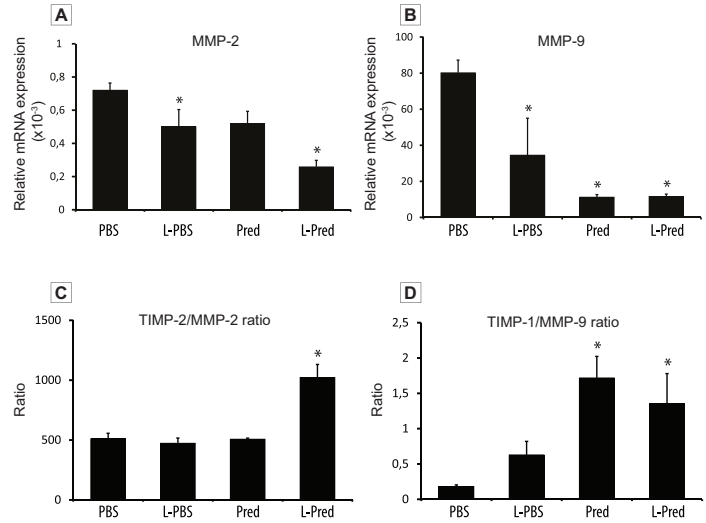


Figure 7. mRNA expression levels of MMP-2, MMP-9 and the ratios of TIMP-2/MMP-2 and TIMP-1/MMP-9 in macrophages after incubation with PBS (control medium), L-PBS, Pred and L-Pred. (A-B) Relative mRNA expression of MMP-2 and MMP-9. (C-D) Ratios of TIMP-2/MMP-2 and TIMP-1/MMP-9. Expression was normalized against GAPDH. (*) $P < 0.05$ compared to PBS.

Discussion

In the present study, we demonstrate that intravenously administered liposomes selectively target the anastomotic region and can effectively improve venous outward remodeling of murine AVF when prednisolone is encapsulated in the liposomes.

Liposomes are one the most prominent drug carrier systems currently available, due to their relative easy preparation using biocompatible components and the high drug payload[10]. Moreover, liposomes can hold their payload while circulating in the vasculature until they extravasate and accumulate at sites of inflammation as a result of enhanced vascular permeability in inflamed tissues, thereby reducing possible systemic adverse side effects[11]. The PEG-coating of liposomes is designed to improve their bioavailability in inflamed tissues as it serves as a steric barrier that minimizes liposomal uptake by circulating mononuclear cells[12]. Once extravasated, the liposomes are recognized as foreign particles and phagocytized by macrophages[10]. Using NIRF and immunohistochemistry, we demonstrated that liposomes indeed accumulate in macrophages in the anastomotic area of murine AVF. These results are consistent with previous studies in rabbits[13] and humans[14] which revealed marked accumulation of liposomes in macrophages within inflammatory atherosclerotic plaques.

GCs are powerful anti-inflammatory drugs that act through binding to cytosolic glucocorticoid receptors in target cells, leading to a reduction in the expression of pro-inflammatory cytokines and diminished recruitment of inflammatory cells[15, 16]. Despite these potent anti-inflammatory effects, chronic and systemic therapeutic use of GCs is limited by the high incidence of serious adverse effects[16]. Moreover, as a result of rapid clearance from the circulation, systemic administration of GCs results in low efficacy of drug delivery at the target location. Therefore, encapsulation of GCs in liposomal nanoparticles has great potential to enhance the therapeutic effect of GCs in inflamed tissues. Previous studies on L-Pred in murine model of arthritis[17] have underscored this potential, as complete remission of the inflammatory response was shown upon a single injection, which was superior to the effect of unencapsulated prednisolone.

Preclinical studies have shown that GCs reduce the formation of both arterial and venous stenotic lesions[18-20]. However, the role of inflammation in vascular remodeling upon AVF surgery has not been elucidated yet. Although various animal studies[3-5, 21] revealed infiltration of inflammatory cells in the venous outflow tract in the early phase after AVF surgery, it is unclear whether this inflammatory response directly contributes to maturation failure. Our experiments revealed that L-Pred resulted in inhibition of vascular inflammation in the AVF, as illustrated by a significant reduction of lymphocytes and granulocytes in the venous outflow tract. Interestingly, treatment with unencapsulated prednisolone resulted solely in a modest reduction in inflammatory cells , suggesting that liposomal encapsulation indeed

resulted in a higher concentration of prednisolone in the venous outflow tract. As shown *in vitro,* L-Pred induced a conversion towards an anti-inflammatory profile of macrophages, as demonstrated previously[22]. Moreover, liposomes themselves contribute to the reduction of the pro-inflammatory profile of macrophages, as illustrated by the reduction of pro-inflammatory cytokines in M1 macrophages upon stimulation with L-PBS. This shift towards an anti-inflammatory profile of macrophages might have inhibited the recruitment of lymphocytes and granulocytes to the injured vessels of the AVF. Alternatively, prednisolone might have had a direct effect on lymphocytes and granulocytes as GCs can easily pass the cellular membrane of macrophages in both directions.

While previous studies evaluated the therapeutic effect of GCs to inhibit IH in various vascular injury models[18-20], none of these studies focused on its effect on vascular remodeling. The question arises how treatment with L-Pred resulted in enhanced outward remodeling in the venous outflow tract of AVF. In order to investigate whether L-Pred influenced VSMC proliferation and collagen production, we directly stimulated cultured murine VSMCs with L-Pred. However, no significant effect on VSMC proliferation and collagen synthesis was observed. (data not shown).

MMPs are a group of proteolytic enzymes involved in vascular remodeling by facilitating the turnover of extracellular matrix components such as collagen and elastin[23]. The effect of MMPs on the vascular remodeling depend on the specific MMPs that are activated and the type of vascular injury[24]. Previous studies in a porcine balloon angioplasty model in peripheral arteries revealed that treatment with the MMP-inhibitor marimastatin resulted in reduced constrictive arterial remodeling in favor of expansive remodeling[25]. The exact contribution of MMPs in vascular remodeling in AVF stills remains to be elucidated. Previous studies suggest that the effect of MMP activation on vascular remodeling in AVF might differ between the arterial and venous segment. Indeed, Castier et al. observed that enhanced MMP-9 activity coincided with increased outward remodeling in the arterial segment of murine AVF, whereas studies by Nieves Torres et al[27] revealed that MMP inhibition enhanced venous outward remodeling in AVF. In the latter study, adventitial delivery of a small hairpin RNA against the MMP ADAMTS-1, resulted in reduced macrophage infiltration, decreased MMP-9 activity and enhanced venous outward remodeling in murine AVF. Although we have not been able to quantify MMP activity *in vivo*, we speculate that the enhanced venous outward remodeling in murine AVF that occurred upon treatment with L-Pred is mediated by the dampened inflammatory response and decreased MMP activity in macrophages. In addition, a recent clinical trial evaluating the efficacy of the MMP-inhibitor doxycycline to inhibit growth of abdominal aortic aneurysms resulted in an unexpected acceleration of the aneurysmal growth[26]. These data suggest that in certain vascular disease conditions, inhibition of MMPs could enhance outward remodeling.

Interestingly, elegant studies by Nieves Torres and coworkers[27] suggest a similar effect of MMP inhibiton on venous outward remodeling in AVF. Indeed, adventitial delivery of a small hairpin RNA against the MMP ADAMTS-1, resulted in reduced macrophage infiltration, decreased MMP-9 activity and enhanced outward remodeling in murine AVF. Although we have not been able to quantify MMP activity *in vivo*, we speculate that the enhanced outward remodeling in murine AVF that occurred upon treatment with L-Pred is mediated by the dampened inflammatory response and decreased MMP activity in macrophages.

In contrast to its effect on outward remodeling, no inhibitory effect of L-Pred on IH in the venous outflow tract was observed. These results deviate from other preclinical studies that evaluated the therapeutic effect of GCs in other vascular injury models, that have reported a strong inhibitory effect of dexamethasone on IH[18-20]. This discrepancy may result from a difference in potency between prednisolone and dexamethasone to inhibit VSMC proliferation[28]. Alternatively, it may relate to the difference in pathophysiological stimuli that contribute to IH after arterial injury, when compared to venous IH in AVF. While hemodynamic stimuli are considered to be of vital importance for IH[29, 30], the contribution of inflammation to IH in AVF might be limited, as suggested by our results. Interestingly, our study showed an increase in OR that was accompanied by a trend towards an increase in IH, which could potentially reduce the luminal area and therefore blood flow. Although the exact explanation for this phenomenon is not fully elucidated, we believe that this is due to the fact that both OR and IH are processes that involves VSMC proliferation. As a consequence, interventions that facilitate OR might therefore also result in a (modest) stimulation of IH. Of note, a stimulatory effect of an intervention on OR is more important for the ultimate luminal surface area than the coinciding effect on IH, as there is a quadratic relationship between radius and surface area of the vessel.

Preclinical studies in pigs[4] revealed that the inflammatory response in the venous outflow tract of AVF is temporal, peaking in the early weeks after surgery. This acute, localized inflammatory response makes the application of L-Pred particularly appealing as a short-term treatment in the first weeks after surgery.

In conclusion, liposomal prednisolone reduces the local inflammatory response and stimulates venous outward remodeling in murine AVF. Therefore, treatment with liposomal prednisolone might be valuable strategy to reduce AVF non-maturation. The efficacy of liposomal prednisolone to enhance AVF maturation in ESRD patients will be evaluated in the LIPMAT trial (clinicaltrial.gov ID NCT0249566), a double-blind, randomized, placebo-controlled trial that will commence in Q4 of 2015.

Methods

Liposomes

Prednisolone polyethylene glycol-coated (PEG)-liposomes were prepared as described in the supplemental data and contained 2 mg prednisolone phosphate per ml. The PEG-liposomes were labeled with Alexa 750 succinimidyl (Invitrogen, Carlsbad, CA, USA) and contained either prednisolone phosphate (Fagron, Capelle aan den IJssel, The Netherlands) or PBS. In order to trace the liposomes microscopically, additional PEG liposomes were coupled to gold particles (Nanoprobes, Yaphank, NY, USA).

Animal experiment

The Institutional Committee for Animal Welfare at the Leiden University Medical Center approved all animal experiments that were performed in accordance with the relevant guidelines and regulations. Adult male C57bl6 mice aged 10-11 weeks were used for the experiments and received an unilateral AVF between the dorsomedial branch of the external jugular vein and the common carotid artery in an end-to-side manner as previously described[3]current murine models of AVF failure do not incorporate the surgical configuration that is commonly used in humans. Because the hemodynamic profile is one of the key determinants that play a role in vascular remodeling in the AVF, it is preferable to use this same configuration in an animal model. Here we describe a novel murine model of AVF failure in which the configuration (end-to-side (supplemental data). At the end of the procedure, either L-Pred (10 mg/kg bodyweight), Pred (10 mg/kg bodyweight) (Fagron), L-PBS or PBS was injected intravenously. The dose was determined according to the guidelines of the Food and Drugs Administration, in which the safe starting dose level of prednisolone was set at 1 mg/kg. The injection volume of L-PBS and PBS was equal to the injected volume of the L-Pred and Pred (200 μL). Due to a positive additive effect of multiple injections as compared to a single injection[31], we injected the mice intravenously at day 2,5 and 10. In addition, 3 separate mice received a single bolus injection intravenously of gold-labeled empty liposomes (130 μL) at day 2 to evaluate liposomal accumulation in the AVF microscopically. All mice were sacrificed 14 days after the surgical procedure.

Near-infrared fluorescence imaging

To assess the accumulation of the liposomes macroscopically, we used the near infrared fluorescence (NIRF) imaging technique3current murine models of AVF failure do not incorporate the surgical configuration that is commonly used in humans. Because the hemodynamic profile is one of the key determinants that play a role in vascular remodeling in

the AVF, it is preferable to use this same configuration in an animal model. Here we describe a novel murine model of AVF failure in which the configuration (end-to-side directly after surgery and at time of sacrifice. After positioning of the Fluorescence Assisted Resection and Exploration (FLARE) imaging system (Center for Molecular Imaging, Boston, MA, USA) approximately 46 cm above the AVF, 200 µl 1% methylene blue (Sterop, Belgium) dissolved in saline was injected in the left femoral vein to assess the patency of the AVF. Video images were captured with 30-frames-per-second. Multiple video channels (color video, 700 nm and 800 nm) were obtained simultaneously with 60 milliseconds exposure times. After computer-controlled image acquisition, color video and NIRF images were displayed individually and merged in real-time. The 800 nm and 700 nm channel were used for imaging the liposomes and methylene blue, respectively.

Tissue harvesting and processing

Fourteen days after surgery, the mice were anesthetized (supplemental data) whereupon the AVF was dissected and assessed using NIRF as described above. Next, the inferior vena cava was transsected followed by mild pressure perfusion fixation with 4% formalin through an intracardiac perfusion. The tissue was processed to paraffin and 5 µm-thick sections of the venous outflow tract were made perpendicular to the vein with an interval of 150 µm.

Morphometric analysis

Morphometric analysis was performed on Weigert's elastin stained sections using quantitative imaging software (Qwin, Leica, Wetzlar, Germany). The intimal area was calculated by subtracting the luminal area from the area within the internal elastic lamina (IEL). The circumference of the vessel was determined by measuring the length of the IEL. Results are expressed as mean ± SEM.

Immunohistochemical staining and analysis

All immunohistochemical quantifications were performed on the first 3 venous sections starting from the anastomosis per AVF. Slides were digitized using an automated microscopic scanner (Panaoramic digital MIDI slice scanner, 3DHISTECH, Hungary). Detailed protocols of the immunohistochemical stainings are listed in supplemental data.

Serial sections from each AVF were stained with the following antibodies: anti- α-smooth muscle actin (α-SMA) for vascular smooth muscle cells and myofibroblasts (Dako, Glostrup, Denmark); anti-CD45 for leukocytes (BD Pharmingen, San Diego, California, USA); anti-F4/80 for macrophages (Abcam, Cambridge, UK); anti-CD-206 for anti-inflammatory (M2) macrophages (Abcam); anti-CD-3 for T-lymphocytes (Abcam) and GR-1 for granulocytes

(from G. Kraal, VUMC, Amsterdam, The Netherlands). To distinguish anti-inflammatory (M2) macrophages from the whole macrophage population anti-F4/80 and anti-CD-206 antibodies were combined in a double immunofluorescence staining.
For the immunohistochemical analysis of the CD206-F4/80 and CD45 staining, the number of positive cells was counted in two random fields of view using a 400x magnification from which the mean was calculated. In view of the limited presence of CD3+ and GR1+ cells, quantification of these cells was performed by counting all positive cells that were present in the venous segment of the AVF. Gold-labeled liposomes were visualized using the LI Silver enhancement kit (Nanoprobes) and combined with the F4/80 staining.

Generation and stimulation of bone marrow derived macrophages

To generate bone marrow-derived macrophages (BMDM) femurs of healthy C57Bl/6 male mice (n=3) were flushed with sterile PBS. Total bone marrow progenitor cells (BMPCs) were centrifuged at 300g at 4 °C for 10 min and incubated for 5 min on ice with erythrocyte lysis buffer (Sigma-Aldrich R7757, St. Louis, MO, USA). After erythrocytes were depleted, remaining cells were washed three times with PBS, centrifuged at 300g at 4 °C for 10 min, and resuspended in RPMI medium supplemented with 20% fetal calf serum (FCS), 2 mmol/L l-glutamine, 100 U/ml penicillin, 100 mg/ml streptomycin (all from PAA, Colbe, Germany). To promote differentiation of BMPCs towards macrophages, cultured medium was supplemented with 10 ng/ml of macrophage colony-stimulating factor (M-CSF) (Peprotech, Rocky Hill, NJ, USA). Cells were seeded at a density of 1.0*106 cells per well, and the medium was replaced on day 3 and 5.
On day 7, cells were stimulated either with LPS (100ng/ml) and IFN-gamma (10ng/ml) to differentiate them towards pro-inflammatory (M1) phenotype or with IL-4 (10ng/ml) and IL-13 (10ng/ml) (all from Preprotech) for anti-inflammatory (M2) phenotype. On the same day Pred (10 μg/ml), L-Pred (10 μg/ml), L-PBS or control medium was added to the cells (n=3). After 24 hours the supernatant was collected and cells were lysed for RNA isolation.

RNA isolation, cDNA synthesis and qPCR

Total RNA was extracted from the macrophages cells using Trizol reagent (Invitrogen, Carlsbad, CA, USA). RNA was reverse transcribed using a 5-minute 65°C incubation of 1 μg total RNA with deoxyribonucleotide triphosphates (Invitrogen) and random primers (Invitrogen). c-DNA was synthesized using an M-MLV First-Strand Synthesis system (Invitrogen), and used for quantitative analysis of mouse genes (supplemental data) with an SYBR Green Master Mix (Applied Biosystems, Foster City, CA, USA). Levels of gene expression were determined by normalization to murine glyceraldehyde 3-phosphate dehydrogenase (GAPDH).

Statistical analysis

All data except the patency outcome were expressed as mean ± SEM. SPSS 20.0 was used for all statistical calculations. Except for the data on AVF patency and animal survival, all measurements were analyzed statistically using One-way ANOVA with Dunett post-hoc test with the PBS group as the reference category. A Fisher's exact test was used for the data on AVF patency and animal survival. A P-value < 0.05 was considered statistically significant.

Acknowledgements

We thank Enceladus Pharmaceuticals BV for generously manufacturing and supplying the liposomes.

Reference List

1. Tordoir,J.H. *et al.* Prospective evaluation of failure modes in autogenous radiocephalic wrist access for haemodialysis. *Nephrol. Dial. Transplant.* **18**, 378-383 (2003).

2. Rothuizen,T.C. *et al.* Arteriovenous access failure: more than just intimal hyperplasia? *Nephrol. Dial. Transplant.* **28**, 1085-1092 (2013).

3. Wong,C.Y. *et al.* Vascular remodeling and intimal hyperplasia in a novel murine model of arteriovenous fistula failure. *J. Vasc. Surg.* **59**, 192-201 (2014).

4. Wang,Y. *et al.* Venous stenosis in a pig arteriovenous fistula model--anatomy, mechanisms and cellular phenotypes. *Nephrol. Dial. Transplant.* **23**, 525-533 (2008).

5. Nath,K.A., Kanakiriya,S.K., Grande,J.P., Croatt,A.J., & Katusic,Z.S. Increased venous proinflammatory gene expression and intimal hyperplasia in an aorto-caval fistula model in the rat. *Am. J. Pathol.* **162**, 2079-2090 (2003).

6. Kaygin,M.A. *et al.* The relationship between arteriovenous fistula success and inflammation. *Ren Fail.* **35**, 1085-1088 (2013).

7. Vandevyver,S., Dejager,L., Tuckermann,J., & Libert,C. New insights into the anti-inflammatory mechanisms of glucocorticoids: an emerging role for glucocorticoid-receptor-mediated transactivation. *Endocrinology* **154**, 993-1007 (2013).

8. Farokhzad,O.C. & Langer,R. Impact of nanotechnology on drug delivery. *ACS Nano.* **3**, 16-20 (2009).

9. Schmidt,J. *et al.* Drug targeting by long-circulating liposomal glucocorticosteroids increases therapeutic efficacy in a model of multiple sclerosis. *Brain* **126**, 1895-1904 (2003).

10. Lasic,D.D. & Papahadjopoulos,D. Liposomes revisited. *Science* **267**, 1275-1276 (1995).

11. Lasic,D.D. Novel applications of liposomes. *Trends Biotechnol.* **16**, 307-321 (1998).

12. Schiffelers,R.M., Banciu,M., Metselaar,J.M., & Storm,G. Therapeutic application of long-circulating liposomal glucocorticoids in auto-immune diseases and cancer. *J. Liposome Res.* **16**, 185-194 (2006).

13. Lobatto,M.E. *et al.* Multimodal clinical imaging to longitudinally assess a nanomedical anti-inflammatory treatment in experimental atherosclerosis. *Mol. Pharm.* **7**, 2020-2029 (2010).

14. van der Valk,F.M. *et al.* Prednisolone-containing liposomes accumulate in human atherosclerotic macrophages upon intravenous administration. *Nanomedicine.* **11**, 1039-1046 (2015).

15. Cronstein,B.N., Kimmel,S.C., Levin,R.I., Martiniuk,F., & Weissmann,G. A mechanism for the antiinflammatory effects of corticosteroids: the glucocorticoid receptor regulates leukocyte adhesion to endothelial cells and expression of endothelial-leukocyte adhesion molecule 1 and intercellular adhesion molecule 1. *Proc. Natl. Acad. Sci. U. S. A* **89**, 9991-9995 (1992).

16. Rhen,T. & Cidlowski,J.A. Antiinflammatory action of glucocorticoids--new mechanisms for old drugs. *N. Engl. J. Med.* **353**, 1711-1723 (2005).

17. Metselaar,J.M., Wauben,M.H., Wagenaar-Hilbers,J.P., Boerman,O.C., & Storm,G. Complete remission of experimental arthritis by joint targeting of glucocorticoids with long-circulating liposomes. *Arthritis Rheum.* **48**, 2059-2066 (2003).

18. Pires,N.M. *et al.* Histopathologic alterations following local delivery of dexamethasone to inhibit restenosis in murine arteries. *Cardiovasc. Res.* **68**, 415-424 (2005).

19. Schepers,A. *et al.* Short-term dexamethasone treatment inhibits vein graft thickening in hypercholesterolemic ApoE3Leiden transgenic mice. *J. Vasc. Surg.* **43**, 809-815 (2006).

20. Villa,A.E. *et al.* Local delivery of dexamethasone for prevention of neointimal proliferation in a rat model of balloon angioplasty. *J. Clin. Invest* **93**, 1243-1249 (1994).

21. Manning,E. *et al.* A new arteriovenous fistula model to study the development of neointimal hyperplasia. *J. Vasc. Res.* **49**, 123-131 (2012).

22. Hofkens,W., Schelbergen,R., Storm,G., van den Berg,W.B., & van Lent,P.L. Liposomal targeting of prednisolone phosphate to synovial lining macrophages during experimental arthritis inhibits M1 activation but does not favor M2 differentiation. *PLoS. One.* **8**, e54016 (2013).

23. Wang,M., Kim,S.H., Monticone,R.E., & Lakatta,E.G. Matrix metalloproteinases promote arterial remodeling in aging, hypertension, and atherosclerosis. *Hypertension* **65**, 698-703 (2015).

24. Galis,Z.S. & Khatri,J.J. Matrix metalloproteinases in vascular remodeling and atherogenesis: the good, the bad, and the ugly. *Circ. Res.* **90**, 251-262 (2002).

25. Sierevogel,M.J. *et al.* Oral matrix metalloproteinase inhibition and arterial remodeling after balloon dilation: an intravascular ultrasound study in the pig. *Circulation* **103**, 302-307 (2001).

26. Meijer,C.A. *et al.* Doxycycline for stabilization of abdominal aortic aneurysms: a randomized trial. *Ann. Intern. Med.* **159**, 815-823 (2013).

27. Nieves Torres,E.C. *et al.* Adventitial delivery of lentivirus-shRNA-ADAMTS-1 reduces venous stenosis formation in arteriovenous fistula. *PLoS. One.* **9**, e94510 (2014).

28. Reil,T.D., Sarkar,R., Kashyap,V.S., Sarkar,M., & Gelabert,H.A. Dexamethasone suppresses vascular smooth muscle cell proliferation. *J. Surg. Res.* **85**, 109-114 (1999).

29. Roy-Chaudhury,P., Spergel,L.M., Besarab,A., Asif,A., & Ravani,P. Biology of arteriovenous fistula failure. *J. Nephrol.* **20**, 150-163 (2007).

30. Asif,A., Roy-Chaudhury,P., & Beathard,G.A. Early arteriovenous fistula failure: a logical proposal for when and how to intervene. *Clin. J. Am. Soc. Nephrol.* **1**, 332-339 (2006).

31. van den Hoven,J.M. *et al.* Optimizing the therapeutic index of liposomal glucocorticoids in experimental arthritis. *Int. J. Pharm.* **416**, 471-477 (2011).

Supplemental Data

Methods

Liposomal prednisolone preparation

Prednisolone phosphate polyethylene glycol-coated (PEG)-liposomes were prepared by injecting 1 mL of an alcoholic lipid solution of 1 Molar (containing dipalmitoyl phosphatidyl choline and dipalmitoyl phosphatidyl glycerol, both from Lipoid GmbH, Germany, and cholesterol (Sigma Aldrich, saint Louis, MO, USA)) in a molar percentage of 62%, 5%, and 33% of total lipid content, respectively), in 9 mL of an aqueous solution of 100 mg/ml prednisolone phosphate disodium salt (Fagron, Capelle aan den IJssel,The Netherlands). Subsequently the 10 ml crude liposome dispersion was sized by multiple extrusion at 60 degrees C using a medium pressure extruder (Lipex) equipped with two stacked polycarbonate membrane filters with 100 nm pores. Alcohol and free prednisolone phosphate (not incorporated in liposomes) were removed by ultrafiltration and replacement of the filtrate with clean phosphate buffered 0.9% saline (pH 7.4). The resulting formulation consisted of liposomes of approximately 105 nm in diameter as measured by dynamic light scattering, with a polydispersity index of 0.05 and a zeta-potential of approximately -30 mV. Content determination was done by extraction using the organic phase for lipid determination (HPLC followed by evaporative light scattering detection) and the aqueous phase to assess the prednisolone phosphate content (UV spectrophotometry at 254 nm). The liposomes contained approximately 2 mg prednisolone phosphate/mL and 70 μmol total lipid/ml. "Empty" liposomes (L-PBS) were prepared in the same manner using phosphate buffered saline instead of the aqueous prednisolone phosphate solution.

The liposomes were labeled with Alexa 750 by first mixing PEG(2000)-DSPE-NH2 and PEG(2000)-DSPE (Avanti Polar Lipids, Birmingham, AL, USA) in a 1:1 molar ratio in 0.1 M sodium bicarbonate solution at pH 8.3. This mixture was then heated at 60°C and Alexa 750 succinimidyl (Invitrogen, Carlsbad, CA, USA) was added, which led to coupling of Alexa 750 to the NH2-PEGylated lipid. This mixture was subsequently added to the liposomes and mixed under repeated temperature cycling between 60°C and room temperature, allowing the PEGylated and Alexa-conjugated lipid to insert in the liposome bilayer. In order to trace the liposomes at a microscopic level, gold-containing PEG-liposomes were prepared by adding to the PEG-liposome lipid mixture described above 0.1mol% dipalmitoyl phosphatidyl ethanolamine coupled to 1.4 nm gold particles (Nanoprobes, Yaphank NY, USA). After formation of the crude liposome dispersion multiple extrusion was performed using the same method as with prednisolone phosphate PEG-liposomes and identical size characteristics were obtained (103 nm, polydispersity index 0.08). The final formulation contained 10 μmol lipid/ml.

Surgical procedure

The animal was anesthetized using isoflurane followed by shaving and disinfection of the skin in the ventral neck area and fixed in a supine position on a heating blanket. The mouse was then injected with buprenorphin (0.1 mg/kg) (MSD, Whitehouse Station, NJ, USA) and 0.5 mL saline. Under a dissecting microscope (Leica, Wetzlar, Germany), an incision in the ventral midline of the neck area was made, followed by a dissection of the right dorsomedial branch of the external jugular vein and ipsilateral common carotid artery after the excision of the sternocleidomastoid muscle using a heat cauterizer. Next, after applying a vascular clamp (S&T, Neuhausen, Switzerland) on the proximal and distal artery an approximate 1 mm incision was made using a micro scissor (Fine Science Tools, Heidelberg, Germany) and the lumen was rinsed with a heparin solution (100 IU/ml) (LEO Pharma, Ballerup, LLDenmark). The vein was then clamped proximally and ligated distally, followed by a transection just proximal to the ligation. After rinsing the vein with a heparin solution, an end-to-side anastomosis was created using 10.0 interrupted sutures (BBraun, Melsungen, Germany). Halfway during the suturing procedure, heparin (0.2 IU/gram bodyweight) together with 200 µL of either L-Pred (10 mg/kg bodyweight), Pred (10 mg/kg bodyweight), L-PBS or PBS was injected intravenously. After completion of the anastomosis, the remaining clamps were removed and patency was assessed. The skin was closed with a 6.0 running suture (BBraun, Melsungen, Germany). Following completion of the surgery 0.5 mL of saline was injected subcutaneously and the mice were kept warm until recovery.

Sacrification and tissue harvesting

Upon sacrifice, mice received an intraperitoneal injection with an anesthetic-mixture containing midazolam (5 mg/kg) (Roche, Basel, Switzerland), medetomidine (0.5 mg/kg) (Orion, Espoo, Finland) and fentanyl (0.05 mg/kg) (Janssen, High Wycombe, UK) whereupon a reincision was made over the scar. The AVF was dissected and assessed using NIRF as described above. After a thoracotomy, the inferior vena cava was transsected followed by a mild pressure perfusion fixation with 4% formalin through an intracardiac perfusion.

Immunohistochemistry and Immunofluorescence

For immunohistochemical stainings, deparaffinization and hydration was followed by a treatment with 1% hydrogen peroxide and 5% bovine serum albumin in order to block the endogenous peroxidase and aspecific binding sites respectively. To unmask the antigens and epitopes antigen retrieval with Citrate Buffer (pH6) at 95-100 °C for 1 hour was done for CD-3, CD-206 and F4/80 antibodies. After 15 min blocking with 3% BSA (Sigma-Aldrich, , St. Louis, MO, USA) in PBS sections were incubated overnight at room temperature with specific

antibodies to goat anti-mouse F4/80 (Abcam, Cambridge, UK), rabbit anti-mouse CD-206 (Abcam, Cambridge, UK), rabbit anti-mouse CD-3 (Abcam, Cambridge, UK) and goat anti-mouse GR-1 (from G. Kraal, VUMC, Amsterdam, The Netherlands). Control sections were incubated with rabbit IgG at 1:200 or 1:1000 dilution for CD-3 or CD-206 respectively or goat IgG at 1:100 or 1:300 dilution for F4/80 or GR-1 respectively. On the next day sections were briefly rinsed in 1% BSA (Sigma-aldrich) in PBS and incubated for 1 hour at room temperature with appropriate secondary antibodies that were goat anti-rabbit IgG labeled with Alexa-488 or goat anti-rat IgG labelled with Alexa-568 (Molecular Probes) for F4/80, CD-206 double immunofluorescence staining or horseradish peroxidase conjugated (Jackson ImmunoResearc bh,Westgrove, PA) goat anti-rat IgG at 1:200 dilution or peroxidase-based EnVision kit (DAKO, Glostrup, Denmark) for GR-1 or CD-3 respectively. For horseradish peroxidase-based stainings (CD-3 and GR-1) immunoreactive tissue was then developed by using a 3,3'-diaminobenzidine peroxidase substrate kit (Dako) and counterstained with hematoxylin. For immunofluorescence F4/80+/CD-206+ double staining sections were coverslipped with ProLong® Gold Antifade with DAPI (Life technologies, California, US) to counterstain nuclei. All slides were further digitized by an automated microscopic scanner (Panoramic digital MIDI slice scanner, 3DHISTECH, Hungary). All histologic evaluations were performed in a blinded manner on the first three venous sections upstream from anastomotic area. Venous part was chosen because most of the stenotic lesions in human AVFs occur in the venous outflow tract. For CD-3 and GR-1 immunohistochemistry the total number of positive cells per section was counted. F4/80 single or CD-206 double positive immunofluorescence staining were quantified as total number of positive cells per field of view in x400 magnification.

Supplemental Data

Video 1-4. In vivo NIRF imaging of the AVF at day 0 and day 14 in mice treated with intravenously administered PBS or Alexa-750 labeled L-Pred. The red color overlay corresponds to the intravenously administered methylene blue visualized on the 700 nm channel. Green color overlay corresponds to the intravenously administered liposomes that are labeled with the Alexa-750 fluorochrome visualized on the 800 nm channel. The animal was oriented in such a fashion that the top of the screen resembles the cranioventral side.

Video 1. In vivo NIRF imaging of the AVF directly after creation (day 0) in an animal that was injected with PBS. Using methylene blue, we confirmed the patency of the AVF.

Video 2. In vivo NIRF imaging of the AVF directly after creation (day 0) in an animal that was injected with L-Pred. Intravascular circulating liposomes was confirmed together with AVF patency.

Video 3. In vivo NIRF imaging of the AVF at time of sacrification in an animal that was injected intravenously with PBS at day 0,2,5 and 10. The neck was dissected bilaterally in order to expose the contralateral side. Suture threads were placed around the venous outflow tract, proximal and distal common carotid artery of the AVF and around the contralateral branch of the external jugular vein. AVF patency was confirmed after administration of intravascular methylene blue.

Video 4. In vivo NIRF imaging of the AVF at time of sacrification in an animal that was injected intravenously with L-Pred at day 0, 2, 5 and 10. Suture threads were placed around the venous outflow tract, proximal and distal common carotid artery of the AVF and around the contralateral branch of the external jugular vein. At day 14, liposomal extravasation was observed around the anastomosis of the AVF and in the wound edges. No circulating liposomes were observed.

Gene	Forward primer	Reversed primer
IL-6	CTGCAAGAGACTTCCATCCAG	AGTGGTATAGACAGGTCTGTTGG
TNF	CCCTCACACTCAGATCATCTTCT	GCTACGACGTGGGCTACAG
IL-10	GCTGGACAACATACTGCTAACC	CCCAAGTAACCCTTAAAGTCCTG
MCP-1	GCACCAGCCAACTCTCAC	CTTCTTGGGGTCAGCACAG
MMP2	CCGAGGACTATGACCGGGATA	GGGCACCTTCTGAATTTCCA
MMP9	CTGGCGTGTGAGTTTCCAAAAT	TGCACGGTTGAAGCAAAGAA
TIMP1	ACACCCCAGTCATGGAAAGC	CTTAGGCGGCCCGTGAT
TIMP2	GTTTATCTACACGGCCCCCTCTT	ATCTTGCCATCTCCTTCTGCCTT
GAPDH	ACTCCCACTCTTCCACCTTC	CACCACCCTGTTGCTGTAG

Table 1. Primers used for in vitro experiments

Chapter 7

Deficiency of TLR4 homologue RP105 aggravates outward remodeling in a murine model of arteriovenous fistula failure

Taisiya Bezhaeva, ChunYu Wong, Margreet R. de Vries, Eric P. van der Veer, Carla M.A. van Alem, Ivo Que, Reshma A. Lalai, Anton Jan van Zonneveld, Joris I. Rotmans and Paul H.A. Quax

Submitted



Abstract

Arteriovenous access dysfunction is a major cause of morbidity for hemodialysis patients with a 1-year primary patency of only 60%. The pathophysiology of arteriovenous fistula (AVF) maturation failure is associated with inflammation, impaired outward remodeling (OR) and intimal hyperplasia. RP105 is a critical physiologic regulator of TLR4 signaling, and is expressed on numerous cell types. In the present study, we investigated the impact of differential RP105 expression on AVF maturation, and defined cell-specific effects of RP105 deficiency on macrophages and vascular smooth muscle cells (VSMCs). Overall, $RP105^{-/-}$ mice displayed a 26% decrease in venous OR. *The inflammatory response in $RP105^{-/-}$ mice* was characterized by an accumulation of the anti-inflammatory macrophage phenotype, a 76% decrease in pro-inflammatory macrophages, a 70% reduction in $CD3^{+}$ T-cells, and a 50% decrease in MMP-activity. *In vitro*, anti-inflammatory macrophages derived from $RP105^{-/-}$ mice were characterized by increased IL10 production, while the levels of MCP1 and IL6 secreted by $RP105^{-/-}$ pro-inflammatory macrophages were elevated, as compared to WT mice. VSMC content in $RP105^{-/-}$ AVFs was markedly decreased. *In vitro*, $RP105^{-/-}$ venous VSMCs proliferation was 50% lower, whereas arterial VSMCs displayed a 50% decrease in migration, relative to WT VSMCs. In conclusion, the marked decrease in venous OR in $RP105^{-/-}$ mice could potentially be the result of a shift in both macrophages and VSMCs towards a regenerative phenotype, identifying a novel relationship between inflammation and VSMC function in AVF maturation.

Introduction

The placement of an arteriovenous fistula (AVF) is currently regarded as the best available option for permanent vascular access in patients requiring chronic hemodialysis. For proper maturation of the AVFs, both a major increase in blood flow and venous diameter are required to allow adequate hemodialysis treatment. However, several clinical trials have shown that the 1-year primary patency rate of AVFs does not exceed 60%, illustrating the fact that the need for further improvement of this access conduit is vital[1,2]. AVF-related complications are frequently encountered shortly after AVF surgery, as 30-60% of the AVF fail to mature adequately to support dialysis therapy[3]. The exact mechanisms that lead to AVF maturation failure remain unknown, but both impaired outward remodeling (OR) and formation of intimal hyperplasia (IH) are regarded as primary contributors to this pathophysiology[4]. Recent studies have shown that the process of vascular adaptation after AVF creation is associated with an excessive inflammatory response[5-8] and proliferation and migration of arterial and venous vascular smooth muscle cells (VSMCs) towards the intima at the site of anastomosis[9-11]. In view of extensive adverse consequences resulting from AVF failure and the subsequent burden for hemodialysis patients, there is increasing emphasis on pathophysiological studies aimed to unravel the complex mechanisms underlying AVF failure. The latter is pivotal in efforts to identify novel molecular therapeutic targets that could potentially improve AVF patency.

Toll-like receptor 4 (TLR4) is a well-known sentry that induces a pro-inflammatory signaling cascade[12]. Its function is modulated not only by exogenous pathogens in the context of microbial infections[13], but also by several endogenous stimuli in inflammatory conditions such as atherosclerosis[14,15] or during vascular remodeling[16-19]. To initiate the TLR4 signaling cascade, activation of its adaptor molecule MD2 is required which is responsible for the recognition of bacterial lipopolysaccharide (LPS) on the cell surface[20]. Due to the hierarchical importance of TLR4 in the innate immune response and its ubiquitous function, the signaling activity of this protein is firmly regulated by several regulatory molecules. One such regulator is RP105 (radioprotective 105, also known as CD180), a cell surface protein expressed by numerous cell types, including inflammatory cells and VSMCs[21,22]. The structure of RP105 is evolutionarily similar to TLR4 and it associates with MD1, a MD2 homologue which promotes RP105 cell surface expression[23,24]. RP105–MD1 exerts dichotomous regulatory activities on TLR4-mediated LPS responses in a cell type-dependent fashion[25]. On B-cells, RP105-MD1 drives cellular proliferation and enhances B-cell-dependent inflammatory processes[26]. In contrast, in myeloid cells, RP105 acts as a natural antagonist of TLR4 signaling[27], while the functional role in VSMCs remains poorly understood. Previous studies from our group have demonstrated that RP105 deficiency results in decreased atherosclerotic lesion formation via alterations on

pro-inflammatory B-cells[28] and a CCR2-dependent decrease in monocyte influx[29]. Strikingly, complete opposite effects were observed in a murine model of vein graft disease, where a 90% increase in graft lesion area was linked to a local increase in macrophage content and lesional levels of monocyte chemoattractant protein-1 (MCP1), expressed by VSMCs[21]. In a model of post-interventional vascular remodeling, artery cuff placement in RP105$^{-/-}$ mice resulted in increased neointima formation, which coincided with an increase in arterial VSMC proliferation *ex vivo*[22].

In the context of both AVF maturation and failure, numerous cell types are involved including inflammatory cells and VSMCs from both the feeding artery[10,30] and local venous wall[31], making it a unique model to unravel specific functional consequences of RP105 on remodeling in AVF. In the present study, we aimed to elucidate the role of RP105 on AVF maturation in a murine model of AVF failure by assessing cell type-specific effects of RP105 deficiency, on macrophage polarization and VSMC behavior.

Results

RP105 deficiency influence AVF maturation

To investigate how differential expression of RP105 could influence AVF maturation, we evaluated AVF material two weeks after creating in wild-type (WT) and RP105$^{-/-}$ mice using morphometric and immunohistochemical approaches. RP105$^{-/-}$ mice showed a 26% smaller circumference of the external jugular vein compared to WT mice (P=0.03) (Figure 1a), indicating that RP105deficiency impacts outward remodeling. As shown in Figure 1b, diminished RP105 expression did not influence IH in the venous outflow tract of the AVF. Importantly, immunohistochemical staining revealed that the vast majority of intimal cells are αSMA^{+} in both WT and RP105$^{-/-}$ mice (Figure 1b).

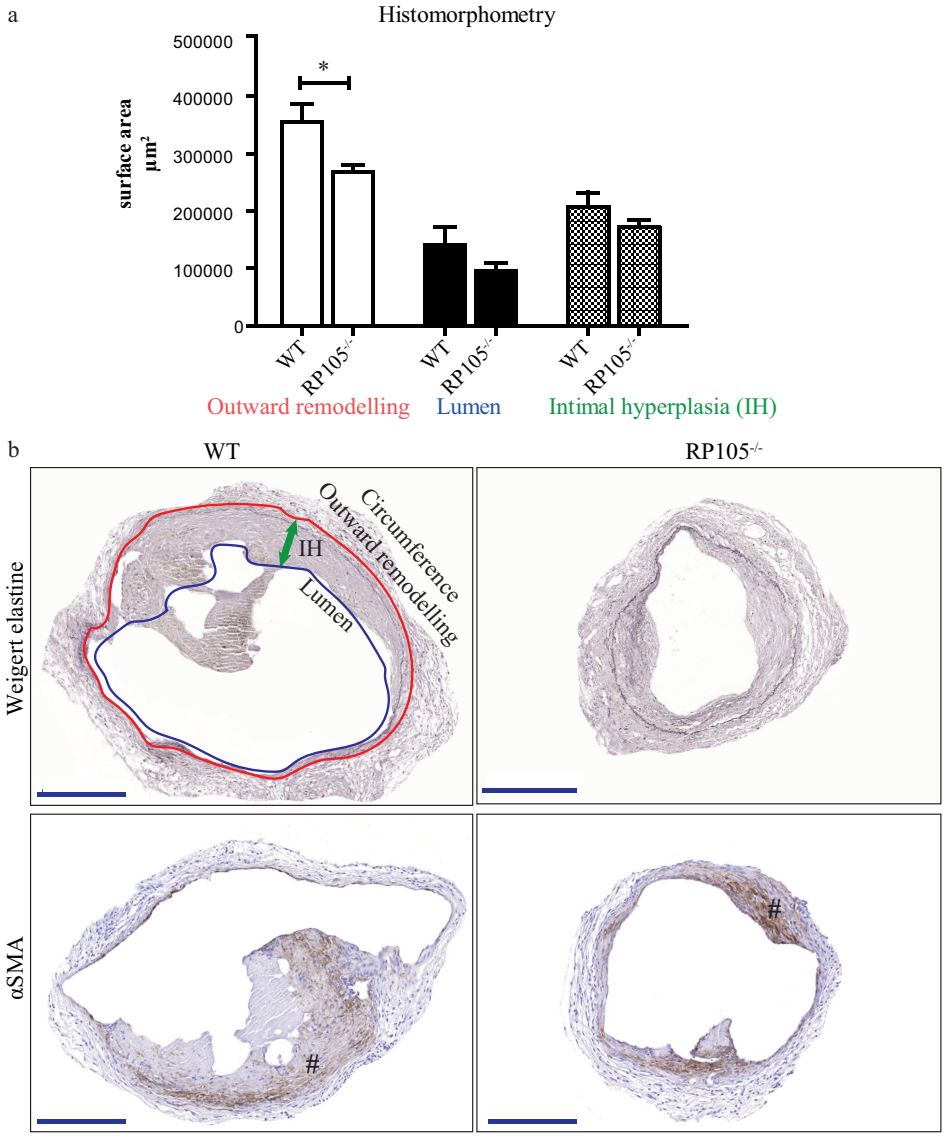


Figure 1. Effect of RP105 deficiency on AVF maturation *in vivo*. (a) Quantification of morphometric parameters. Decrease in vessel circumference (outward remodeling) in RP105 deficient mice was observed 14 days after AVF creation, as compared to WT. Lumen and intimal hyperplasia did not differ between RP105$^{-/-}$ and WT mice. (b) Histological staining of venous outflow tract 14 days after surgery. Weigert elastin staining was used to determine histomorphometrical parameters of the vessel. Circumference (internal elastic lamina area) was used to quantify outward remodeling (red line). Intimal hyperplasia (green arrow) measured as a difference between luminal area (blue line) and vessel circumference. αSMA staining shows area of intimal hyperplasia 14 days after AVF creation. (#) intimal hyperplasia; (*) P<0.05; n=11 per group. Bar=200 µm: 100x magnification.

RP105 deficiency leads to reduced VSMC content in AVF lesions

Given this VSMC enrichment in the intimal region of mature AVF, we sought to determine the proliferation capacity of these cells immunohistochemically. For this, we quantitated the amount of proliferating αSMA^{+}/Ki67^{+} cells in AVF sections. These studies revealed a 31% decrease in αSMA^{+}/Ki67^{+} VSMCs in RP105$^{-/-}$ mice, as compared to WT mice (Figure 2a). Since we cannot discriminate between arterial and venous VSMCs *in vivo*, this borderline significance in the number of αSMA^{+}/Ki67^{+} VSMCs (P=0.07) might be relevant (Figure 2b).

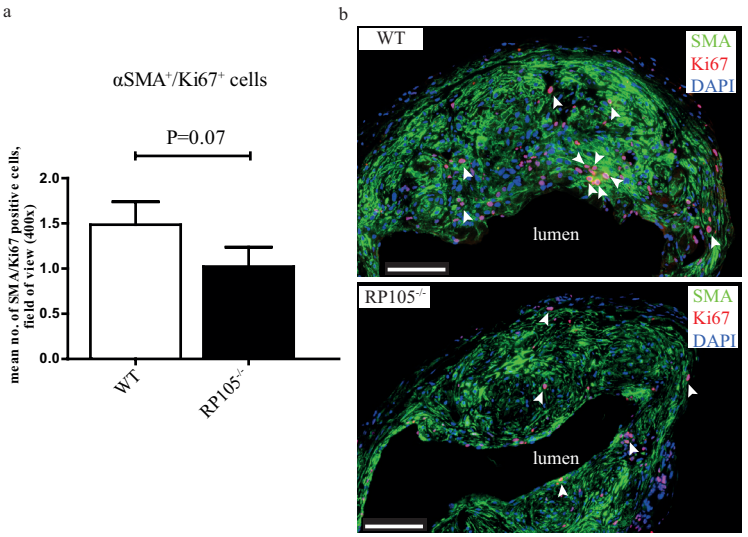


Figure 2. Effect of RP105 deficiency on VSMC proliferation *in vivo*. Quantification (a) and immunofluorescent staining (b) of αSMA+/Ki67+ cells (white arrows) revealed reduction in number of proliferating VSMCs in AVF lesions of RP105$^{-/-}$ mice compared to WT 14 days after AVF surgery. n=11 per group. Bar=100 μm.

Diminution of RP105 differently affects arterial and venous VSMC function

To further dissect the contribution of arterial and venous VSMCs to AVF maturation and failure, we elected to study the consequences of differential RP105 expression in arterial and venous VSMCs *ex vivo*. For this, we cultured explant material from the carotid artery and vena cava of WT and RP105$^{-/-}$ mice for 2 weeks. Morphologically, we observed that arterial VSMCs possessed an elongated phenotype, whereas venous cells had a more stellate appearance (Figure 3a). This phenotypic difference was maintained throughout cell culture, and the vascular origin of the cells was confirmed by assessing EphB4 expression levels, an established embryological marker of venous origin, which was increased in cultured venous VSMCs up to 2 weeks after isolation (Figure 3b).

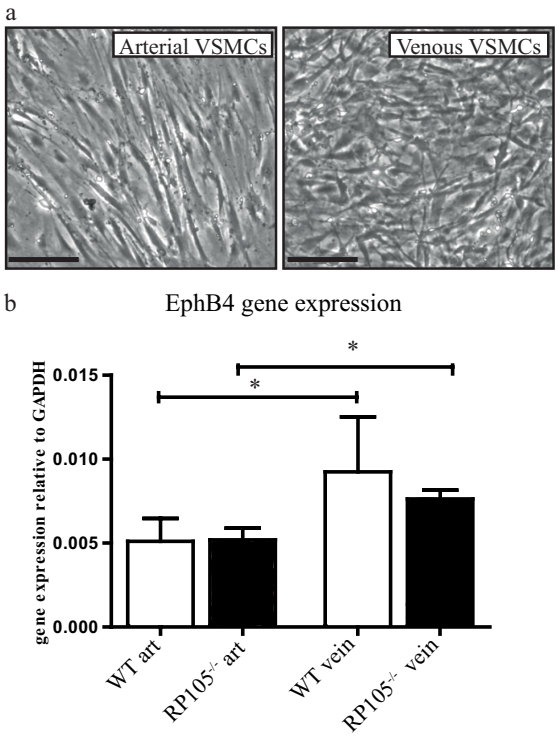


Figure 3. Proliferation and migration of arterial and venous SMCs *in vitro*. (a) A reduction in the proliferative rate was limited to SMCs isolated from RP105$^{-/-}$ veins. (b) Decrease in migration of SMCs isolated from RP105$^{-/-}$ mice was restricted to arterial cells only. Cells were maintained in culture for 14 days. Proliferation and migration were measured over 16 h time period. (*) P<0.05; n=3.

Next, we further determine expression levels of RP105 associating molecules. Interestingly, RT-PCR analysis of RP105 and its accessory molecule MD1 by WT VSMCs also revealed a striking > 100-fold increase in gene expression on venous VSMCs compared to arterial VSMCs (Figure 4a,b). Furthermore, mRNA expression levels of the inflammatory marker TLR4 was also elevated by 48% in venous cells, as compared to arterial VSMCs (Figure 4c). Expression of the TLR4 accessory molecule MD2 did not differ between WT and RP105$^{-/-}$ mice arterial and venous VSMCs (Supplementary Figure 1).

Functionally, venous VSMCs derived from RP105$^{-/-}$ mice displayed a 50% reduction in their rate of proliferation, relative to VSMCs derived from WT mice, while arterial VSMCs proliferation was unaltered (Figure 5a). In contrast, migratory capacity was reduced by 50% over a 16h time period in arterial VSMCs derived from RP105$^{-/-}$, venous SMCs showed no difference in migration between WT and RP105$^{-/-}$ mice (Figure 5b).

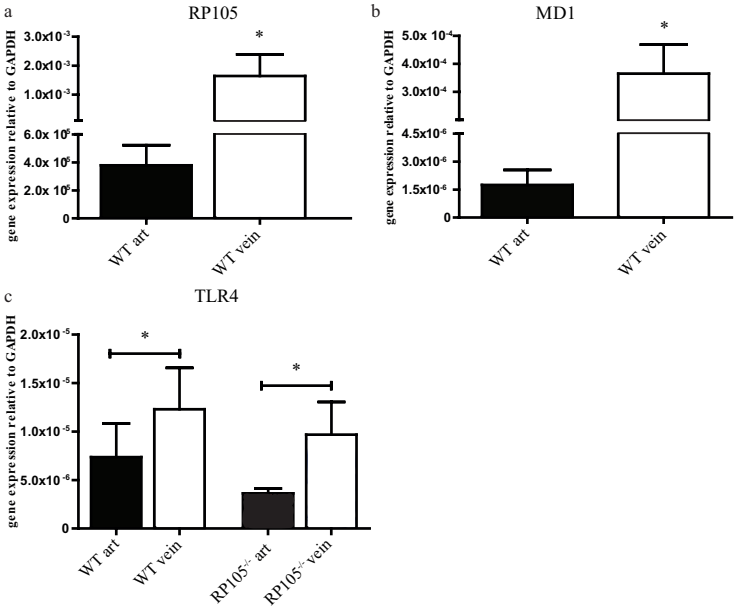


Figure 4. Difference in mRNA expression levels between arterial and venous SMCs *in vitro.* (a) RP105, (b) MD1, (c) TLR4. The relative expression normalized to GAPDH. (*)P<0.05; n=3.

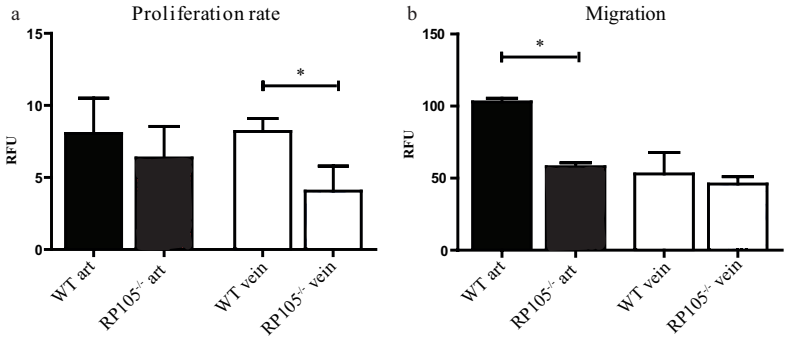


Figure 5. *In vitro* cultured arterial and venous SMCs. (a) Microscopic representation of morphological difference between cultured arterial and venous SMCs. Bar=100μm, x200 magnification. (b) Stable increase in EphB4 mRNA levels was detected in venous SMCs isolated from WT and RP105$^{-/-}$ mice. Cells were maintained in culture for 14 days. (*) P<0.05; n=3.

RP105 deficiency impacts the inflammatory status of AVF infiltrating cells

To gain insight into the consequences of differential expression of RP105 on the inflammatory response to injury *in vivo*, we evaluated the inflammatory cell composition of AVFs in $RP105^{-/-}$ and WT mice. Analysis of AVF material 2 weeks after surgery revealed a 76% reduction in $MAC3^{+}/CCR2^{+}$ pro-inflammatory macrophages cell number in the venous lesions of $RP105^{-/-}$ mice. Furthermore, the number of infiltrating $MAC3^{+}/CD206^{+}$ anti-inflammatory macrophages was increased by 35%, as compared to WT mice (Figure 6a). The number of $CD3^{+}$ T-lymphocytes in $RP105^{-/-}$ mice was decreased by 70% (Figure 6b). Interestingly, we observed an enrichment of these inflammatory cells in the adventitial layer of the vessel (Figure 6a, b). No changes between $RP105^{-/-}$ and WT mice were found in the number of $MCP1^{+}$ cells in the AVF lesions at 2 weeks after surgery (Supplementary Figure 2).

Notably, the distribution of the total population of macrophages in $RP105^{-/-}$ 2 weeks after AVF creation was skewed towards a tissue repair, or regenerative state. More than 90% of all $MAC3^{+}$ cells were $CD206^{+}$, a cell surface protein that defines the anti-inflammatory macrophage phenotype, whereas but 6% of these $MAC3^{+}$ macrophages were found to express CCR2, the pro-inflammatory macrophage marker.

Macrophage-mediated cytokine production is affected by RP105 expression levels

Having identified that AVFs in $RP105^{-/-}$ mice are enriched for anti-inflammatory macrophages, we subsequently isolated bone marrow from WT and $RP105^{-/-}$ mice and polarized bone marrow-derived macrophages towards either pro- or anti-inflammatory phenotypes with LPS/IFN-gamma or IL4/IL13 treatment for 24h, respectively. We observed an augmented inflammatory response by pro-inflammatory macrophages derived from $RP105^{-/-}$ mice as evidenced by a 40% increase in MCP1 secretion and a 73% up regulation in IL6 production, as compared to macrophages obtained from WT mice (Figure 7a). Macrophages that were isolated from $RP105^{-/-}$ mice and driven towards the anti-inflammatory phenotype exhibited a 72% increase in anti-inflammatory cytokine IL10 production as compared to WT macrophages (Figure 7b).

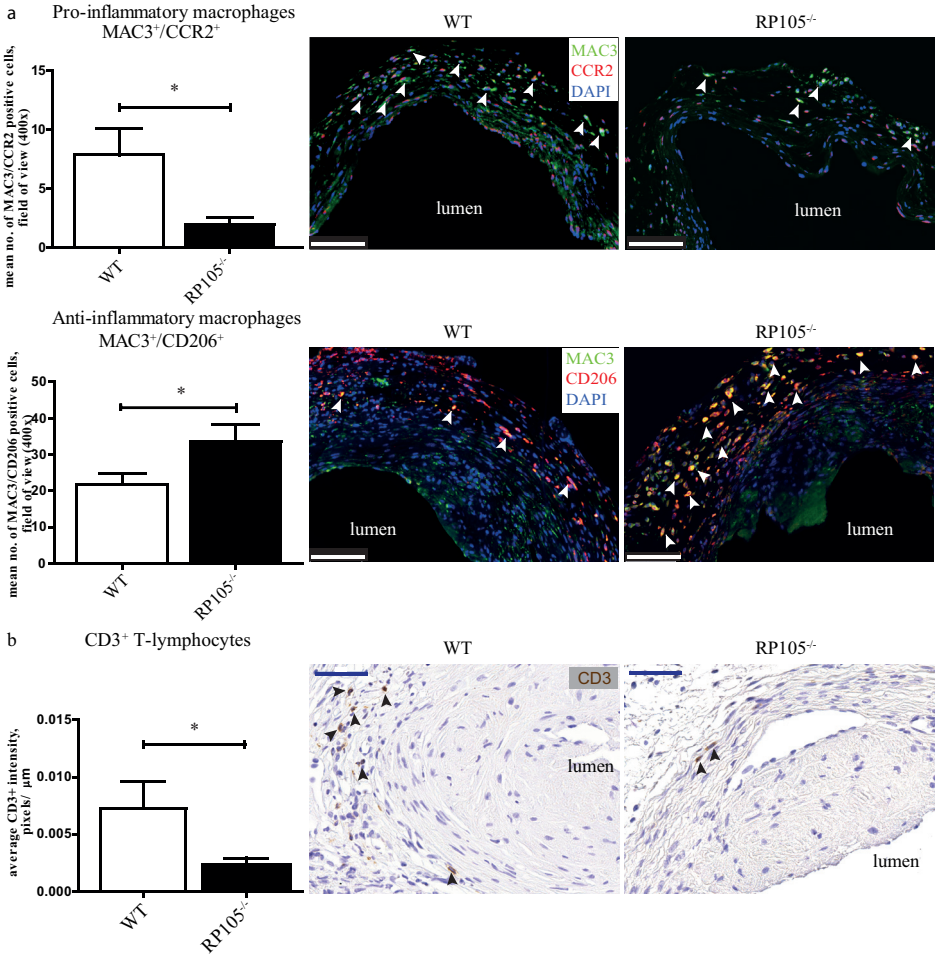


Figure 6. Effects of RP105 deficiency on inflammatory response *in vivo*. Quantification and immunohistochemical staining of (a) MAC3+/CCR2+ macrophages and MAC3+/CD206+ macrophages (white arrows) and (b) CD3+ T-lymphocytes (black arrows) in AVF lesions 14 days after surgery. Decrease in cell number of pro-inflammatory macrophages and upregulation of anti-inflammatory macrophages upon RP105 deletion was observed. Bar=100 µm. Number of CD3+ T-lymphocytes was reduced in RP105$^{-/-}$ as compared to WT. Bar=50 µm: 400x magnification. (*) P<0.05; n=11 per group.

MMP activity is decreased in AVF lesions of RP105 deficient mice

Matrix metalloproteinases (MMPs) are known for the role they play in extracellular matrix (ECM) remodeling, such as collagen and elastin. MMP-mediated degradation of the ECM is critically involved in vascular remodeling following AVF placement and during AVF maturation[32]. We assessed MMP activity in the lesions using *in vivo* near-infrared fluorescent imaging. We observed

a two-fold reduction (6.3±1.6 WT vs. 2.9±0.2 RP105$^{-/-}$ AU) in fluorescence intensity indicating reduced *in vivo* MMP activity in RP105$^{-/-}$ mice as compared to WT (Figure 8).

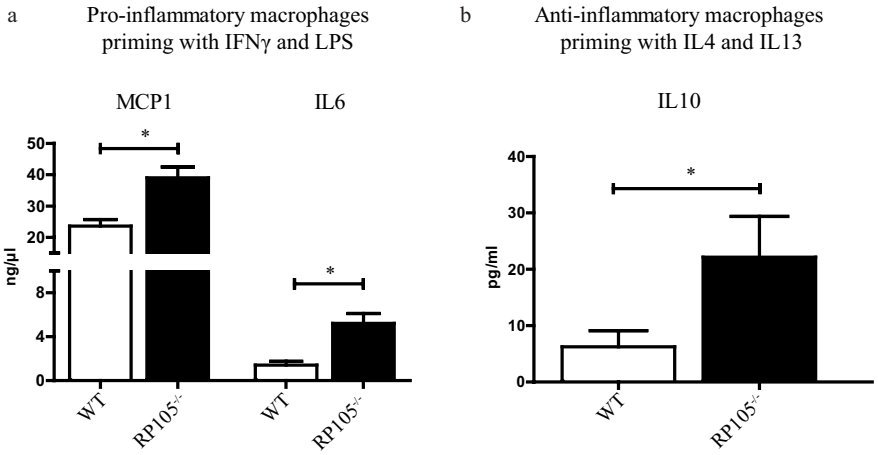


Figure 7. Effect of RP105 deficiency on macrophage function. (a) Bone marrow-derived macrophages from RP105$^{-/-}$ primed towards pro-inflammatory phenotype secrete increased levels of MCP1 and IL6 as compared to WT control mice. (b) Anti-inflammatory macrophages from RP105$^{-/-}$ secrete increased levels of anti-inflammatory cytokine IL10. (*) P<0.05; n=3.

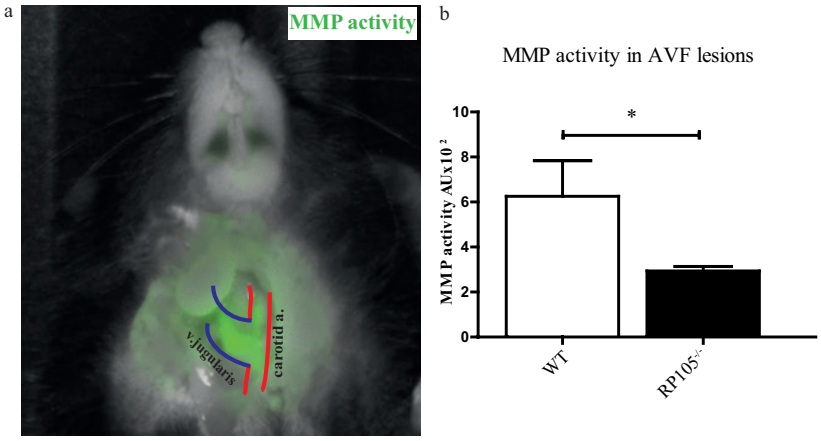


Figure 8. In vivo near-infrared biofluorescent imaging and quantitative analysis of MMP activity. (a) Quantitative analysis of fluorescent intensity revealed a decrease in MMP activity in RP105$^{-/-}$ mice, as compared to WT. (b) Visual representation of near-infrared signal from active MMPs. Accumulation of green color can be seen in the anastomotic region 24 h after injection of MMPSense™ 680 probe. (*) P<0.05; n=4 per group.

Discussion

In this study, we addressed the specific role of TLR4 homologue RP105 in vascular remodeling, inflammation and VSMCs function in a murine model of AVF failure. The process of AVF maturation is complex and integrates several cellular responses, including the infiltration of inflammatory cells shortly after AVF surgery[5,33]. In addition, VSMCs play a pivotal role in AVF maturation as they contribute to thickening of the venous vessel wall and the concurrent outward remodeling. Here, we clearly show that RP105 deficiency affects the inflammatory and VSMC-mediated response to injury during the course of AVF maturation, accumulating in an impaired outward remodeling 14 days after the placement of an AVF.

Contribution of VMSCs proliferation to AVF maturation in RP105 deficient mice

A vital aspect of AVF maturation involves the outward remodeling response, a vessel widening process that is tightly coupled with VSMC proliferation. While VSMC proliferation in IH is generally considered to be detrimental, the process is beneficial for vascular adaptation in AVF, especially in the early phase of AVF maturation. To this end, the reduction in venous outward remodeling in RP105$^{-/-}$ mice, coupled with a reduction in proliferating venous SMC within AVFs and ex vivo, suggests that inhibiting VSMCs proliferation (and migration) could be detrimental for long-term AVF maturation.

Distinct *in vitro* effects of RP105 deficiency on arterial and venous VSMCs

A striking observation in our studies was that RP105 diminution differentially affected arterial and venous SMCs, as evidenced by RP105-specific effects on venous proliferation and arterial migration. The endogenous expression levels of RP105 in arterial and venous SMCs support this finding, along with differential expression profiles of associating TLR4-family members (including TLR4 and MD-1). Collectively, these findings suggest that the susceptibility for inflammatory stimuli could potentially differ between arterial and venous VSMCs. Importantly, our studies support the notion that numerous cell sources are involved in venous IH in AVF (including resident venous cells, infiltrating arterial cells, and circulating bone marrow-derived cells[7,34-37]). Furthermore, our studies illustrate the need for continued investigation of the phenotypic properties and functional characteristics of VSMCs in AVFs, in particular due to the contrasting lineage tracing studies detailing a predominance of arterial SMCs10 versus venous SMCs[31] in venous IH following AVF placement.

RP105 targets both the pro-inflammatory and repair associated arms of the immune system

Increased expression of the pro-inflammatory mediators IL6, TNF and MCP1 are associated with AVF failure[8,38,39], while the reduction of anti-inflammatory molecule heme oxygenase-1 (HO-1) is linked to AVF failure[40-42]. In our study, we demonstrated that the polarization of macrophages isolated from the bone marrow of RP105$^{-/-}$ mice towards the pro- or anti-inflammatory phenotypes appears to remove a regulatory repressor, as both phenotypes displayed an up regulation of signature cytokines being produced. The augmentation of pro-inflammatory cytokine production in RP105$^{-/-}$ macrophages is in keeping with RP105 being an antagonist of pro-inflammatory TLR4 signaling[25,27,43], while the spike in IL10 production is supported by recent reports that low grade inflammation triggers bone marrow-derived macrophages to generate anti-inflammatory cytokines in a TLR4 dependent fashion[44].

AVF placement in RP105$^{-/-}$ mice yielded decreased MAC3^{+}/CCR2^{+} macrophages and CD3^{+} T-lymphocytes. A noteworthy observation two weeks after AVF placement in RP105$^{-/-}$ mice was the attenuation of vessel wall MMP activity. While the type of vascular injury impacts the degree by which MMPs remodel the vascular wall, these factors also play a role in determining which MMPs are activated[45], and could differ between arterial and venous segments. Castier *et al.* reported that increased MMP-9 activity coincided with increased OR in the arterial segment of the AVF[46], while Nieves Torres *et al.* demonstrated that MMP inhibition enhanced venous OR in AVF[47]. Our studies contradict this finding, and suggest instead that decreased MMP limits venous OR in maturating AVFs.

During the process of vascular remodeling the initial pro-inflammatory reaction is gradually changing towards resolution of inflammation characterized by accumulation of anti-inflammatory cells[48-51]. The specific dynamics with regard to pro-/anti- inflammatory response in the context of AVF maturation is still unknown. In our murine model, RP105 deficiency caused significant increase in MAC3^{+}/CD206^{+} anti-inflammatory macrophages in the venous lesions of AVF, compared to controls. Overall prevalence in anti-inflammatory population (93.7%), compared to 6.3% of pro-inflammatory macrophages at 2 weeks after AVF creation might suggest either that in the current model pro-inflammatory response is completed at earlier time points or that anti-inflammatory macrophages play a dominant role in the tissue response in murine AVF. Thus, despite the increased production of both pro- and anti-inflammatory cytokines by macrophages *in vitro*, the effect of RP105 deletion on anti-inflammatory macrophages was dominant in the venous lesions of murine AVF.

Study limitations

Current study is performed in mice, which do not precisely mimic the human inflammatory response to injury; however this model remains highly useful for studying the vital pathophysiological aspects of AVF maturation and failure. Another limitation is the absence of uremia, given that a recent *in vivo* study by Kang et al. demonstrated that fistula maturation in mice is affected by CKD[42]. Here, the chronic accumulation of waste products and uremic toxins in the blood impacted AVF flow, resulting in increased venous wall thickness and thrombus formation. Also, future studies should include flow measurements, as the rate of blood flow is critical functional parameter of AVF.

In conclusion, our study demonstrates the complex role of RP105 in VSMCs and macrophages in a murine model of AVF. The design and implementation of therapeutic strategies targeting the TLR4/RP105 axis to prevent AVF failure must include cell specific targeting approaches and be temporally controlled.

Material and Methods

Animals

Murine model of AVF failure

This study was performed in compliance with Dutch government guidelines and the Directive 2010/63/EU of the European Parliament. All animal experiments were approved by the Institutional Committee for Animal Welfare of Leiden University Medical Center. RP105$^{-/-}$ mice (C57BL/6 background) were obtained from the local animal breeding facility, WT C57BL/6 mice were obtained from Charles River. Adult male mice aged 10-11 weeks were used for the experiments. AVF were created in an end-to-side manner between the dorsomedial branch of the external jugular vein and the common carotid artery as previously described[5,52] (Supplementary Methods S1). The mice were euthanized at 2 weeks after AVF surgery.

In vivo near-infrared MMPs assay

In vivo MMP activity of endogenous MMP-2, -3, -9, -12 and -13 was assessed by injecting fluorescent imaging agent MMPSense™ 680 from PerkinElmer's (Waltham, MA, USA) which is activated in the presence of active MMPs[53]. First, AVF was created as described above (n=4 per group). 14 days later mice were anesthetized under isoflurane and 4 nmol of MMPSense™ 680 probe were injected into the tail vein. 24 hours later, mice were placed under anesthesia, AVF was dissected and mice were scanned using the Optix MX2 optical imaging system. Excitation was performed with a 670-nm pulsing laser, and emission was detected with a 693-

nm long-pass filter. Lifetime analysis was used to confirm the specificity of MMP-activated probes. Fluorescence intensities and fluorescence lifetime were expressed in pseudo colors and projected on the bright field grayscale image of the mouse. Quantification of the fluorescent intensity was performed using the Optiview 2.2 software as described previously[54].

Tissue harvesting and processing

14 days after surgery, the mice were anesthetized using isoflurane whereupon the AVF was dissected. After a thoracotomy, the inferior vena cava was transsected followed by a mild pressure perfusion fixation with 4% formalin through an intracardiac perfusion. The tissue was embedded in paraffin and 5 µm-thick sections of the venous outflow tract were made perpendicular to the vein with an interval of 150 µm.

Morphometric and histological analysis

Morphometric analysis was performed on Weigert's elastin stained sections using ImageJ software. Vessel circumference as a parameter displaying the process of outward remodeling was determined by measuring the length of the internal elastic lamina (IEL). The intimal hyperplasia was calculated by subtracting the luminal area from the area within the IEL.
Immunohistochemical staining was performed for macrophages (MAC3, 1:200, BD-Pharmingen, SanDiego, USA) in a combination with CCR2 for pro-inflammatory phenotype (1:400, Abcam, Cambrigde, UK) or CD206 (1:1000, Abcam) for anti-inflammatory phenotype, T-lymphocytes (CD3, 1:300, Abcam) and VSMCs (αSMA, 1:1000, Dako, Glostrup, Denmark) in a combination with Ki67 (1:200, Abcam) to detect proliferating cells. For the immunohistochemical analysis of the MAC3/CD206, MAC3/CCR2 and αSMA/Ki67 staining, the number of positive cells was counted in 3 random fields of view using a 400x magnification from which the mean was calculated. Quantification of $CD3^+$ cells was performed with ImageJ software by calculating % DAB positive area from the total vessel area. All immunohistochemical quantifications were performed on the first 3 venous sections starting from the anastomosis per AVF. Slides were digitized using an automated microscopic scanner (Panoramic digital MIDI, 3DHISTECH, Hungary). Results are expressed as mean±standard error of the mean.

Cell culture

Vascular smooth muscle cells

Primary arterial and venous vascular smooth muscle cells were isolated from murine carotid artery and vena cava of C57Bl/6 and $RP105^{-/-}$ mice (n=3 per group) respectively. Connective tissues were removed and vessels cut open. Endothelial monolayer was detached by gentle scraping with sterile surgical forceps. The carotid artery and caval vein were dissected into

small pieces and plated onto Petri dish 100 mm or 60 mm diameter coated with 0.1 mg/ml fibronectine. After 14 days of culture with DMEM medium supplemented with 20% FCS, 2 mmol/l l-glutamine, 100 U/ml penicillin and 100 µg/ml streptomycin, cells were trypsinized and re-plated onto 6 or 12 well plates and left for 7 days in culture. Upon enrichment in 80-90% confluence VSMCs were trypsinized and seeded at required density for further functional assays.

Macrophages

Macrophages were derived from bone marrow by flushing tibia and femur of healthy C57Bl/6 or RP105$^{-/-}$ mice (n=3 per group) and seeded at a density of 500.000 cells/well in 6-wells plates. Cells were cultured for 7 days in RPMI GlutaMax (Gibco) supplemented with 100 U/ml penicillin/streptavidin, 25% Fetal Calf Serum (FCS) and 20 mg/ml M-CSF (Myltec Biotechnologies) as described previously[6]. On day 7, cells were stimulated either with LPS (100 ng/ml) and IFN-gamma (10 ng/ml) to differentiate them towards pro-inflammatory phenotype or with IL4 (10 ng/ml) and IL13 (10 ng/ml) (all from Preprotech) for anti-inflammatory phenotype. After 24 hours the supernatants were collected for ELISA assays and cells were lysed with Trizol reagent (Invitrogen, Carlsbad, CA, USA) for RNA isolation.

VSMC proliferation assay

Murine VSMCs, explanted from aortas and veins of control or RP105$^{-/-}$ mice, were subsequently cultured as described above, and proliferation was measured using neutral red cell proliferation and cytotoxicity assay kit from **Boster Bio (Pleasanton, CA, USA)** according to the manufacturer protocol (Supplementary Methods S2).

VSMC migration assay

Primary arterial and venous VSMCs from control and RP105$^{-/-}$ mice were grown to confluence and then made quiescent in cultured medium supplemented with 1% FCS for 24 hours. Cells were detached from the surface using Accutase Cell Detachement Solution (Innovative Cell Technologies, Inc., San Diego, CA, USA) and suspended at a concentration of 100.000 cells/ml in culture medium supplemented with 1% FCS. Migration was assayed with a polycarbonate membrane inserts having 8 µm-pores in 24-well chemotaxis chambers using commercial CytoSelect Cell Migration Assay Kit (Cell Biolabs, Inc., San Diego, CA, USA) over 16 hours towards the 20% FCS gradient. All migratory cells were lysed and labeled with fluorescent dye (CyQuant GR). Quantification was performed on a fluorescence plate reader at 480nm/520nm.

ELISA assays

ELISA assays for MCP1, IL6 and IL10 production were performed with cell free supernatant collected from bone marrow-derived macrophages after 24 hours polarization towards pro- or anti-inflammatory phenotype using commercial available kits following the instructions of the manufacturer (BD Biosciences, San Jose, CA, USA: MCP1- Catalog No 555260; IL6- Catalog No 555240, IL10- Catalog No 555252).

RT-PCR

Total RNA was extracted from the macrophages and VSMCs using Trizol reagent (Invitrogen) according to the manufacturer's protocol. RNA was reverse transcribed using a 5-minute 65°C incubation of 1 μg total RNA with deoxyribonucleotide triphosphates (Invitrogen) and random primers (Invitrogen). c-DNA was synthesized using an M-MLV First-Strand Synthesis system (Invitrogen), and used for quantitative analysis of mouse genes (Supplementary Table 1) with an SYBR Green Master Mix (Applied Biosystems, Foster City, CA, USA). The relative mRNA expression levels were determined by normalization to murine glyceraldehyde 3-phosphate dehydrogenase (GAPDH) using $2[-\Delta\Delta C(T)]$ method.

Statistical analysis

Results are expressed as mean±SEM and considered statistically significant for $p<0.05$; t tests and Mann-Whitney tests for parametric and nonparametric data, respectively, were used as appropriate. All *in vitro* experiments were performed in biological n=3 in experimental triplicates.

Acknowledgements

This study was supported by a grant from the Dutch Kidney Foundation (KJPB 08.0003).

Reference List

1. Tordoir, J.H., *et al.* Prospective evaluation of failure modes in autogenous radiocephalic wrist access for haemodialysis. *Nephrology, dialysis, transplantation : official publication of the European Dialysis and Transplant Association - European Renal Association* **18**, 378-383 (2003).

2. Dember, L.M., *et al.* Effect of clopidogrel on early failure of arteriovenous fistulas for hemodialysis: a randomized controlled trial. *JAMA : the journal of the American Medical Association* **299**, 2164-2171 (2008).

3. Lazarides, M.K., Georgiadis, G.S., Antoniou, G.A. & Staramos, D.N. A meta-analysis of dialysis access outcome in elderly patients. *Journal of vascular surgery* **45**, 420-426 (2007).

4. Rothuizen, T.C., *et al.* Arteriovenous access failure: more than just intimal hyperplasia? *Nephrology, dialysis, transplantation : official publication of the European Dialysis and Transplant Association - European Renal Association* **28**, 1085-1092 (2013).

5. Wong, C.Y., *et al.* Vascular remodeling and intimal hyperplasia in a novel murine model of arteriovenous fistula failure. *Journal of vascular surgery* (2013).

6. Wong, C., *et al.* Liposomal prednisolone inhibits vascular inflammation and enhances venous outward remodeling in a murine arteriovenous fistula model. *Scientific reports* **6**, 30439 (2016).

7. Wang, Y., *et al.* Venous stenosis in a pig arteriovenous fistula model--anatomy, mechanisms and cellular phenotypes. *Nephrology, dialysis, transplantation : official publication of the European Dialysis and Transplant Association - European Renal Association* **23**, 525-533 (2008).

8. Nath, K.A., Kanakiriya, S.K., Grande, J.P., Croatt, A.J. & Katusic, Z.S. Increased venous proinflammatory gene expression and intimal hyperplasia in an aorto-caval fistula model in the rat. *The American journal of pathology* **162**, 2079-2090 (2003).

9. Lee, T. & Haq, N.U. New Developments in Our Understanding of Neointimal Hyperplasia. *Advances in chronic kidney disease* **22**, 431-437 (2015).

10. Liang, M., *et al.* Migration of smooth muscle cells from the arterial anastomosis of arteriovenous fistulas requires Notch activation to form neointima. *Kidney international* **88**, 490-502 (2015).

11. Roy-Chaudhury, P., *et al.* Neointimal hyperplasia in early arteriovenous fistula failure. *American journal of kidney diseases : the official journal of the National Kidney Foundation* **50**, 782-790 (2007).

12. Akira, S., Takeda, K. & Kaisho, T. Toll-like receptors: critical proteins linking innate and acquired immunity. *Nature immunology* **2**, 675-680 (2001).

13. Kawai, T. & Akira, S. The role of pattern-recognition receptors in innate immunity: update on Toll-like receptors. *Nature immunology* **11**, 373-384 (2010).

14. Ding, Y., *et al.* Toll-like receptor 4 deficiency decreases atherosclerosis but does not protect against inflammation in obese low-density lipoprotein receptor-deficient mice. *Arteriosclerosis, thrombosis, and vascular biology* **32**, 1596-1604 (2012).

15. Lu, Z., Zhang, X., Li, Y., Jin, J. & Huang, Y. TLR4 antagonist reduces early-stage atherosclerosis in diabetic apolipoprotein E-deficient mice. *The Journal of endocrinology* **216**, 61-71 (2013).

16. Hollestelle, S.C., *et al.* Toll-like receptor 4 is involved in outward arterial remodeling. *Circulation* **109**, 393-398 (2004).

17. Karper, J.C., *et al.* Toll-like receptor 4 is involved in human and mouse vein graft remodeling, and local gene silencing reduces vein graft disease in hypercholesterolemic APOE*3Leiden mice. *Arteriosclerosis, thrombosis, and vascular biology* **31**, 1033-1040 (2011).

18. Karper, J.C., *et al.* Blocking toll-like receptors 7 and 9 reduces postinterventional remodeling via reduced macrophage activation, foam cell formation, and migration. *Arteriosclerosis, thrombosis, and vascular biology* **32**, e72-80 (2012).

19. Vink, A. In Vivo Evidence for a Role of Toll-Like Receptor 4 in the Development of Intimal Lesions. *Circulation* **106**, 1985-1990 (2002).

20. Akashi-Takamura, S. & Miyake, K. TLR accessory molecules. *Current opinion in immunology* **20**, 420-425 (2008).

21. Wezel, A., *et al.* Deficiency of the TLR4 analogue RP105 aggravates vein graft disease by inducing a pro-inflammatory response. *Scientific reports* **6**, 24248 (2016).

22. Karper, J.C., *et al.* TLR accessory molecule RP105 (CD180) is involved in post-interventional vascular remodeling and soluble RP105 modulates neointima formation. *PloS one* **8**, e67923 (2013).

23. Divanovic, S., *et al.* Inhibition of TLR-4/MD-2 signaling by RP105/MD-1. *Journal of endotoxin research* **11**, 363-368 (2005).

24. Ohto, U., Miyake, K. & Shimizu, T. Crystal structures of mouse and human RP105/MD-1 complexes reveal unique dimer organization of the toll-like receptor family. *Journal of molecular biology* **413**, 815-825 (2011).

25. Schultz, T.E. & Blumenthal, A. The RP105/MD-1 complex: molecular signaling mechanisms and pathophysiological implications. *Journal of leukocyte biology* (2016).

26. Divanovic, S., *et al.* Regulation of TLR4 signaling and the host interface with pathogens and danger: the role of RP105. *Journal of leukocyte biology* **82**, 265-271 (2007).

27. Divanovic, S., *et al.* Negative regulation of Toll-like receptor 4 signaling by the Toll-like receptor homolog RP105. *Nature immunology* **6**, 571-578 (2005).

28. Karper, J.C., *et al.* An Unexpected Intriguing Effect of Toll-Like Receptor Regulator RP105 (CD180) on Atherosclerosis Formation With Alterations on B-Cell Activation. *Arteriosclerosis, thrombosis, and vascular biology* **33**, 2810-2817 (2013).

29. Wezel, A., *et al.* RP105 deficiency attenuates early atherosclerosis via decreased monocyte influx in a CCR2 dependent manner. *Atherosclerosis* **238**, 132-139 (2015).

30. Rotmans, J.I. & Bezhaeva, T. The battlefield at arteriovenous crossroads: invading arterial smooth muscle cells occupy the outflow tract of fistulas. *Kidney international* **88**, 431-433 (2015).

31. Skartsis, N., *et al.* Origin of neointimal cells in arteriovenous fistulae: bone marrow, artery, or the vein itself? *Seminars in dialysis* **24**, 242-248 (2011).

32. Wong, C.Y., *et al.* Elastin is a key regulator of outward remodeling in arteriovenous fistulas. *European journal of vascular and endovascular surgery : the official journal of the European Society for Vascular Surgery* **49**, 480-486 (2015).

33. Roy-Chaudhury, P., *et al.* Pathogenetic role for early focal macrophage infiltration in a pig model of arteriovenous fistula (AVF) stenosis. *The journal of vascular access* **15**, 25-28 (2014).

34. Caplice, N.M., *et al.* Neoangiogenesis and the presence of progenitor cells in the venous limb of an arteriovenous fistula in the rat. *American journal of physiology. Renal physiology* **293**, F470-475 (2007).

35. Tanaka, K., *et al.* Circulating progenitor cells contribute to neointimal formation in nonirradiated chimeric mice. *FASEB journal : official publication of the Federation of American Societies for Experimental Biology* **22**, 428-436 (2008).

36. Misra, S., *et al.* Adventitial remodeling with increased matrix metalloproteinase-2 activity in a porcine arteriovenous polytetrafluoroethylene grafts. *Kidney international* **68**, 2890-2900 (2005).

37. Li, L., *et al.* Cellular and morphological changes during neointimal hyperplasia development in a porcine arteriovenous graft model. *Nephrology, dialysis, transplantation : official publication of the European Dialysis and Transplant Association - European Renal Association* **22**, 3139-3146 (2007).

38. Croatt, A.J., *et al.* Characterization of a model of an arteriovenous fistula in the rat: the effect of L-NAME. *The American journal of pathology* **176**, 2530-2541 (2010).

39. Juncos, J.P., *et al.* MCP-1 contributes to arteriovenous fistula failure. *Journal of the American Society of Nephrology : JASN* **22**, 43-48 (2011).

40. Tsapenko, M.V., *et al.* Increased production of superoxide anion contributes to dysfunction of the arteriovenous fistula. *American journal of physiology. Renal physiology* **303**, F1601-1607 (2012).

41. Lin, C.C., *et al.* Length polymorphism in heme oxygenase-1 is associated with arteriovenous fistula patency in hemodialysis patients. *Kidney international* **69**, 165-172 (2006).

42. Kang, L., *et al.* A new model of an arteriovenous fistula in chronic kidney disease in the mouse: beneficial effects of upregulated heme oxygenase-1. *American journal of physiology. Renal physiology* **310**, F466-476 (2016).

43. Liew, F.Y., Xu, D., Brint, E.K. & O'Neill, L.A.J. Negative regulation of Toll-like receptor-mediated immune responses. *Nat Rev Immunol* **5**, 446-458 (2005).

44. Sanin, D.E., Prendergast, C.T. & Mountford, A.P. IL-10 production in macrophages is regulated by a TLR-driven CREB-mediated mechanism that is linked to genes involved in cell metabolism(). *Journal of immunology (Baltimore, Md. : 1950)* **195**, 1218-1232 (2015).

45. Galis, Z.S. & Khatri, J.J. Matrix metalloproteinases in vascular remodeling and atherogenesis: the good, the bad, and the ugly. *Circulation research* **90**, 251-262 (2002).

46. Castier, Y., Ramkhelawon, B., Riou, S., Tedgui, A. & Lehoux, S. Role of NF-kappaB in flow-induced vascular remodeling. *Antioxidants & redox signaling* **11**, 1641-1649 (2009).

47. Nieves Torres, E.C., *et al.* Adventitial Delivery of Lentivirus-shRNA-ADAMTS-1 Reduces Venous Stenosis Formation in Arteriovenous Fistula. *PloS one* **9**, e94510 (2014).

48. Mantovani, A., Biswas, S.K., Galdiero, M.R., Sica, A. & Locati, M. Macrophage plasticity and polarization in tissue repair and remodelling. *The Journal of pathology* **229**, 176-185 (2013).

49. Jetten, N., *et al.* Anti-inflammatory M2, but not pro-inflammatory M1 macrophages promote angiogenesis in vivo. *Angiogenesis* **17**, 109-118 (2014).

50. Lichtnekert, J., Kawakami, T., Parks, W.C. & Duffield, J.S. Changes in macrophage phenotype as the immune response evolves. *Current opinion in pharmacology* **13**, 555-564 (2013).

51. Perdiguero, E.G. & Geissmann, F. The development and maintenance of resident macrophages. *Nature immunology* **17**, 2-8 (2015).

52. Wong, C.Y., *et al.* A Novel Murine Model of Arteriovenous Fistula Failure: The Surgical Procedure in Detail. *Journal of visualized experiments : JoVE*, e53294 (2016).

53. de Vries, M.R., *et al.* Plaque rupture complications in murine atherosclerotic vein grafts can be prevented by TIMP-1 overexpression. *PloS one* **7**, e47134 (2012).

54. Kaijzel, E.L., *et al.* Multimodality imaging reveals a gradual increase in matrix metalloproteinase activity at aneurysmal lesions in live fibulin-4 mice. *Circulation. Cardiovascular imaging* **3**, 567-577 (2010).

Chapter 8

Summary and Discussion



Thanks to the invention of the first dialysis machine by Kolff in 1943 combined with the development of vascular access methods that was started by Scribner[1, 2], there finally was a treatment for end stage renal disease (ESRD) patients. At present, kidney transplantation has become the preferred modality in kidney replacement therapy. Although the number of patients with a functioning donor kidney in the Netherlands is increasing, the shortage of suitable donors still persists. The remaining group of patients that is dependent on dialysis is therefore still a considerable one (40%)[3]. Hemodialysis is the most widely used option in chronic dialysis treatment and requires a suitable vascular access. Unfortunately, this vascular access suffers from a high number of failures responsible for a high morbidity and health care costs.

In **chapter 2** the pathophysiology of arteriovenous fistula (AVF) failure is discussed. Although the exact pathophysiology of AVF failure remains unclear, there is a general consensus among researchers that it is multifactorial. At an anatomical level, the two main processes that are responsible for AVF failure are intimal hyperplasia (IH) and inadequate outward remodelling (OR). The vascular adaptation process is mainly driven by altered haemodynamical factors that starts with the surgical procedure in which the low-pressure vein is connected to the high-pressure arterial system. The result is an immediate increase in blood flow through both the feeding artery and the draining vein[4, 5]. This rapid increase in flow results both in passive vascular distension and in an nitric oxide (NO) driven active distension in which the endothelial cells(ECs) produce NO that in its turn relaxes the vascular smooth muscle cells (VSMCs)[6, 7]. Concomitantly, a more structural form of vascular remodelling is initiated as the body is trying to normalize the increased wall shear stress and wall tension by increasing the luminal diameter and increasing vessel wall thickness, respectively[8]. It is believed that the endothelial and vascular smooth cell are the key players, and that the process starts with the EC that converts haemodynamic stimuli into biochemical signals such as vasodilating agents, growth factors, cellular adhesion molecules, cathepsins and matrix metalloproteinases (MMPs). Intimal hyperplasia is the pathologic lesion in AVFs that may result in stenosis and ultimately thrombosis. At a histological level, IH is characterized primarily by alpha smooth muscle actin (α-SMA) positive cells from which the vast majority exhibit a myofibroblast or synthetic VSMC phenotype. The pathophysiology of intimal hyperplasia is believed to be multifactorial and has been well described in literature. One of the factors associated with IH is unfavourable haemodynamic profile in the form of low flow and oscillating flow pattern. Also, ESRD associated pathologies such as a chronic inflammatory state[9, 10], uremia[11, 12] and increased baseline levels of oxidative stress[13] all seem to contribute to IH formation. Moreover, pre-existing venous IH and vascular calcification both can influence AVF maturation in a negative way. The net resultant of the unbeneficial IH formation and beneficial OR will

ultimately determine luminal calibre, flow and long term patency. Due to the potential positive contribution to AVF maturation and its assumed role in luminal calibre preservation, we pledge for more research emphasis on the role of outward remodelling.

In order to study the complex effects that is involved in AVF failure, we decided to utilize an in-vivo animal model that mimics the human situation as closely as possible. Numerous animal models have been developed over het past decades in order to unravel vascular access related pathology. Large animals such as baboons, pigs, goats, sheep and dogs have the advantage that the vascular dimensions approaches the human situation more closely than in smaller animals. This is important due to the fact that hemodynamical factors are considered to be an important contributor to AVF failure. These larger animal models are very suitable for experimental set-ups aimed at surgical and interventional techniques. However, the high costs and moderate availability associated with large animals have to be taken into account. In contrary, smaller animals such as rodents are less costly and are more easily available. More importantly, due to the availability of transgenic mice, murine models are very well suited for studies aimed at unravelling the molecular mechanisms. However, due to the small dimensions a surgeon that is skilled in microsurgery is a requirement. In 2006, Castier et al.[14] introduced an improved murine model of AVF failure in which he was the first to describe a vascular anastomosis using only sutures, thus eliminating the presence of an intravascular catheter. However, the arterial end to venous side vascular anastomosis configuration that was used, does not resemble the most frequently used configuration that is used in humans. This has a great impact on the hemodynamical profile in the AVF.

In **chapter 3** we describe a new murine model that we have developed together with the group of Roy-Chaudhury in which we incorporate a venous end to arterial side anastomosis, resembling the human situation as closely as possible. In this model we connected the right common carotid artery to an ipsilateral branch of the external jugular vein. We analysed the AVF histologically at different time points (day 0, 7, 14 and 28) and observed that IH is mainly located in the venous outflow tract. Chronologically, these lesions appear to start with a mural thrombus that in time is popularized by alpha smooth muscle actin (α-SMA) positive cells. Both the location and the cellular composition of the IH resemble the human vascular pathology that is seen in failed AVFs. The growth of IH increases in a linear fashion in the course of time. The second process that will determine the luminal area is outward remodeling. In our model, OR is only present during the first two weeks after AVF creation. Due to the progressive growth of IH during the whole period and the ceasing of OR after 2 weeks, the luminal area will decrease starting from week 2 ultimately leading to an occlusion of the AVFs at week 4. Postoperatively, we observed a disrupted lining of endothelial cells that that seemed to grew back in a time dependant manner.

Following AVF creation, CD45 positive cells seem to migrate into the vessel wall from the neovascularization in the adventitia. This is different from the traditional concept that the recruitment of inflammatory cells starts from the luminal side. The consequence of this finding is that future therapies directed against the influx of (inflammatory) cells should perhaps be targeted against the adventitia. Moreover, this finding confirms the involvement of inflammation in AVF failure.

The assessment of the patency of the murine AVF using only visual and physical confirmation can sometimes be difficult. Other visualisation techniques such as ultrasonography and magnetic resonance imaging can aid in this assessment. Unfortunately, we were not able to successfully assess the patency of the AVF using the abovementioned techniques due to technical reasons. As an alternative, we used Near Infrared Fluoroscopy (NIRF) This method requires an intravenous injection of indocyanine green, which is then visualized using a specialized camera that captures video images in real-time. This technique proved to be a safe and technical easy to perform vascular patency assessment in our model. In order to help in the surgical training, we described (**chapter 4**) the technically challenging procedure in detail in a step-by-step protocol that also includes a video that demonstrates the key steps.

As described above, following AVF creation the involved vessels need to adapt (mature) in order to become an adequate vascular access point for haemodialysis. The complex process requires the vessel wall to remodel. The vascular wall consists of multiple structures, from which the extracellular matrix (ECM) takes up most of the volume. One of the most prominent proteins in the ECM is elastin. Elastin production begins with the synthesis and secretion of the soluble precursor tropoelastin by VSMCs and is then subsequently crosslinked by lysyl-oxidase to form elastic fibers. These fibers are located concentrically in a group-wise manner, forming the elastic laminae. This structure is responsible for the mechanical properties that is unique and essential for proper function.

In **chapter 5** we studied the effect of elastin on vascular remodelling in our murine AVF model by incorporating a mouse that is haplodeficient for the elastin gene ($eln^{+/-}$). In literature the phenotype has been well described, although it is mainly focused on the artery. Histologically, we observed a reduced amount of elastic fibers in the vein of $eln^{+/-}$ mice prior to surgery, without a compensatory increase in the number of rings of elastic lamellae as is seen in the aorta of these animals[15]. After AVF creation, the amount of elastic fibers in the venous vessel wall is reduced in both the $eln^{+/-}$ and wild type (WT) mice. At 3 weeks the mRNA expression levels of mELN was 53% lower when compared to WT mice. Interestingly, with this decrease in elastin presence we observed an increased OR (21%) in $eln^{+/-}$ mice. We hypothesize that this is due to the reduced mechanical strength in blood vessels of $eln^{+/-}$ mice. This mechanical effect is elegantly demonstrated in a study by Li et al.[15], in which the aorta of $eln^{+/-}$ mice show a reduced extensibility at higher pressures.

Interestingly, elastin did not seem to have an effect on IH formation, though it has been shown that elastin has an anti-proliferative effect on VSMCs. It is not clear why this effect was not seen in our AVF model. Perhaps this is due to the fact that in our model IH is initiated and dependant on the primary thrombus formation after vascular injury, in contrast to the pathophysiology that is seen in haplodeficient mice and humans[15].

While the size of the intimal area did not differ between the WT en $eln^{+\backslash -}$ mice, we did observe a larger content of α-sma positive cells in the venous outflow tract of the $eln^{+/-}$ mice. The latter results from a higher density of α-sma positive cells in the intima. In addition, the enhanced OR response in $eln^{+/-}$ mice also resulted in a larger VSMCs content in the adventitia and media. This observation supports the hypothesis that VSMC proliferation in the initial phase after AVF surgery is required in order to keep pace with the expansion of the venous outflow tract, as demonstrated previously in flow induced arterial OR in rats[16].

The data from this study in which we observed an enlarged OR in the elastin haplodeficient mice provides support for the hypothesis that low elastin content in the venous outflow tract might facilitate AVF maturation. Therapies aimed at lowering the elastin content, such as topical application of pancreatic elastase on AVFs[17], would therefore be a viable strategy to improve AVF maturation.

Animal studies have shown that the adaptive response that occurs upon AVF creation, is characterized by marked vascular inflammation as illustrated by the infiltration of macrophages and lymphocytes[18] as well as the up regulation of pro-inflammatory cytokines[19]. In addition, clinical studies suggest an association between increased inflammatory blood markers and AVF dysfunction[9, 20]. In line with these clinical findings, we observed a marked influx of CD45-positiveinflammatory cells in the vessel wall after AVF creation in our murine model (**chapter 3**), confirming the involvement of inflammation in AVF failure.

Glucocorticoids (GCs) are powerful anti-inflammatory drugs that act through binding to cytosolic glucocorticoid receptors in target cells, leading to a reduction in the expression of pro-inflammatory cytokines and diminished recruitment of inflammatory cells[21, 22]. Despite these potent anti-inflammatory effects, chronic and systemic therapeutic use of GCs is limited by the high incidence of serious adverse effects[23]. Moreover, as a result of rapid clearance from the circulation, systemic administration of GCs results in low efficacy of drug delivery at the target location. Therefore, encapsulation of GCs in liposomal nanoparticles holds great potential, as it can hold their payload while circulating in het vasculature until they extravasate and accumulate at sites of inflammation as a result of enhanced vascular permeability in inflamed tissues, thereby reducing possible systemic side effects and more importantly, increasing the local availability of its payload.

In **chapter 6** we set out to elucidate the role of inflammation in AVF failure, by suppressing the inflammatory reaction in our murine model using liposomal prednisolone (L-Pred). Firstly, we have demonstrated by using near infrared fluoroscopy (NIRF) and immunohistochemistry that the liposomes extravasate and accumulate in macrophages in the anastomotic area of the AVF. More specifically, we believe that the liposomes extravasate from the neovascularization in the adventitia. Interestingly, this is the same area in which IH is most prominent. Therefore, delivery of GCs in this area would be desirable.

At a morphometrical level, treatment with L-Pred resulted in an increase in OR of 27%, a 47% increase in luminal area and a trend towards a higher IH area when compared to the PBS treated group. Control groups that were administered either liposomal PBS or unencapsulated prednisolone did not show any effect on the morphometry. This interesting finding is accompanied by the anti-inflammatory effect of prednisolone. We have confirmed this reaction histologically and in in-vitro experiments. Histologically, we observed an 83% reduction in the amount of CD45 positive cells in animals treated with L-Pred when compared to PBS treated controls. Looking more closely at the specific type of inflammatory cells, we observed a reduction of 86% and 51% in T-cells and granulocytes, respectively.

Interestingly, liposomes themselves contribute to the reduction of the pro-inflammatory profile of macrophages, as illustrated by the reduction of pro-inflammatory cytokines in M1 macrophages upon stimulation with L-PBS. This shift towards an anti-inflammatory profile of macrophages might have inhibited the recruitment of lymphocytes and granulocytes to the injured vessels of the AVF. Alternatively, prednisolone might have had a direct effect on lymphocytes and granulocytes as GCs can easily pass the cellular membrane of macrophages in both directions.

The exact mechanism by which liposomal prednisolone resulted in increased OR in murine AVF is not clear. We speculate that matrix metalloproteinases might be involved in this response. MMPs are a group of proteolytic enzymes involved in vascular remodeling by facilitating the turnover of extracellular matrix components such as collagen and elastin[24]. The effect of MMPs on the vascular remodeling depend on the specific MMPs that are activated and the type of vascular injury[25]. Previous studies in a porcine balloon angioplasty model in peripheral arteries revealed that treatment with the MMP-inhibitor marimastatin resulted in reduced constrictive arterial remodeling in favor of expansive remodelling[26]. In addition, a recent clinical trial evaluating the efficacy of the MMP-inhibitor doxycycline to inhibit growth of abdominal aortic aneurysms resulted in an unexpected acceleration of the aneurysmal growth[27]. These data suggest that in certain vascular disease conditions, inhibition of MMPs could enhance outward remodeling. Interestingly, elegant studies by Nieves Torres and coworkers[28] suggest a similar effect of MMP inhibiton on venous outward remodeling

in AVF. Indeed, adventitial delivery of a small hairpin RNA against the MMP ADAMTS-1, resulted in reduced macrophage infiltration, decreased MMP-9 activity and enhanced outward remodeling in murine AVF. We have demonstrated that L-pred effectively increases MMP2 and MMP9 expression in cultured macrophages. Although we have not been able to quantify MMP activity *in vivo*, we speculate that the enhanced outward remodeling in murine AVF that occurred upon treatment with L-Pred is mediated by the dampened inflammatory response and decreased MMP activity in macrophages.

In contrast to its effect on outward remodeling, no effect of L-Pred on IH in the venous outflow tract was observed. These results deviate from other preclinical studies that evaluated the therapeutic effect of GCs in other vascular injury models, that have reported a strong inhibitory effect of dexamethasone on IH[29-31]. This discrepancy may result from a difference in potency between prednisolone and dexamethasone to inhibit VSMC proliferation[32]. Alternatively, it may relate to the difference in pathophysiological stimuli that contribute to IH after arterial injury, when compared to venous IH in AVF. While hemodynamic stimuli are considered to be of vital importance for IH[33, 34], the contribution of inflammation to IH in AVF might be limited, as suggested by our results. Ultimately, the net result of vascular remodelling in the AVF was an increased luminal area in the venous outflow tract, that was mainly accountable by the OR process alone.

In conclusion, liposomal prednisolone reduces the local inflammatory response and stimulates venous outward remodeling in murine AVF. Therefore, treatment with liposomal prednisolone might be valuable strategy to reduce AVF non-maturation. Based on the results of this study, a double-blind, randomized, placebo-controlled clinical trial was initiated that will evaluate the efficacy of liposomal prednisolone to enhance AVF maturation in ESRD patients.

In **chapter 7** we study the effects of the Toll-Like Receptor 4 (TLR4) inhibitor RP105 on AVF maturation. Based on the hypothesis that TLR4 mediated inflammatory responses contribute to vascular remodeling in several pathophysiological processes, we expected an increased AVF maturation in mice that are deficient of the TLR4 inhibitor RP105. Surprisingly we observed a slight but significant reduction in outward remodeling in the venous limb of the AVFs in $RP105^{-/-}$ mice. More detailed analysis of the effects of RP105 deficiency on the inflammatory response revealed an unexpected reduction in pro-inflammatory macrophages (M1) and a strong shift towards anti-inflammatory M2 macrophages. This was accompanied by a 70% reduction in CD3+ T-cells and a reduction in MMP activity. Moreover, we observed strong effects on proliferation of smooth muscle cells of both arterial and venous origin. Since the expression of RP105 in the latter group of smooth muscle cells is much higher, the inhibitory effects on proliferation of venous smooth muscle cells , the cells that most likely are the strongest contributors to outward remodeling of the arteriovenous fistulas, are the most prominent

effects observed. These results demonstrate that the concept of inhibiting the inhibitor of TLR4 in order to stimulate the TLR4 mediated inflammatory driven outward remodeling is too simple and a better understanding of the complex interaction of the various cell types involved in fistula maturation and especially the role of RP105 in these multifactorial processes is essential before any therapeutic options can be defined on this concept.

Final conclusion

Arteriovenous fistula failure is a major clinical problem that is responsible for high morbidity and healthcare cost in patients that are in need of a chronic hemodialysis vascular access. Despite all the research that has been committed, the exact pathophysiology remains unknown. One of the objectives was to develop a murine model of AVF failure that was different compared to the existing murine models in the way that it resembles the vascular configuration in humans. In the murine model that was used prior to our newly introduced model, the anastomosis was configurated in an venous-side to arterial-end manner, whereas we introduced a configuration that consisted of an arterial-side to venous-end. This difference in configuration is important in that it leads to a different hemodynamical profile, which in itself also seems to contribute to the pathophysiology of AVF failure. We successfully created a novel murine model that showed similar histological pathologies as is seen in failed human arteriovenous fistulas. This model can be used to study the pathophysiology of AVF failure and to explore possible future therapies. Interestingly, our model showed that the characteristic intimal hyperplasia that is seen in AVF failure is firstly initiated by thrombus formation, followed by the popularisation of α-smooth muscle actin positive cells. This suggests that prevention of thrombus formation would decrease intimal hyperplasia and therefore AVF failure. However, anti-coagulatory/ anti platelet therapies in the clinical setting never have shown an improvement in maturation failure on the long term[35]. Moreover, the administration of vitamin K antagonism even seems to increase intimal hyperplasia in rats[36].

Although chronic kidney disease (CKD) seems to accelerate the development of intimal hyperplasia in mice who received an AVF[37], most of the research, including ours, were conducted in an non CKD animal. For future research we would propose to combine our model with a CKD model such as described by Kang et. al[38].

Following the development of a novel AVF model, we then focused on the unravelling of the pathophysiology behind AVF failure. We first explored the role of the extra cellular matrix protein elastin and showed that a reduction in elastin increases the outward remodelling process, due to the altered mechanical composition of the blood vessel. This concept is now

being researched in a clinical trial, in which human type 1 pancreatic elastase (PRT-201) is locally applied on AVFs[17] and arteriovenous grafts[39]. The first results are promising, but it will need to be confirmed in larger studies.

Next, we focused on the role of inflammation in AVF failure. In our AVF model we observed a marked influx of CD-45 positive cells in the vessel wall, suggesting that inflammation is involved in AVF maturation. To further explore this, we reduced the inflammatory response by administering liposomal prednisolone, which led to an increased outward remodelling and luminal area of the venous outflow tract of the AVF. Suggesting that the localised delivery of prednisolone via liposomes has a beneficial effect in AVF maturation. This hypothesis will be investigated in a double-blind, randomized, placebo-controlled trial in humans that commenced in 2015.

In contrast to the study with liposomal prednisolone, we also wanted to explore the effect on AVF maturation when the inflammation was increased via the TLR4 pathway by removing the TLR4 inhibitor RP105 using KO mice. To our surprise, we observed an unexpected anti-inflammatory effect that led to an decreased outward remodeling of the AVF. This effect may relate to a shift of macrophages towards the M2 phenotype, reduction in MMP activity and a decreased proliferation rate of VSMCs. This unexpected result towards an anti-inflammatory effect, demonstrates that the TLR4 mediated pathway is more complex than anticipated and that more understanding of this process is needed before we can define a therapeutic strategy for this pathway.

Reference List

1. Quinton W, Dillard D, Scribner BH. Cannulation of blood vessels for prolonged hemodialysis. Hemodial Int 2004 Jan 1;8(1):6-9.

2. Scribner BH, Buri R, Caner JE, Hegstrom R, Burnell JM. The treatment of chronic uremia by means of intermittent hemodialysis: a preliminary report. 1960. J Am Soc Nephrol 1998 Apr;9(4):719-26.

3. Renine.nl. 2015.

4. Saucy F, Haesler E, Haller C, Deglise S, Teta D, Corpataux JM. Is intra-operative blood flow predictive for early failure of radiocephalic arteriovenous fistula? Nephrol Dial Transplant 2010 Mar;25(3):862-7.

5. Tordoir JH, Rooyens P, Dammers R, van der Sande FM, de HM, Yo TI. Prospective evaluation of failure modes in autogenous radiocephalic wrist access for haemodialysis. Nephrol Dial Transplant 2003 Feb;18(2):378-83.

6. Cooke JP, Rossitch E Jr, Andon NA, Loscalzo J, Dzau VJ. Flow activates an endothelial potassium channel to release an endogenous nitrovasodilator. J Clin Invest 1991 Nov;88(5):1663-71.

7. Tronc F, Wassef M, Esposito B, Henrion D, Glagov S, Tedgui A. Role of NO in flow-induced remodeling of the rabbit common carotid artery. Arterioscler Thromb Vasc Biol 1996 Oct;16(10):1256-62.

8. Corpataux JM, Haesler E, Silacci P, Ris HB, Hayoz D. Low-pressure environment and remodelling of the forearm vein in Brescia-Cimino haemodialysis access. Nephrol Dial Transplant 2002 Jun;17(6):1057-62.

9. Liu BC, Li L, Gao M, Wang YL, Yu JR. Microinflammation is involved in the dysfunction of arteriovenous fistula in patients with maintenance hemodialysis. Chin Med J (Engl) 2008 Nov 5;121(21):2157-61.

10. Sezer S, Ozdemir FN, Arat Z, Turan M, Haberal M. Triad of malnutrition, inflammation, and atherosclerosis in hemodialysis patients. Nephron 2002 Jul;91(3):456-62.

11. Bolton CH, Downs LG, Victory JG, Dwight JF, Tomson CR, Mackness MI, et al. Endothelial dysfunction in chronic renal failure: roles of lipoprotein oxidation and pro-inflammatory cytokines. Nephrol Dial Transplant 2001 Jun;16(6):1189-97.

12. Ghiadoni L, Cupisti A, Huang Y, Mattei P, Cardinal H, Favilla S, et al. Endothelial dysfunction and oxidative stress in chronic renal failure. J Nephrol 2004 Jul;17(4):512-9.

13. Himmelfarb J, Stenvinkel P, Ikizler TA, Hakim RM. The elephant in uremia: oxidant stress as a unifying concept of cardiovascular disease in uremia. Kidney Int 2002 Nov;62(5):1524-38.

14. Castier Y, Lehoux S, Hu Y, Foteinos G, Tedgui A, Xu Q. Characterization of neointima lesions associated with arteriovenous fistulas in a mouse model. Kidney Int 2006 Jul;70(2):315-20.

15. Li DY, Faury G, Taylor DG, Davis EC, Boyle WA, Mecham RP, et al. Novel arterial pathology in mice and humans hemizygous for elastin. J Clin Invest 1998 Nov 15;102(10):1783-7.

16. Buus CL, Pourageaud F, Fazzi GE, Janssen G, Mulvany MJ, De Mey JG. Smooth muscle cell changes during flow-related remodeling of rat mesenteric resistance arteries. Circ Res 2001 Jul 20;89(2):180-6.

17. Hye RJ, Peden EK, O'Connor TP, Browne BJ, Dixon BS, Schanzer AS, et al. Human type I pancreatic elastase treatment of arteriovenous fistulas in patients with chronic kidney disease. J Vasc Surg 2014 Aug;60(2):454-61.

18. Wang Y, Krishnamoorthy M, Banerjee R, Zhang J, Rudich S, Holland C, et al. Venous stenosis in a pig arteriovenous fistula model--anatomy, mechanisms and cellular phenotypes. Nephrol Dial Transplant 2008 Feb;23(2):525-33.

19. Nath KA, Kanakiriya SK, Grande JP, Croatt AJ, Katusic ZS. Increased venous proinflammatory gene expression and intimal hyperplasia in an aorto-caval fistula model in the rat. Am J Pathol 2003 Jun;162(6):2079-90.

20. Kaygin MA, Halici U, Aydin A, Dag O, Binici DN, Limandal HK, et al. The relationship between arteriovenous fistula success and inflammation. Ren Fail 2013 Sep;35(8):1085-8.

21. Cronstein BN, Kimmel SC, Levin RI, Martiniuk F, Weissmann G. A mechanism for the antiinflammatory effects of corticosteroids: the glucocorticoid receptor regulates leukocyte adhesion to endothelial cells and expression of endothelial-leukocyte adhesion molecule 1 and intercellular adhesion molecule 1. Proc Natl Acad Sci U S A 1992 Nov 1;89(21):9991-5.

22. Rhen T, Cidlowski JA. Antiinflammatory action of glucocorticoids--new mechanisms for old drugs. N Engl J Med 2005 Oct 20;353(16):1711-23.

23. Metselaar JM, Wauben MH, Wagenaar-Hilbers JP, Boerman OC, Storm G. Complete remission of experimental arthritis by joint targeting of glucocorticoids with long-circulating liposomes. Arthritis Rheum 2003 Jul;48(7):2059-66.

24. Wang M, Zhao D, Spinetti G, Zhang J, Jiang LQ, Pintus G, et al. Matrix metalloproteinase 2 activation of transforming growth factor-beta1 (TGF-beta1) and TGF-beta1-type II receptor signaling within the aged arterial wall. Arterioscler Thromb Vasc Biol 2006 Jul;26(7):1503-9.

25. Galis ZS, Khatri JJ. Matrix metalloproteinases in vascular remodeling and atherogenesis: the good, the bad, and the ugly. Circ Res 2002 Feb 22;90(3):251-62.

26. Sierevogel MJ, Pasterkamp G, Velema E, de Jaegere PP, de Smet BJ, Verheijen JH, et al. Oral matrix metalloproteinase inhibition and arterial remodeling after balloon dilation: an intravascular ultrasound study in the pig. Circulation 2001 Jan 16;103(2):302-7.

27. Meijer CA, Stijnen T, Wasser MN, Hamming JF, van Bockel JH, Lindeman JH. Doxycycline for stabilization of abdominal aortic aneurysms: a randomized trial. Ann Intern Med 2013 Dec 17;159(12):815-23.

28. Nieves Torres EC, Yang B, Roy B, Janardhanan R, Brahmbhatt A, Leof E, et al. Adventitial delivery of lentivirus-shRNA-ADAMTS-1 reduces venous stenosis formation in arteriovenous fistula. PLoS One 2014;9(4):e94510.

29. Pires NM, Schepers A, van der Hoeven BL, de Vries MR, Boesten LS, Jukema JW, et al. Histopathologic alterations following local delivery of dexamethasone to inhibit restenosis in murine arteries. Cardiovasc Res 2005 Dec 1;68(3):415-24.

30. Schepers A, Pires NM, Eefting D, de Vries MR, van Bockel JH, Quax PH. Short-term dexamethasone treatment inhibits vein graft thickening in hypercholesterolemic ApoE3Leiden transgenic mice. J Vasc Surg 2006 Apr;43(4):809-15.

31. Villa AE, Guzman LA, Chen W, Golomb G, Levy RJ, Topol EJ. Local delivery of dexamethasone for prevention of neointimal proliferation in a rat model of balloon angioplasty. J Clin Invest 1994 Mar;93(3):1243-9.

32. Reil TD, Sarkar R, Kashyap VS, Sarkar M, Gelabert HA. Dexamethasone suppresses vascular smooth muscle cell proliferation. J Surg Res 1999 Jul;85(1):109-14.

33. Roy-Chaudhury P, Spergel LM, Besarab A, Asif A, Ravani P. Biology of arteriovenous fistula failure. J Nephrol 2007 Mar;20(2):150-63.

34. Asif A, Roy-Chaudhury P, Beathard GA. Early arteriovenous fistula failure: a logical proposal for when and how to intervene. Clin J Am Soc Nephrol 2006 Mar;1(2):332-9.

35. Dember LM, Beck GJ, Allon M, Delmez JA, Dixon BS, Greenberg A, et al. Effect of clopidogrel on early failure of arteriovenous fistulas for hemodialysis: a randomized controlled trial. JAMA 2008 May 14;299(18):2164-71.

36. Zaragatski E, Grommes J, Schurgers LJ, Langer S, Kennes L, Tamm M, et al. Vitamin K antagonism aggravates chronic kidney disease-induced neointimal hyperplasia and calcification in arterialized veins: role of vitamin K treatment? Kidney Int 2015 Oct 14.

37. Kokubo T, Ishikawa N, Uchida H, Chasnoff SE, Xie X, Mathew S, et al. CKD accelerates development of neointimal hyperplasia in arteriovenous fistulas. J Am Soc Nephrol 2009 Jun;20(6):1236-45.

38. Kang L, Grande JP, Hillestad ML, Croatt AJ, Barry MA, Katusic ZS, et al. A new model of an arteriovenous fistula in chronic kidney disease in the mouse: beneficial effects of upregulated heme oxygenase-1. Am J Physiol Renal Physiol 2016 Mar 15;310(6):F466-F476.

39. Dwivedi AJ, Roy-Chaudhury P, Peden EK, Browne BJ, Ladenheim ED, Scavo VA, et al. Application of human type I pancreatic elastase (PRT-201) to the venous anastomosis of arteriovenous grafts in patients with chronic kidney disease. J Vasc Access 2014 Sep;15(5):376-84.

Chapter 9

Nederlandse Samenvatting

Curriculum Vitae

List of Publications

Dankwoord



Nederlandse Samenvatting

Dankzij de ontwikkeling van de hemodialyse machine in 1943 door Kolff en vaattoegangs mogelijkheden door Scribner, was er eindelijk een behandeling voor patiënten met eind stadium nierfalen. In de loop van de jaren zijn de behandelopties uitgebreid en verbeterd, waarbij de transplantatie van een nier in de meerderheid van de gevallen de voorkeur geniet boven dialyse. Hoewel het aantal patiënten met een functionerende donornier toeneemt in Nederland, blijft het probleem bestaan dat het aanbod van donornieren kleiner is dan de vraag. De groep patiënten die geen niertransplantaat hebben en dus van dialyse afhankelijk zijn blijft groot (40%). Hemodialyse is de meest toegepaste vorm van dialyse, maar dit vereist wel dat er sprake moet zijn van een goede vaattoegang waarmee het bloedsomloop van de patiënt gekoppeld kan worden aan het dialyse apparaat. Helaas, zijn er veel problemen met deze vaattoegang welke leidt tot een hoge morbiditeit en ziektekosten.

In **hoofdstuk 2** wordt de pathofysiologie van arterioveneus fistel (AVF) falen bediscussieerd. Hoewel de exacte pathofysiologie hiervan grotendeels onbekend blijft, is er in de literatuur wel een consensus dat het gaat om multifactoriële factoren die hieraan ten grondslag liggen. Op het anatomisch niveau zijn er een tweetal processen die we kunnen identificeren, namelijk; intima hyperplasie (IH) en inadequate outward remodeling (OR). De vasculaire aanpassing die het bloedvat moet ondergaan wordt hoofdzakelijk gedreven door de veranderde hemodynamische factoren die ontstaan nadat bij de chirurgische procedure een vene waarin een lage druk heerst, wordt aangesloten op een arterie waar juist een hoge druk heerst. Dit resulteert in een directe toename in bloedflow van de zowel de arterie als de vene. Deze snelle stijging in bloedflow leidt tot zowel een passieve- als in een door stikstof oxide (NO) gedreven actieve vaatdistensie. Deze laatste wordt door de endotheelcellen geproduceerd en leidt tot relaxatie van de vaatwand via de gladde spiercellen (VSMCs). Vanuit een functioneel/mechanisch oogpunt van vaatremodelering, zal het lichaam proberen de veranderde hemodynamiek zoals een toename in “wall shear stress” en druk op de vaatwand te compenseren door respectievelijk toe te nemen in diameter en vaatwanddikte. De endotheelcel en gladde spiercel lijken hierin een hoofdrol te spelen, waarbij de endotheelcel hemodynamische stimuli omzetten in biochemische signalen zoals vasodilaterende factoren, groeifactoren, cellulaire adhesie moleculen, cathepsines en matrix metalloproteinases (MMPs).
Intima hyperplasie is de pathologische laesie in AVFs die kan leiden tot stenose en uiteindelijk trombose. Op histologisch niveau wordt IH gekenmerkt door alpha-smooth muscle actin (α-SMA) positieve cellen, waarvan de meerderheid een myofibroblast of synthetische VSMC fenotype heeft. De pathofysiologie van IH is multifactorieel. Een van de factoren die hierin een

rol speelt zijn ongunstige hemodynamische profielen zoals een lage flow en een oscillerende flow patronen. Daarnaast zijn de pathologische processen die vaak gepaard gaan met eindstadium nierfalen zoals een chronisch verhoogde inflammatoire status, hyperuremie en verhoogde oxidatieve stress ook allen bijdragend aan IH vorming. Naast de hierbovengenoemde ongunstige factoren, blijkt er ook nog eens dat pre-existente IH laesies en vasculaire verkalking beiden een negatieve invloed hebben op AVF maturatie.
Het netto resultaat van het ongunstige IH vorming en het gunstige OR zal uiteindelijke het lumen kaliber, bloed flow en de lange termijns patency bepalen. Hoewel in de literatuur met name wordt gekeken naar mogelijkheden om IH te remmen, pleiten wij er juist voor om ook aandacht te besteden aan het stimuleren van OR.
Om de complexe processen te bestuderen die betrokken zijn in AVF falen, wilden wij een diermodel gebruiken die de klinische situatie het dichtst mogelijk benaderd. In de loop van de jaren zijn er meerdere diermodellen ontwikkeld die worden gebruikt om AVF falen te bestuderen. Dieren van een groot formaat zoals bavianen, varkens, geiten, schapen en honden hebben het voordeel dat de vasculaire dimensies dichtbij die van de mens zitten. Dit is met name van belang doordat de hemodynamiek een belangrijke rol speelt. Deze diermodellen zijn zeer geschikt voor experimentele opzetten die gericht zijn op chirurgische en interventionele technieken. Helaas zijn de faciliteiten hiervoor beperkt en zijn de kosten relatief hoog. Het gebruik van kleine proefdieren zoals muizen en ratten is daarentegen juist relatief goedkoop en de faciliteiten zijn beter beschikbaar. Een ander belangrijk voordeel van het gebruik van muizen is dat deze de mogelijkheid bieden tot genetische modificatie. Dit maakt een muismodel uitermate geschikt om mechanistische vraagstukken te onderzoeken. Het nadeel van een muismodel is dat de dimensies klein zijn, waardoor het chirurgisch technisch uitdagender wordt. In 2016 introduceerde Castier et al. een muismodel voor AVF falen, waarin voor het eerst gebruik werd gemaakt van alleen hechtingen om de anastomose te maken. Hiermee werd het gebruik van een kunststof katheter verlaten. De configuratie van de anastomose (arteriële end naar veneuze side) is echter niet gelijkend op de situatie zoals deze meestal in de klinische setting is (Veneuze end naar arteriële side). Dit laatste is van belang omdat met een andere configuratie er ook sprake is van een andere hemodynamiek.

In **hoofdstuk 3** beschrijven we een nieuw muismodel die samen met de onderzoeksgroep van dr. Roy-Chaudhury werd ontwikkeld en waarin een arteriële side naar veneuze end anastomose gebruikt wordt, zoals deze ook in de klinische setting meestal wordt gebruikt. In dit model wordt de rechter carotis communis met de ipsilaterale tak van de vena jugularis externa verbonden met 10.0 hechtingen. De AVF werd op verschillende tijdspunten (Dag 0, 7, 14 en 28) histologisch geanalyseerd, en daaruit bleek dat de IH voornamelijk gelokaliseerd was

in het veneuze uitstroomgebied. Chronologisch gezien lijken deze IH laesies te beginnen als een wandtrombus dat naarmate de tijd vordert gepopulariseerd wordt door α-SMA positieve cellen. Zowel de locatie als de cellulaire compositie van de IH vertoont gelijkenis met die van gefaalde humane AVFs. De groei van de IH laesies verloopt op lineaire wijze. Als we kijken naar OR in ons model zien we dat deze alleen in de eerste 2 weken na de operatie aanwezig is. Door de lineaire groei van IH en het stoppen van OR na 2 weken neemt het luminale oppervlak vanaf week 2 geleidelijk af. In ongeveer de helft van de gevallen leidt dit proces tot een totale occlusie op week 4.
In de eerste week na de operatie is er een duidelijk verlies van endotheelcellen in de vaatwand. In de loop van de tijd wordt dit echter wel weer hersteld.
Na de creatie van de AVF lijkt het erop dat er een migratie van CD45 positieve cellen plaatsvindt beginnend vanuit de neovascularisatie in de adventitia. Toekomstige therapieën zouden dan zich dan hierop kunnen richten.
Het fysisch objectiveren van de functionaliteit van de AVF in de muis kan lastig zijn. Diagnostische hulpmiddelen zoals echografie en MRI zou hierin mogelijk kunnen helpen. Helaas was het gebruik van de hierbovengenoemde modaliteiten niet succesvol gebleken in onze handen. Als alternatief hiervoor hebben we met succes met Near Infrared Fluoroscopy (NIRF) de AVF functioneel kunnen visualiseren. Deze methode vereist een intraveneuze injectie met een contrastmiddel die dan wordt gevisualiseerd met behulp van een gespecialiseerde camera die de videobeelden in realtime kan genereren.

Om de complexe ingreep verder te verduidelijken hebben we in **hoofdstuk 4** de operatieprocedure gefilmd en de belangrijkste stappen gemonteerd in een video.

Na de succesvolle ontwikkeling van het diermodel, wordt de aandacht gericht op de mechanistische processen die in het bloedvat plaatsvinden na het aanleggen van de AVF. Een van de belangrijkste eiwitten die in een bloedvat zit is elastine. Dit eiwit geeft het bloedvat zijn elastische eigenschappen die nodig zijn voor een goede functie. In **hoofdstuk 5** bestuderen we het effect hiervan op OR en IH door muizen te opereren die haplo-deficiënt ($eln^{+/-}$) zijn voor het tropo-elastine gen. Deze muizen hebben een 53% reductie in mRNA expressie van tropoelastine in de veneuze vaatwand leidend tot een afname van elastische vezels. De haplo-deficiënte muizen laten 21 dagen na het aanleggen van een AVF een 21 % toename van het omtrek zien. Onze hypothese is dat dit veroorzaakt wordt doordat elastine een belangrijke mechanisch component is die bijdraagt aan de sterkte van het bloedvat. Het wegnemen van een dergelijk component zal er dan toe leiden dat deze minder tegendruk kan geven aan de toegenomen bloeddruk, met als gevolg dat het bloedvat meer zal uitzetten.

Het reduceren van elastine in de bloedvaten leidt in ons diermodel niet tot een toename van IH. Wel wordt er een toename gezien in het aantal α-SMA positieve cellen in de $eln^{+/-}$ muizen. Dit laatste wordt mogelijk verklaard doordat VSMC proliferatie nodig is om OR te kunnen bewerkstelligen. Het reduceren van elastine in de AVF lijkt dus gunstig te zijn op de OR en derhalve zou een therapie die dit bewerkstelligt gunstig kunnen zijn.

In **hoofdstuk 6** wordt de rol van inflammatie in de AVF bekeken in ons muismodel. We hebben eerder in ons diermodel gezien dat er postoperatief sprake was van een duidelijke influx van CD-45 positieve ontstekingscellen. Om het effect van deze ontstekingsreactie op AVF maturatie te bestuderen hebben we de muizen postoperatief het anti-inflammatoire prednisolon toegediend. Om het prednisolon maximaal op lokaal niveau van de AVF te krijgen via een systemische intraveneuze toediening, werd deze verpakt in een liposoom. Een liposoom is een transporter dat ervoor zorgt dat de prednisolon die in de bloedsomloop circuleert niet actief kan worden, totdat deze uit het bloedsomloop treedt via lekkende vaten die aanwezig zijn in inflammatoir weefsel. We zien in ons diermodel dat deze liposomen inderdaad met name rondom de anastomose uittreden en worden gefagocyteerd door macrofagen. Het remmen van de inflammatie leidt tot een toename van OR en lumen oppervlak van respectievelijk 27% en 47%. Hoewel statistisch niet significant, leek de IH hoger in de dieren die met liposomaal prednisolon waren behandeld. We speculeren dat dit effect veroorzaakt wordt door een reductie in activiteit van MMPs. Het remmen van de inflammatoire respons na AVF chirurgie lijkt dus een positieve invloed te hebben op AVF maturatie. Op basis van deze studie werd in 2016 een dubbel geblindeerde, gerandomiseerde en placebo gecontroleerde klinische trial gestart waarbij hetzelfde liposomale prednisolon gebruikt wordt in patiënten met nierfalen.

In **hoofdstuk 7** gaan we verder in op de rol van inflammatie op AVF maturatie. We hebben specifiek gekeken naar de effecten, wanneer de inflammatie gestimuleerd zou worden via de Toll-like receptor 4 (TLR4) pathway door het remmend RP105 complex uit te schakelen middels het gebruik van RP105 knock out muizen ($RP105^{-/-}$). Dit bleek echter een ander effect te hebben dan gedacht. Er was sprake van juist een anti-inflammatoir effect met hierbij een toename van het aantal anti-inflammatoire M2 macrofagen en afname van T-cellen. Hierbij werd ook een afname in MMP activiteit en VSMC proliferatie gezien in de $RP105^{-/-}$ muizen die leiden tot afwijkende OR.

Ten slotte geeft **hoofdstuk 8** een beschouwing en discussie van alle studies die in dit proefschrift zijn beschreven.

Curriculum Vitae

Chun-Yu Wong werd op 17 augustus 1982 geboren in Leidschendam. In 2000 behaalde hij het VWO eindexamen aan het Alfrink College in Zoetermeer, waarna hij geneeskunde ging studeren aan de Universiteit van Leiden. Tijdens de studie geneeskunde werkte hij mee aan verschillende wetenschappelijke artikelen op de afdeling Heelkunde bij dr. G.N. Jukema. In 2007 behaalde hij zijn arts-examen, waarna hij tot 2009 heeft gewerkt als arts-assistent niet in opleiding tot specialist (ANIOS) op de spoedeisende hulp en later op de afdeling heelkunde in het Bronovo Ziekenhuis (opleider dr. H.J. Smeets). Hierna is hij in 2009 gestart als arts-onderzoeker bij de afdeling Nierziekten en afdeling Heelkunde en het Einthoven Laboratory for Experimental Vascular Medicine van het Leids Universitair Medisch centrum onder de begeleiding van dr. J.I. Rotmans, Prof. dr. A.J. Rabelink en Prof. dr. P.H.A. Quax.
Sinds 2013 is hij gestart met de opleiding tot chirurg aan het Leids Universitair Medisch Centrum (opleider prof. dr. J.F. Hamming) . De opleiding werd sinds 2015 vervolgd in het Alrijne Ziekenhuis (opleider dr. A.M. Zeillemaker) waar hij zich zal specialiseren in de vaatchirurgie.

List of Publications

Wong C, Rothuizen TC, Quax PH, van Zonneveld AJ, Rabelink TJ, Rotmans JI.
Arteriovenous access failure:more than just intimal hyperplasia?
Nephrol Dial Transplant. 2013 May;28(5):1085-92

Wong CY, de Vries MR, Wang Y, van der Vorst JR, Vahrmeijer AL, van Zonneveld AJ, Roy-Chaudhury P, Rabelink TJ, Quax PH,Rotmans JI.
Vascular remodeling and intimal hyperplasia in a novel murine model of arteriovenous fistula failure.
J Vasc Surg. 2014 Jan;59(1):192-201

Wong CY, de Vries MR, Wang Y, van der Vorst JR, Vahrmeijer AL, van Zonneveld AJ, Hamming JF, Roy-Chaudhury P, Rabelink TJ, Quax PH, Rotmans JI.
A Novel Murine Model of Arteriovenous Fistula Failure: The Surgical Procedure in Detail.
J Vis Exp. 2016 Feb 3;(108)

Wong CY, Rothuizen TC, de Vries MR, Rabelink TJ, Hamming JF, van Zonneveld AJ, Quax PH, Rotmans JI.
Elastin is a key regulator of outward remodeling in arteriovenous fistulas.
Eur J Vasc Endovasc Surg. 2015 Apr;49(4):480-6

Wong CY, Bezhaeva T, Rothuizen TC, Metselaar JM, de Vries MR, Verbeek FP, Vahrmeijer AL, Wezel A, van Zonneveld AJ, Rabelink TJ, Quax PH, Rotmans JI.
Liposomal prednisolone inhibits vascular inflammation and enhances venous outward remodeling in a murine arteriovenous fistula model.
Sci Rep. 2016 Jul 27;6:30439

Dankwoord

Dit proefschrift is tot stand gekomen met medewerking van velen. Graag wil ik enkelen in het bijzonder bedanken.

Beste **Ton**, allereerst wil ik jou bedanken voor alle hulp en begeleiding. Jouw efficiëntie en visie zijn inspirerend.

Joris, dank voor jouw vertrouwen, ondersteuning en de fijne begeleiding. De ontwikkeling van een nieuw diermodel was de eerste en tegelijkertijd de grootste opdracht die we wilden vervullen. Dankzij jouw steun hebben we dit na 1,5 jaar hard werken met succes volbracht. Een prestatie waar wij samen denk ik erg trots op zijn!

Paul, jij hebt mij met open armen ontvangen in jouw onderzoeksgroep. Ik heb met veel plezier veel tijd gespendeerd in jouw laboratorium en heb daar heel veel geleerd over de verschillende technieken die gepaard gingen met ons onderzoek; van opereren tot histologische analyse. Dank voor al jouw vaderlijke steun en begeleiding die je mij gegeven hebt.

Jaap, dank voor de fijne begeleiding tijdens mijn onderzoeksperiode en het vertrouwen die je mij hebt gegeven. Jouw oordeel was bepalend geweest voor mijn vervolgopleiding tot chirurg.

Anton Jan, dank voor jouw steun en begeleiding. Onze wekelijkse lab meetings waren van grote waarde voor mijn vorming als wetenschapper.

Dear **Prabir**, thank you for your hospitality, cooperation and for sharing scientific knowledge that was crucial for my thesis. Your contribution in our scientific field is impressively outstanding and very inspiring.

Hajo, veel dank voor het helpen meedenken aan het begin van het onderzoek. Ik waardeer het zeer dat jij ondanks een drukke werkschema altijd tijd hebt weten te maken om mij te helpen. Jouw kennis, maar vooral ook jouw bescheidenheid zijn inspirerend.

Bart, jouw input heeft dit proefschrift naar een hoger niveau getild. Dankzij jouw bijdrage hebben wij het daadwerkelijk voor elkaar gekregen om wetenschap te bedrijven van “bench to bedside”!

Michel, hoewel onze experimenten in grote proefdieren het proefschrift niet gehaald hebben wil ik jou bedanken voor jouw bijdrage hieraan. Onze samenwerking heeft zeker bijgedragen aan mijn wens om mij verder te specialiseren in de vaatchirurgie.

Dear **Yang**, I would like to thank you for teaching me how to perform microsurgical procedures and for your kind hospitality during my stay in the United States.

Margreet, onze "murine" topchirurg en wetenschapper. Jij hebt mij onbaatzuchtig al jouw kennis op het gebied van opereren en weefselanalyse met mij gedeeld. Hier is de "dronken generaal" jou zeer erkentelijk voor!

Reshma en **Iris**, ik wil jullie bedanken voor al jullie hulp bij de analyses.

Sherley en **Hoang**, dank voor jullie inzet en output die jullie hebben geleverd.

Ben en **Fred**, dank voor de goede zorg die jullie hebben geleverd aan de proefdieren. Ik heb erg genoten van onze professionele en vooral gezellige samenwerking.

Speciale dank gaat uit naar mijn paranimfen. **Carolien**, partner in crime. Jouw management skills zijn ongeëvenaard en iets om jaloers op te zijn! Daarnaast heb je als bureaubuurvrouw altijd voor mij klaar gestaan in de leuke en ook minder leuke periodes. Jouw vermogen om een positieve draai aan dingen te geven is bijzonder knap en effectief. Dank dat jij mij als paranimf wil bijstaan.
Nienke, ochtendmens en altijd vrolijk. Ik bewonder jouw discipline en jouw vermogen om hard te werken. Jij zorgde er altijd voor dat wij tijdens het werken genoeg vermaak hadden op de werkkamer. Dank dat je mij wilt bijstaan bij mijn proefschriftverdediging.

Graag wil ik alle **co-auteurs** bedanken voor hun bijdrage aan de manuscripten.

De oude kamergenoten van C7 wil ik graag bedanken voor hun bijdrage op wetenschappelijk en vriendschappelijk gebied. **Yuana**, **Patricia, Begüm, Bernardine, Inge, Sherida**, **Nienke** en **Carolien**. Wij waren het voorbeeld van een goede kruisbestuiving en samenwerking van verschillende disciplines.

Graag wil ik alle mensen die betrokken zijn bij de laboratoria van de **Nierziekten, Heelkunde** en **Einthoven** groep bedanken voor al hun hulp bij de experimenten. Zonder hun vrijgevigheid

van kennis en middelen was de totstandkoming van het proefschrift niet mogelijk geweest.
Als laatste wil ik mijn familie bedanken voor hun steun en interesse in mijn promotieonderzoek. **Hoi-Wing** en **Hoi-Yee**, dank voor jullie steun en begrip ook gedurende mijn promotietraject. Ons hechte band en zorgzaamheid naar elkaar is voor mij heel bijzonder.

In het bijzonder wil ik mijn **ouders** bedanken voor alle opofferingen die ze hebben gedaan om mij een goede opvoeding te laten genieten. Ik heb van jullie geleerd dat je van hard werken grootse dingen kunt bereiken. Dit laatste was een cruciaal ingrediënt voor de totstandkoming van mijn proefschrift.

Lieve **pap**, ik vind het jammer dat je niet bij mijn verdediging aanwezig zal zijn, maar ik beloof dat ik de verdediging met volle inzet en gepaste bescheidenheid zal aangaan, zoals ik dat van jou heb geleerd.